Biochar Adsorption of CO_2 from Gas Mixtures, A Study of Dry and Wet Conditions

by

© Zahra, Ghanbarpour Mamaghani B.Sc. M.Sc.

A thesis submitted to the School of Graduate Studies

in partial fulfilment of the requirements for the degree of

Doctor of Philosophy

Department of Process Engineering

Faculty of Engineering and Applied Science

Memorial University of Newfoundland

December 2023

St. John's Newfoundland

Abstract

Biochar, a green adsorbent produced from the thermochemical conversion of biomass, has proved its CO_2 capture potential in many research works. Nevertheless, when considering industrial-scale utilization, it becomes crucial to explore scenarios that closely resemble real-world emission points beyond the adsorption capacity of the adsorbent. In this work, we conducted a thorough review of the existing literature to assess whether all potential barriers and challenges related to the industrial-scale application of biochar as a CO_2 adsorbent have been investigated and addressed. In later parts, we conducted research focused on areas we identified as research gaps in our review of the literature.

A careful scanning of the literature revealed that the majority of research studies on biochar CO_2 adsorption are concentrated on its adsorption of pure CO_2 or binary CO_2/N_2 mixtures. However, in actual emission scenarios, CO_2 is never discharged as a pure gas; instead, it is emitted as part of a gas mixture. Water vapor is a component that is always present in flue gas/gasification syngas and can adversely impact the adsorption of many common CO_2 adsorbents, such as zeolites, by strongly adsorbing to the adsorption sites. For this reason, a pre-treatment drying stage is necessary for many of the commercial adsorbents, adding to the capital and operational costs. The literature was obscure regarding whether biochar performance would be negatively impacted in the presence of water vapor.

Our investigation on the water vapor impact on woody biochar CO_2 adsorption

via computational and experimental methods revealed that the adsorption rate and capacity of the biochar were not negatively impacted by the water vapor. In fact, the biochar CO_2 adsorption capacity was improved at higher CO_2 partial pressures (>80 vol.%). The experiments were performed with binary CO_2/N_2 mixtures (20-80 vol.% CO_2 balanced with N_2) at 20 °C and 1.2 bar under dry and humid conditions. For the wet experiments, N_2 was saturated with water at 20 °C before being mixed with CO_2 resulting in 20-80% relative humidity (0.5-1.8 vol% H_2O). The results showed that for 20-60 vol.% CO_2, the biochar CO_2 adsorption capacity was not impacted by the presence of water; however, at 80 vol.% CO_2, the adsorption capacity was improved by approximately 38% potentially due to carbonate formation as a result of CO_2 solution/reaction with water.

Another component that is often co-released with CO_2 either due to incomplete combustion of fuel in the flue gas or as one of the main components in gasification syngas is CO. From our observation, no available literature experimentally challenged the biochar co-adsorption of CO and CO_2. In this work, the biochar CO/CO_2 co-adsorption was examined both by computational and experimental methods. The binding energy calculations indicated that the adsorption of CO_2 on the biochar would release more energy than the adsorption of CO, demonstrating a stronger affinity of biochar for CO_2. Moreover, considering the adsorption capacities for pure CO and CO_2 on biochar (with a higher capacity observed for CO_2 (2.325 mmol/g) compared to CO (0.700 mmol/g)) led us to predict that if both gases were present in

the feed gas, biochar would exhibit a preference for CO_2 over CO. However, biochar binary CO/CO_2 co-adsorption experiments were necessary for a reliable conclusion.

The breakthrough curves of dynamic biochar CO/CO_2 co-adsorption experiments (10-90 vol.% CO_2 balanced with CO) at 20 °C and 1.2 bar showed that although CO and CO_2 were both adsorbed on biochar when the adsorption bed was fresh, some/all of the CO molecules were later removed by the more strongly adsorbed CO_2, resulting in 0 mmol/g biochar CO adsorption for experiments with lower partial pressures of CO (10-50 vol% CO). As the flue gas/gasification syngas are released at higher temperatures, examining the temperature impact on the biochar CO/CO_2 co-adsorption was necessary. The pure CO and CO_2 adsorption tests performed in the temperature range of 20-100 °C revealed that although biochar CO_2 adsorption capacity decreased as the temperature increased, biochar CO adsorption capacity was not impacted by temperature. Selected biochar binary CO/CO_2 co-adsorption tests repeated at 100 °C showed that the reduction of biochar CO_2 adsorption capacity at 100 °C compared to 20 °C resulted in lower removal of adsorbed CO molecules by CO_2, which consequently resulted in a higher CO adsorption from the binary mixtures at 100 °C compared to 20 °C.

Acknowledgements

Firstly, I would like to express my heartfelt gratitude to my supervisor, Dr. Kelly Hawboldt, for her unwavering guidance, support, and patience throughout the entire research process. Her invaluable mentorship has been instrumental in shaping my research and academic journey. I am also deeply thankful to my co-supervisor, Dr. Stephanie MacQuarrie, for her valuable insights and constructive feedback which have significantly contributed to the quality and depth of this thesis.

I would like to extend my sincere appreciation to Dr. Michael Katz, a valued member of my supervisory committee whose mentorship and support went beyond the typical committee role. Dr. Katz not only provided invaluable guidance but also generously granted me access to his laboratory and research facilities, enabling me to conduct my research effectively. I also wish to express my deep gratitude to Dr. Peter Fransham for his valuable guidance. His constructive suggestions and the wealth of knowledge he shared, stemming from his extensive experience in pyrolysis systems, have greatly enriched my understanding and contributed significantly to the success of my research.

I would also like to thank the research consultants at ACENET, especially Dr. Oliver Stueker (Memorial University of Newfoundland) and Dr. Serguei Vassiliev (University of New Brunswick), for their support during the molecular modeling parts of this thesis. I also wish to express my sincere gratitude to the technical services staff from Memorial University of Newfoundland, especially Jeff Keats, and

graduate students who helped with this project, especially Etienne Guinand and Dr. Mason Lawrence, for their valuable contributions.

Last but not least, I wish to dedicate a heartfelt appreciation to my mom, Khadijeh, my sisters, Masoumeh and Sara, and my boyfriend, Pedram. Mom, your unwavering love and sacrifices have been my guiding light throughout this journey. My sisters, your understanding and support have provided me with the strength to overcome obstacles. To my boyfriend, your constant encouragement and patient listening have made this endeavor all the more worthwhile. Each of you has been a source of inspiration for me. Thank you for being the pillars of strength in my life and for making this journey truly special.

Contents

List of Tables

List of Figures

Table of Acronyms

Page number indicates the first significant reference.

MEA :	Monoethanolamin (p. 2).
MOFs :	Metal-organic frameworks (p. 4).
LHV :	Lower heating value (p. 19).
FTIR :	Fourier-transform infrared spectroscopy (p. 30).
AC :	Activated carbon (p. 54).
ACFs :	Activated carbon fibers (p. 54).
RH :	Relative humidity (p. 54).
TEPA :	Tetraethylenepentamine (p. 54).
PSA :	Pressure swing adsorption (p. 56).
CMR :	Catalytic Membrane Reactor (p. 59).
ABR :	Automated breakthrough analyzer (p. 101).
PFD :	Process flow diagram (p. 103).
BET :	Brunauer-Emmett-Teller (p. 104).

BJH : Barrett-Joyner-Halenda (p. 104).

TGA : Thermogravimetric analysis (p. 104).

DTG : Differential thermogravimetry (p. 104).

MS : Mass spectrometry (p. 108).

MFC : Mass flow controller (p. 108).

IAST : Ideal adsorbed solution theory (p. 150).

Table of Symbols

Page number indicates the first significant reference. Although not all symbols are explicitly referenced below, their definitions are obvious from the context.

E : Energy (kJ/mol) (p. 106).

q : Adsorption capacity (mmol/g) (p. 109).

F : Volumeteric flowrate (mL/min) (p. 109).

C : Adsorbate concentration in the adsorption column outlet gas (mmol/L) (p. 109).

C_0 : Adsorbate concentration in the adsorption column inlet gas (mmol/L) (p. 109).

m : Adsorbent mass (g) (p. 109).

t : Time (min) (p. 109).

q_e : Adsorption capacity at the equilibrium state (mmol/g) (p. 110).

k_1 : Pseudo-first-order kinetic rate constant (1/min) (p. 110).

k_2 : Pseudo-second-order kinetic rate constant (g/(mmol min)) (p. 110).

k_A : Avrami kinetic constant (1/min) (p. 110).

q_{exp} : Experimental adsorption capacity (mmol/g) (p. 121).

R^2 : Coefficient of determination (p. 127).

q_m : Maximum adsorption capacity (mmol/g) (p. 148).

K_L : Inverse of the Langmuir coefficient (1/kPa) (p. 148).

P : Pressure (kPa) (p. 148).

K_F : The Freundlich coefficient (mmol/(g $kPa^{1/n}$)) (p. 149).

n : The isotherm constant (the Freundlich and the Langmuir-Freundlich isotherms) (p. 149).

K_{LF} : The Langmuir-Freundlich coefficient (1/kPa) (p. 149).

K_{L1} : The Dual-site Langmuir coefficient (1/kPa) (p. 150).

K_{L2} : The Dual-site Langmuir coefficient (1/kPa) (p. 150).

q_{m1} : Maximum adsorption capacity for adsorption sites type 1 (mmol/g) (p. 150).

q_{m2} : Maximum adsorption capacity for adsorption sites type 2 (mmol/g) (p. 150).

x_i : Mole fraction of component i (p. 150).

q_i : Adsorbent adsorption capacity for component i (mmol/g) (p. 150).

q_t : Total adsorption capacity for all components in the gas mixture (mmol/g) (p. 150).

N : Number of components in the gas mixture (p. 150).

Chapter 1

Introduction and Overview

1.1 Introduction

Over time, climate change has emerged as one of the foremost worldwide concerns [1, 2]. This global temperature surge is primarily driven by increasing levels of greenhouse gases (GHGs) in the atmosphere, resulting from numerous human activities [2]. Among different GHGs, such as CO_2, CH_4, and N_2O, CO_2 is the component with the most pronounced influence primarily due to its higher emission levels [2, 3]. The CO_2 level was reported as 414.7 ppm in the atmosphere in 2019, which is an approximate 45% increase compared to CO_2 level in the 1980s [4]. The global CO_2 emission from fossil-fuel combustion was 36.1 Gt 2022 [5].

Fossil fuel-fired power plants are responsible for approximately 33-40% of the CO_2 emissions, with coal-fired power plants being the predominant source [4]. Carbon capture and storage offers a promising solution to mitigate the impacts of greenhouse gas emissions. By capturing CO_2 from its emission points, a significant portion of CO_2 can be prevented from entering the atmosphere [1, 6, 7].

There are different available technologies for CO_2 capture, including absorption, adsorption, membrane separation, and cryogenic separation [8]. CO_2 absorption using amine solvents, such as monoethanolamine (MEA), is the most conventional CO_2 removal technique [9, 10]. The main drawbacks of this method are possible system corrosion by amine solvents, possible degradation of the solvent (which can be thermal degradation due to high regeneration temperatures or chemical degradation caused by the presence of O_2 or some oxides), and high energy requirements for

solvent regeneration (can be up to 4-6 MJ/kg CO_2 for chemical solvents) [10].

Separation of CO_2 using membranes is straightforward and cost-effective; however, its application for flue gas CO_2 removal has some challenges. The membrane needs to have a high selectivity to remove CO_2 at low partial pressures from flue gas. There is also the possibility of thermal and chemical degradation due to high flue gas temperature and the presence of sulfur-containing materials, respectively. Therefore, some pretreatment stages might be inevitable [11]. Cryogenic separation is a relatively new approach among CO_2 capture methods, in which CO_2 is transformed into a solid on the surface of a heat exchanger [9]. Although this method offers the advantage of not requiring any chemical (as a solvent/adsorbent), there are some challenges ahead of its way to commercialization, including the need for perfect thermal insulation of the system to prevent heat transfer with the surrounding area and the possible reduction of the heat transfer efficiency as the layers of solid CO_2 appear on heat exchanger surface [9, 10]. In addition, the gas stream impurities, such as water vapor, need to be removed before the process due to the possible destructive impacts on the system, such as ice clogging the pipes or corrosive acids forming [10].

CO_2 adsorption occurs using solid adsorbents [12]. Among the technologies for CO_2 capture, adsorption is the most cost-effective one due to adsorbents lower regeneration energy requirements compared to absorption [12–14]. Carbon-based adsorbents have generally shown a great CO_2 capture potential [12]. The utilization of carbon-based adsorbents produced from biomass (which is an abundant and re-

newable source) is a sustainable process in two ways: it is used for CO_2 capture and sequestration, and it addresses biomass disposal concerns [1, 15].

Biochar, a carbon-based adsorbent produced from the thermochemical conversion of biomass, has proved its CO_2 capture capability [16–18]. Most of the research on CO_2 capture is focused on biochar adsorption from pure CO_2 or binary CO_2/N_2 [19]. However, CO_2 is never released as a pure gas in the real-life industrial-scale emission points [19, 20]. For instance, flue gas from a coal-fired power plant is typically composed of CO_2, N_2, H_2O, and O_2 with traces of NOx and SOx [21], while syngas from gasification is a mixture of CO, H_2, CO_2, N_2 along with some hydrocarbons, such as CH_4, and possible traces of H_2S, NH_3, and tars [20]. Therefore, before the industrial-scale application of biochar, it is necessary to conduct comprehensive research to assess its performance in the presence of different impurities.

No matter what the flue gas source is, there is typically water present [22–24]. Some of the common CO_2 adsorbents, such as several zeolites and metal-organic frameworks (MOFs), show such a great affinity toward water that CO_2 adsorption is reduced in the humid conditions [23]. Carbon-based adsorbents are generally considered to be hydrophobic [24], so water may not have a drastic impact on their CO_2 adsorption. However, there is not sufficient research assessing CO_2 adsorption by carbon-based adsorbents, especially biochar, under humid conditions to have an ultimate conclusion on this matter [19].

Another impurity in gas emissions containing CO_2 is CO, whether it is the result

of incomplete combustion of fuel [25] or in syngas as one of the main components [26]. Therefore, it is important to study the simultaneous adsorption of CO and CO_2 on biochar. There are limited research works predicting CO and CO_2 co-adsorption on carbon-based adsorbents by simulations or by comparing their pure gas adsorptions [27, 28]. However, from our review of the literature, no prior research work has experimentally challenged the CO/CO_2 co-adsorption on biochar.

1.2 Objectives

The overall objective of this thesis is to investigate the challenges that need to be addressed prior to the industrial-scale application of biochar as a CO_2 adsorbent. We focused on two of the most important challenges ahead of the larger scale utilization of biochar, which are: 1. the impact of water vapor on biochar CO_2 adsorption and 2. biochar simultaneous adsorption of CO_2 and CO (the impact of CO on biochar CO_2 adsorption).

The biochar in this work was produced from softwood sawdust via fast pyrolysis in an auger reactor at 500 °C at 1 kg/hr under a slight vacuum. The schematic diagram of a pyrolysis process is presented in Figure 1.1. The physical and chemical characteristics, such as elemental compositions, surface areas, and functionalities of the biochar and softwood, were examined and compared to each other. Several dynamic tests at different conditions were performed to obtain satisfactory conclusions for the primary research objectives of this thesis.

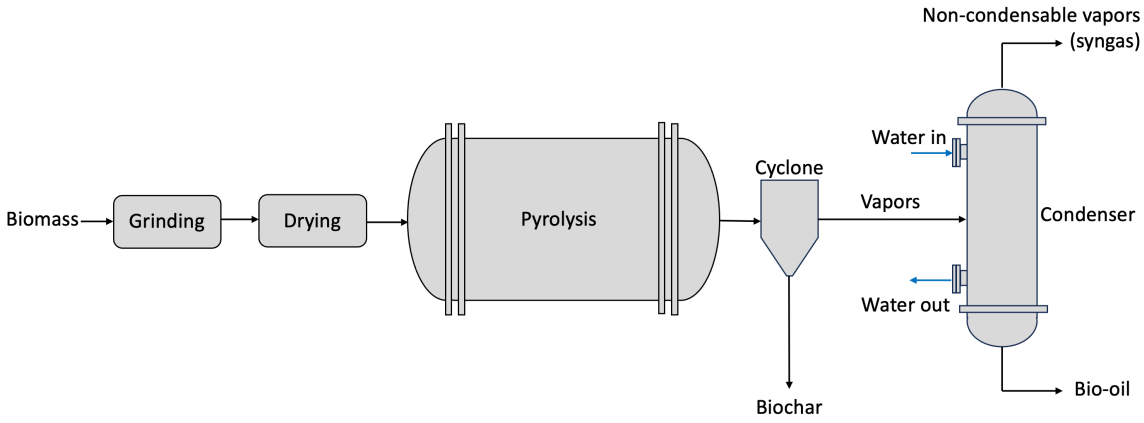

Figure 1.1: Schematic diagram of pyrolysis process

This thesis consists of manuscripts that are either published or under review or ready to be submitted to the journals. An outline of the chapters is provided in the following:

Chapter 2 has been published in the Journal of Environmental Chemical Engineering. This chapter provides all the necessary information on different methods for biochar production and biochar characteristics (which can vary greatly depending on its feedstock and production conditions) impacting its CO_2 capture ability. This article provides a thorough examination of studies focused on the adsorption of CO_2 from gas mixtures by carbon-based adsorbents and clearly points out the lack of research in the area of biochar CO_2 adsorption from gas mixtures. In addition, this article critically reviews the literature focused on carbon-based adsorbents CO_2 adsorption under humid conditions. A thorough review of possible applications of

biochar in syngas H_2 purification is also presented in this chapter.

Chapter 3 is under review in the Journal of Fuel. In this chapter, the production of biochar from softwood sawdust via fast pyrolysis is discussed, and the physical and chemical properties of the biochar and softwood biomass are examined and compared. This chapter discusses the impact of water vapor on CO_2 adsorption on biochar via computational and experimental methods. The biochar and CO_2 binding energy was calculated via molecular modeling for the dry and wet conditions (in the presence of water as a solvent). The results were compared to have a rough estimation before the adsorption tests. The impact of water vapor on biochar CO_2 adsorption was then tested with adsorption experiments of binary CO_2/N_2 mixture under dry and partially saturated conditions. The adsorption capacities for similar concentrations under dry and wet conditions were calculated and compared. In addition, the adsorption rates of the experiments under dry and wet conditions were compared to investigate the possible impact of water vapor on the rate of adsorption. A conclusion based on the results of biochar CO_2 adsorption performance under dry and wet conditions was presented, and suggestions for future work were provided.

Chapter 4 is under review in the Journal of Separation and Purification Technology. This chapter examines the co-adsorption of CO and CO_2 with the purpose of inspecting the impact of CO on CO_2 adsorption on biochar. The co-adsorption of CO and CO_2 were studied by computational and experimental methods. The calculation and comparison of binding energies of CO/CO_2 on biochar provided an estimation

of the affinity of biochar for these two gases before doing the experiments. The dynamic adsorption tests for pure and binary CO/CO_2 mixture were conducted at different concentration levels of CO and CO_2 (at 20 °C and 1.2 bar), and the results were analyzed to determine the impact of CO on CO_2 adsorption on biochar. As the CO_2 containing emitted gases are released at higher temperatures than ambient, the pure and selected binary tests were re-performed at different temperatures ranging from 20-100 °C. The results from this set of experiments enabled us to put together a conclusion in which the impact of CO under conditions closer to an industrial-scale emission could be predicted. In addition, some suggestions on the suitable next stage of the research were presented.

Chapter 5 includes conclusions based on the results achieved in each of the chapters of this thesis. This chapter also includes a series of recommendations for the next steps of this research based on the conclusions reached. A summary of the overview and objectives of each chapter is presented in Figure 1.2.

Chapter 2	A thorough review of the available literature on: 1. biochar CO_2 adsorption from gas mixtures, 2. biochar CO_2 adsorption under humid conditions, 3. biochar potential application in H_2 purification from syngas is presented and the research gaps are pointed out.
Chapter 3	The production of biochar from softwood biomass via fast pyrolysis in an auger reactor is discussed and biochar and softwood are characterized. The biochar CO_2 adsorption capacity and rate under dry and humid conditions is studied using both computational and experimental methods.
Chapter 4	The co-adsorption of CO and CO_2 on the woody biochar is predicted using molecular modeling. The adsorption of pure and binary CO/CO_2 mixtures on biochar at different temperatures are examined via dynamic adsorption tests.
Chapter 5	The conclusions based on the results achieved in each chapter are discussed. The suggested steps for the future research in this area are point out.

Figure 1.2: Summary of each chapter overview and objectives

Bibliography

[1] C. Quan, Y. Zhou, J. Wang, C. Wu, and N. Gao, "Biomass-based carbon materials for co2 capture: A review," *Journal of CO2 Utilization*, vol. 68, p. 102373, 2023.

[2] M. Hanifa, R. Agarwal, U. Sharma, P. Thapliyal, and L. Singh, "A review on co2 capture and sequestration in the construction industry: Emerging approaches and commercialised technologies," *Journal of CO2 Utilization*, vol. 67, p. 102292, 2023.

[3] D. A. Lashof and D. R. Ahuja, "Relative contributions of greenhouse gas emissions to global warming," *Nature*, vol. 344, no. 6266, pp. 529–531, 1990.

[4] K. O. Yoro and M. O. Daramola, "Co2 emission sources, greenhouse gases, and the global warming effect," in *Advances in carbon capture*, pp. 3–28, Elsevier, 2020.

[5] Z. Liu, Z. Deng, S. Davis, and P. Ciais, "Monitoring global carbon emissions in 2022," *Nature Reviews Earth & Environment*, vol. 4, no. 4, pp. 205–206, 2023.

[6] N. Abuelnoor, A. AlHajaj, M. Khaleel, L. F. Vega, and M. R. Abu-Zahra, "Activated carbons from biomass-based sources for co2 capture applications," *Chemosphere*, vol. 282, p. 131111, 2021.

[7] A. González, M. Plaza, F. Rubiera, and C. Pevida, "Sustainable biomass-based

carbon adsorbents for post-combustion co2 capture," *Chemical engineering journal*, vol. 230, pp. 456–465, 2013.

[8] B. Sreenivasulu, D. Gayatri, I. Sreedhar, and K. Raghavan, "A journey into the process and engineering aspects of carbon capture technologies," *Renewable and Sustainable Energy Reviews*, vol. 41, pp. 1324–1350, 2015.

[9] A. Sattari, A. Ramazani, H. Aghahosseini, and M. K. Aroua, "The application of polymer containing materials in co2 capturing via absorption and adsorption methods," *Journal of CO2 Utilization*, vol. 48, p. 101526, 2021.

[10] C. Song, Q. Liu, S. Deng, H. Li, and Y. Kitamura, "Cryogenic-based co2 capture technologies: State-of-the-art developments and current challenges," *Renewable and sustainable energy reviews*, vol. 101, pp. 265–278, 2019.

[11] S. E. Zanco, J.-F. Pérez-Calvo, A. Gasós, B. Cordiano, V. Becattini, and M. Mazzotti, "Postcombustion co2 capture: a comparative techno-economic assessment of three technologies using a solvent, an adsorbent, and a membrane," *ACS Engineering Au*, vol. 1, no. 1, pp. 50–72, 2021.

[12] A. E. Creamer and B. Gao, "Carbon-based adsorbents for postcombustion co2 capture: a critical review," *Environmental science & technology*, vol. 50, no. 14, pp. 7276–7289, 2016.

[13] N. Z. M. Azmi, A. Buthiyappan, A. A. A. Raman, M. F. A. Patah, and S. Sufian,

"Recent advances in biomass based activated carbon for carbon dioxide capture–a review," *Journal of Industrial and Engineering Chemistry*, vol. 116, pp. 1–20, 2022.

[14] L. Jiang, A. Gonzalez-Diaz, J. Ling-Chin, A. Roskilly, and A. Smallbone, "Post-combustion co2 capture from a natural gas combined cycle power plant using activated carbon adsorption," *Applied Energy*, vol. 245, pp. 1–15, 2019.

[15] H. Bamdad, K. Hawboldt, and S. MacQuarrie, "A review on common adsorbents for acid gases removal: Focus on biochar," *Renewable and Sustainable Energy Reviews*, vol. 81, pp. 1705–1720, 2018.

[16] S. Jung, Y.-K. Park, and E. E. Kwon, "Strategic use of biochar for co2 capture and sequestration," *Journal of CO2 Utilization*, vol. 32, pp. 128–139, 2019.

[17] A. N. Shafawi, A. R. Mohamed, P. Lahijani, and M. Mohammadi, "Recent advances in developing engineered biochar for co2 capture: An insight into the biochar modification approaches," *Journal of Environmental Chemical Engineering*, vol. 9, no. 6, p. 106869, 2021.

[18] S. Guo, Y. Li, Y. Wang, L. Wang, Y. Sun, and L. Liu, "Recent advances in biochar-based adsorbents for co2 capture," *Carbon Capture Science & Technology*, p. 100059, 2022.

[19] Z. G. Mamaghani, K. A. Hawboldt, and S. MacQuarrie, "Adsorption of co2

using biochar-review of the impact of gas mixtures and water on adsorption," *Journal of Environmental Chemical Engineering*, p. 109643, 2023.

[20] Y. Zhang, Y. Cui, P. Chen, S. Liu, N. Zhou, K. Ding, L. Fan, P. Peng, M. Min, Y. Cheng, *et al.*, "Gasification technologies and their energy potentials," in *Sustainable resource recovery and zero waste approaches*, pp. 193–206, Elsevier, 2019.

[21] X. Dong, J. Zhang, L. Gang, P. Xiao, P. Webley, and Y.-c. ZHAI, "Effect of water vapor from power station flue gas on co2 capture by vacuum swing adsorption with activated carbon," *Journal of Fuel Chemistry and Technology*, vol. 39, no. 3, pp. 169–174, 2011.

[22] J. J. Manyà, D. García-Morcate, and B. González, "Adsorption performance of physically activated biochars for postcombustion co2 capture from dry and humid flue gas," *Applied Sciences*, vol. 10, no. 1, p. 376, 2020.

[23] F. Yang, T. Ge, X. Zhu, J. Wu, and R. Wang, "Study on co2 capture in humid flue gas using amine-modified zif-8," *Separation and Purification Technology*, vol. 287, p. 120535, 2022.

[24] J. M. Kolle, M. Fayaz, and A. Sayari, "Understanding the effect of water on co2 adsorption," *Chemical Reviews*, vol. 121, no. 13, pp. 7280–7345, 2021.

[25] D. Nicks Jr, J. Holloway, T. Ryerson, R. Dissly, D. Parrish, G. Frost, M. Trainer, S. Donnelly, S. Schauffler, E. Atlas, *et al.*, "Fossil-fueled power plants as a source

of atmospheric carbon monoxide," *Journal of environmental monitoring*, vol. 5, no. 1, pp. 35–39, 2003.

[26] A. Molino, S. Chianese, and D. Musmarra, "Biomass gasification technology: The state of the art overview," *Journal of Energy Chemistry*, vol. 25, no. 1, pp. 10–25, 2016.

[27] G. P. Lithoxoos, L. D. Peristeras, G. C. Boulougouris, and I. G. Economou, "Monte carlo simulation of carbon monoxide, carbon dioxide and methane adsorption on activated carbon," *Molecular Physics*, vol. 110, no. 11-12, pp. 1153–1160, 2012.

[28] S. M. Wilson, D. A. Kennedy, and F. H. Tezel, "Adsorbent screening for co2/co separation for applications in syngas production," *Separation and Purification Technology*, vol. 236, p. 116268, 2020.

Chapter 2

Literature Review

A modified version of this chapter has been published; Z. Ghanbarpour Mamaghani, K. Hawboldt, S. MacQuarrie. Adsorption of CO2 using biochar - Review of the impact of gas mixtures and water on adsorption. Journal of Environmental Chemical Engineering.

Abstract

Biochar produced from sources such as forestry, agricultural, and marine wastes has demonstrated an ability to adsorb CO_2. The adsorption capacity is a function of biochar surface properties, which subsequently depend on biochar feedstock and production conditions. This is a comprehensive review on the use of biochar as a carbon capture adsorbent with a particular focus on the impact of the properties of biochar and feed gas composition CO_2 adsorption. Applying biochar in carbon capture at the industrial scale requires detailed knowledge of the impact of co-adsorption effects of other gases. This is particularly true of water, biogas, syngas, and other gas streams. The study of these impacts is diffuse across the literature, where only one other gas is typically studied. This review brings these studies together to give a comprehensive picture of the impact of gas mixtures as a function of biochar properties on carbon capture. This review highlights the limited study in this area, where the bulk of research work is focused on gas mixtures, demonstrating more work is required on this topic.

Examining biochar affinity toward various gases can also indicate if biochar has potential applications in gas separations to recover gases such as H_2. Articles focused on H_2 purification from gas mixtures using carbon-based adsorbents are also studied. This review indicates the potential for biochar to separate H_2 from syngas, particularly using biochar produced during gasification to then purify syngas, making it a closed-loop system.

Keywords: Biochar; Biomass Utilization; Carbon Capture; Adsorption; Carbon dioxide; Gas treatment; Mixtures

2.1 Introduction

Mitigation of carbon dioxide (CO_2) emissions involves both minimization and capture/sequestration [1, 2]. The overall goal of carbon capture, sequestration or storage is carbon neutrality or carbon negativity [2]. However, in the development of any CO_2 capture process, the nature of the gas mixture must be considered as CO_2 is rarely produced as a single component gas but rather as a gas mixture. In addition, combustion, syngas, and other CO_2-rich exhaust gases are typically rich in water vapor, which could change the properties of the biochar surface and/or the adsorption behavior of CO_2.

Post-combustion gas streams from fossil fuel/biomass combustion consist of CO_2 and N_2, with varying amounts of volatile organic compounds (VOCs), H_2O, O_2, CO, sulfur oxides (SOx), and nitric oxides (NOx) [3, 4] depending on the fuel source and combustion conditions [3]. In addition to the combustion of fossil fuels and biomass, gasification is becoming increasingly used in fuels [5]. Gasification product gases are dominated by H_2, CO, CO_2, CH_4, and lower weight hydrocarbons where the composition depends on the biomass feedstock and gasification conditions [6, 7]. For instance, if the air is the gasifying agent, a large amount of N_2 is present in the syngas resulting in lower concentrations of other components [7]. A summary of some

syngas compositions from different gasification processes is presented in Table 2.1 as an example of how CO_2 is always emitted with other gases. Since gasification is becoming increasingly used in fuels, the heating value is also an important characteristic of the produced syngas. The syngas heating value is determined by the oxidizer used for the gasification step. Air, which is the least costly option, produces the lowest heating value syngas (4-7 MJ/Nm^3), whereas oxygen as the oxidizer produces the highest heating value syngas (12-28 MJ/Nm^3) [8]. Therefore, the heating values of the syngases have been reported in Table 2.1 as well. Another source of CO_2 release is biogas from anaerobic digestion of the organic waste. Biogas can be used as fuel and is typically a mixture of around 50-75 % of CH_4, 25-50 % of CO_2, 2-8 % N_2, and smaller amounts of gases such as H_2S, NH_3, H_2, and other volatile organic compounds [9]. This review focuses on the impact of the gases associated with combustion (due to the ubiquitous nature of fossil fuel and biomass combustion) and/or thermochemical biomass conversion (CO, CO_2, H_2O, and N_2) as biochar is typically produced as a by-product.

Table 2.1: Compositions and lower heating values (LHV) of gasification syngas products

feedstock	gasifier	gasifying agent	temperature (°C)	Syngas Composition (vol.%)				LHV (MJ/Nm^3)	Ref.
				H_2	CO	CO_2	CH_4		
Coffee husk	Bubbling fluidized bed	Air	740	8.74	9.84	7.1	3.97	3.61	[10]
Coffee husk	Bubbling fluidized bed	Air	700	7.68	9.49	7.2	3.88	3.42	[10]
Sawdust	Bubbling fluidized bed	Air	740	6.9	9.1	9.8	8.1	4.8	[10]
Sawdust	Bubbling fluidized bed	Air	700	5.9	7.6	8.9	5.4	3.53	[10]
Coal	Fluidized bed	Air	813	27.7	10.87	13.35	3.9	5.19	[11]
Dried sewage sludge	Fluidized bed	Air	813	14.64	12.39	10.91	5.36	6.11	[11]
Straw pellet	Fluidized bed	Steam	685	13.42	9.38	69.96	4.34	6.5	[12]
Straw pellet	Fluidized bed	Steam	767	20.22	16.18	57.21	4.01	7.1	[12]
Straw pellet	Fluidized bed	Steam	824	19.52	24.67	49.46	4.66	7.9	[12]
Wood pellet	Fluidized bed	Steam	661	16.87	12.55	63.28	4.72	6.8	[12]
Wood pellet	Fluidized bed	Steam	720	23.84	19.15	49.82	4.87	8.2	[12]
Wood pellet	Fluidized bed	Steam	790	22.18	26.52	44.62	5.01	8.0	[12]
Wood chips	Fixed bed	Air	700-1000	17.3	17.1	11.9	1.7	4.7	[13]
Rice straw	Fluidized bed	O_2 enriched air	600	1.04	13.73	32.28	5.89	3.94	[14]
Rice straw	Fluidized bed	O_2 enriched air	800	7.51	19.46	2.45	5.9	5.4	[14]
Pine Cone	Fixed bed	Air	701-1046	18.76	23.62	11.87	1.83	N/A	[15]
Wood Pellet	Fixed bed	Air	701-1046	21.62	27.74	9.43	2.30	N/A	[15]
White pine	Fluidized bed	Air	750	8.13	10.36	15.13	2.37	3	[16]
White pine	Fluidized bed	Air-Steam	750	12.18	6.45	17.70	1.92	2.8	[16]
Citrus peels	Fluidized bed	Air	750	10.50	12.40	18.30	3.70	4	[16]
Citrus peels	Fluidized bed	Air-Steam	750	20.00	11.40	19.40	3.40	4.8	[16]
Posidonia Oceanica	Fluidized bed	Air	750	11.76	12.73	14.12	3.04	4	[16]
Posidonia Oceanica	Fluidized bed	Air-Steam	750	16.35	11.18	16.04	2.78	4.2	[16]

Separation of CO_2 from these gas streams can both recover CO_2 for alternative use and/or sequestration [17] and potentially purification of the gas stream for subsequent use (e.g., H_2 production) [18].

There are several processes used for CO_2 removal, such as absorption, adsorption, membrane separation, and cryogenic separation [19, 20]. In absorption, the liquid solvent (typically amine for CO_2) is in contact with the gas mixture in a packed or tray column and CO_2 is absorbed into the solvent. The CO_2-rich solvent is then sent to a stripper unit in which the solvent is regenerated by applying heat [21, 22]. These systems typically require a large equipment footprint, high energy needs for solvent regeneration, and relatively high corrosion rate of the equipment [23]. Membrane processes have the advantage of high selectivity [24], not requiring a separate phase (e.g., dissolving CO_2 in solvent) [25], and potentially having lower operational costs as there are no solvent regeneration requirements [26]. However, there are still issues related to mechanical and thermal stability of membranes over time [27]. Cryogenic processes remove CO_2 through condensation by lowering the temperature and raising the flue gas pressure. The condensation process can be followed by a distillation step if high purity of CO_2 is required [28]. This process requires a high amount of energy and subsequently a high operational cost [27]. Adsorption uses a solid adsorbent to remove target gases [29] (e.g., porous carbons, MOFs (metal-organic frameworks), zeolites, mesoporous silica [30]). Adsorbent regeneration (if required) is a much less costly and energy intensive process compared to absorption systems [31]. The

primary disadvantage of adsorption over absorption is the gas-solid mass transfer rate (i.e., CO_2 removal) is lower compared to gas-liquid mass transfer. The rate can be modified using different materials, but this could increase capital cost [32].

Porous carbon-based adsorbents from biomass wastes have attracted much attention for selective CO_2 adsorption [33, 34]. Biomass-based adsorbents, where the biomass is residue from forestry or agricultural activities, are attractive as they repurpose the biomass, thereby decreasing CO_2 emissions associated with storage and disposal [33]. Biomass-based carbon adsorbents are generally labeled as low-cost materials due to the fact that the feedstock is abundant and renewable [35]. These adsorbents are not only easily regenerated [35, 36] but have also shown stable performance after multiple regenerations [36]. They have also exhibited high stability in the presence of water, unlike some commercial adsorbents such as zeolites and MOFs [35].

Biochar is a solid carbonaceous adsorbent produced from pyrolysis, gasification, torrefaction, or hydrothermal processing of biomass [37]. It can be produced from a variety of biomass such as woody biomass [38], animal manures [39], food wastes [40], and marine biomass such as seaweed [41]. The porous structure of the biochar as well as its surface functional groups have made this material an excellent candidate for carbon capture and sequestration [42]. Some of the advantages of using biochar as a CO_2 adsorbent compared to other commercial adsorbents are:

- It is environmentally friendly and sustainable as its feedstock is biomass.

- It can store CO_2 for further utilization (e.g. in soil).
- It is cost-effective as its feedstock is abundant.
- Other than CO_2 capture and storage, it addresses the biomass disposal concerns.

There are multiple articles available discussing biochar adsorption of pure CO_2 [43–45]. However, CO_2 is rarely produced as a pure component. The adsorption of CO_2 from gas mixtures requires knowledge of the impact of the other gases on the adsorption capacity [46]. Gases can compete for adsorbent sites, form complexes with adsorbed compounds, and interact in the gas phase which will impact adsorption efficiency [47].

One of the most common impurities in the gas streams is water vapor. Whether the CO_2 is adsorbed in post-combustion or pre-combustion stage, notable amount of water is present in the gas stream [48]. Post-combustion flue gas (e.g., coal combustion) contains approximately 6-12 % H_2O (vol.%) while the syngas product from gasification (e.g., coal gasification) is approximately 2-28 % H_2O (vol.%) [48]. Water in the mixture can cause issues for adsorbents such as zeolites and metal-organic frameworks, which have higher affinity toward water molecules compared to CO_2 molecules [49]. Previous studies have proposed H_2O removal before the gas contacts the adsorbent, such as inserting a layer of a moisture adsorbent material (e.g. alumina) [50–52]. However, dehumidification units add to the overall capital and

operating costs [49, 53] Although carbon adsorbents have generally shown more hydrophobicity and fewer issues with water vapor, given the ubiquitous nature of water in these streams, studying biochar performance when H_2O is present is required [53].

CO_2 adsorption can also help purification of certain compounds. For instance, in the case of syngas from gasification, the main purpose of CO_2 adsorption may be H_2 purification and the focus can be on using biochar to slip H_2 and adsorb CO_2 [54, 55]. This paper reviews the literature focused on biochar as a CO_2 adsorbent, including impact of competing gases, water vapor, and integrated purification/sequestration process (e.g.,hydrogen separation from synthesis gas).

2.2 Biochar Production

Biochar is produced from the thermochemical conversion of biomass in low oxygen or oxygen-free conditions [56]. Biochar is different from ash in the sense that ash is the result of Incineration (burning in the presence of oxygen), where almost all the carbon leaves the biomass structure as CO_2, and what is left as ash is mostly minerals [57]. Thermochemical processes include pyrolysis, gasification, torrefaction, and hydrothermal carbonization [58]. The elemental composition, surface properties (including surface area and functional groups), and applications of biochar are determined by its biomass precursor, production temperature, and residence time [58, 59]. For instance, biomass containing high carbon content, such as lignocellulosic biomass from forestry and agricultural sources [60], has shown good potential as

a carbon sequestration material [61]. The two most common processes that produce biochar are pyrolysis and gasification. Pyrolysis is increasingly common for converting low-quality biomass (waste residues from forestry and agriculture) to value-added products. In slow pyrolysis, the primary product is biochar, and in fast pyrolysis and gasification, bio-oil and syngas are the primary products, respectively. Biochar, whether a primary or secondary product, can be used in fuel, soil, and adsorbent applications [62]. These processes are appealing as they are able to produce energy and sequester carbon [63].

2.2.1 Pyrolysis

Pyrolysis is performed at temperatures between 400-600 °C [64] in the absence of O_2 [65]. Liquid bio-oil, solid biochar, and non-condensable gases are the three main products [65, 66]. Based on the final temperature and the residence time of reaction, pyrolysis can be loosely classified into two groups: slow and fast pyrolysis [58]. In slow pyrolysis, longer residence times (minutes to days) at approximately 400 °C results in higher yield for char, whereas fast pyrolysis favors bio-oil production with shorter vapor residence time ($<$ 10s) at approximately 500 °C (Table 2.2) [58, 67]. The heating rate can vary from 0.1-10 °C/min for slow pyrolysis, and 10-1000 °C/min for fast pyrolysis [68]. Although slow pyrolysis has a higher biochar yield, biochars produced from fast pyrolysis exhibit a more defined pore structure and potentially more surface functionality [69].

As mentioned before, biochar chemical and physical characteristics is determined by the type of biomass feedstock and pyrolysis conditions [70, 71]. Even biochar yield during pyrolysis is affected by the feedstock and production condition. Studies have shown that biochar yield decreases with increasing pyrolysis temperature [72–75] and at the same pyrolysis temperature, biomass with higher ash results in higher biochar yield due to higher inorganic content [73, 76]. A summary of product yields of several pyrolysis processes is shown in Table 2.2.

Table 2.2: Pyrolysis yields with respect to process conditions

Feedstock	Pyrolysis type	Reactor	Temperature	Heating rate	Pyrolysis time	Product yield (wt%)			Ref.
			(°C)	(°C/min)	(min)	Biochar	Bio-oil	Syngas	
Beech wood	Fast	Drop tube reactor	450	NA	20-90	40.6	47.5	6.1	[77]
Beech wood	Fast	Drop tube reactor	500	NA	20-90	13.6	62.4	15	[77]
Beech wood	Fast	Drop tube reactor	550	NA	20-90	10.3	48.3	25.6	[77]
Beech wood	Fast	Drop tube reactor	650	NA	20-90	8.2	39.7	51.5	[77]
Wood sawdust	Slow	Semi batch	350	10	NA	55.11	26.23	18.66	[78]
Wood sawdust	Slow	Semi batch	500	10	NA	41.01	41.10	23.05	[78]
Wood sawdust	Slow	Semi batch	650	10	NA	28.97	34.19	36.12	[78]
Wood sawdust	Slow	Semi batch	350	50	NA	52.85	27.86	19.29	[78]
Wood sawdust	Slow	Semi batch	500	50	NA	44.08	44.16	25.07	[78]
Wood sawdust	Slow	Semi batch	650	50	NA	26.19	34.24	39.42	[78]
Rice husk	Fast	Downdraft circulating fluidized bed	550	NA	0.033	26.0	48.1	25.9	[79]
Oak	Fast	Fluidized bed	500	NA	0.032	14.1	65.7	20.2	[80]
Eukalyptus	Fast	Fluidized bed	500	NA	0.032	14.9	59.2	25.9	[80]
Pitch pine	Fast	Fluidized bed	500	NA	0.032	16.5	61.6	21.9	[80]
Japanese cedar	Fast	Fluidized bed	500	NA	0.032	13.9	62.6	23.5	[80]
Yellow poplar wood	Fast	Fluidized bed	400	NA	0.02	28.9	50.2	20.9	[81]
Yellow poplar wood	Fast	Fluidized bed	550	NA	0.02	7.9	63.9	28.2	[81]
Yellow poplar wood	Fast	Fluidized bed	500	NA	0.063	8.9	61.8	21.8	[81]
Yellow poplar wood	Fast	Fluidized bed	500	NA	0.128	17.9	51.6	30.5	[81]
Halophyte grass	Slow	Stainless steel reactor	300	10	120	48	18	34	[82]
Halophyte grass	Slow	Stainless steel reactor	500	10	120	33	27	41	[82]
Halophyte grass	Slow	Stainless steel reactor	700	10	120	24	23	54	[82]
Cashew nutshell	Slow	Batch	700	22.5	50	30.4	10.7	31	[83]
Potato peel waste	Fast	Auger reactor	450	NA	0.13	30.5	22.7	NA	[84]
Hybrid poplar	Fast	Auger reactor	450	NA	0.13	15.2	40.1	NA	[84]
Tobacco residue	Slow	Tubular	400	7	NA	20.60	48.74	15.30	[85]
Tobacco residue	Slow	Tubular	550	7	NA	27.05	32.11	25.30	[85]
Tobacco residue	Slow	Tubular	700	7	NA	23.92	28.37	31.15	[85]
Tobacco residue	Fast	Tubular	400	300	NA	36.83	26.39	21.75	[85]
Tobacco residue	Fast	Tubular	550	300	NA	25.73	29.78	26.20	[85]
Tobacco residue	Fast	Tubular	700	300	NA	23.61	27.59	31.42	[85]
Softwood shavings	Fast	Auger reactor	450	NA	NA	21	53	NA	[86]
Hardwood sawdust	Fast	Auger reactor	450	NA	NA	22	55	NA	[86]
Softwood bark	Fast	Auger reactor	460	NA	NA	30	39	NA	[86]

The elemental ratios in biochars are one of the important factors in determining their adsorption performance. The H/C can be indicative of biochar aromaticity [87, 88], while O/C can be a representative of deoxygenation, extent of charring [87] and polarity [89]. Ji et al. [88] produced three biochars at 300, 500, and 700 °C with a heating rate of 5 °C/min. The decrease in H/C ratio from 1.08-0.24 when the biochar production temperature increased from 300-700 °C indicates an increase in aromaticity with temperature. The decreasing O/C ratios (0.49-0.26) reported for the same temperature increase indicates a reduction of the polarity with temperature increase. Biochars with lower H/C and O/C values usually exhibit a higher microporosity [90] and lower O/C value (lower polarity) generally results in higher CO_2 capture capacity [91]. The relationships between these ratios as a function of temperature and feedstock are represented in Table 2.3.

During the thermal conversion, volatiles evolve, and high-density aromatic rings are formed in the solid. The level of aromaticity relates to the level of fixed carbon in the biochar and that can be related to the amount of carbon sequestered from the biomass during its production [98]. Therefore, biochar is not only taking part in carbon sequestration during adsorption, but carbon sequestration also happens during the very production step of biochar [61]. Another important characteristic of biochar that affects its adsorption capacity is its surface area [99]. Creamer et al. [100] surface area analysis results of biochars produced at a temperature range of 300-600 °C from sugarcane baggase and hickory wood indicated that biochars

Table 2.3: Biochar atomic ratios with regards to the production conditions

Feedstock	Pyrolysis type	Temperature (°C)	Heating rate (°C/min)	Pyrolysis time (min)	H/C	O/C	Ref.
Moso bamboo	NM	300	NM	30	0.71	0.32	[92]
Moso bamboo	NM	400	NM	30	0.58	0.20	[92]
Moso bamboo	NM	500	NM	30	0.43	0.12	[92]
Moso bamboo	NM	600	NM	30	0.28	0.09	[92]
Moso bamboo	NM	700	NM	30	0.22	0.06	[92]
Bamboo	NM	700	15	NM	0.237	0.052	[93]
Spent coffee grounds	Slow	400	5	60	0.63	0.10	[94]
Spent coffee grounds	Slow	500	5	60	0.51	0.06	[94]
Spent coffee grounds	Slow	600	5	60	0.43	0.02	[94]
Date palm waste	NM	300	5	240	0.84	0.27	[95]
Date palm waste	NM	400	5	240	0.63	0.13	[95]
Date palm waste	NM	500	5	240	0.35	0.05	[95]
Date palm waste	NM	600	5	240	0.28	0.03	[95]
Date palm waste	NM	700	5	240	0.19	0.03	[95]
Date palm waste	NM	800	5	240	0.14	0.02	[95]
Rice husk	Slow	350	5	120	0.87	0.26	[96]
Rice husk	Fast	550	NM	NM	0.75	0.25	[96]
Rice husk	NM	400	5	30	0.882	0.228	[97]
Rice husk	NM	600	5	30	0.420	0.192	[97]
Rice husk	NM	800	5	30	0.197	0.152	[97]
Peach branch	Slow	550	5	120	0.46	0.11	[96]
Peach branch	Fast	550	NM	NM	0.57	0.19	[96]
Mixed wood sawdust	Fast	550	NM	NM	0.62	0.20	[96]
Corn stem	Slow	350	5	120	0.89	0.27	[96]
Corn stem	Slow	550	5	120	0.47	0.13	[96]
Yak manure	Slow	350	5	120	1.06	0.23	[96]
Yak manure	Slow	550	5	120	0.5	0.13	[96]
Eucalyptus softwood	Slow	350	5	120	0.81	0.26	[96]
Eucalyptus softwood	Slow	550	5	120	0.39	0.09	[96]
Walnut shell	Slow	350	5	120	0.78	0.27	[96]
Walnut shell	Slow	550	5	120	0.44	0.11	[96]
Wheat straw	Slow	350	5	120	0.86	0.25	[96]
Wheat straw	Slow	550	5	120	0.43	0.11	[96]
Pine wood	NM	400	5	30	0.658	0.203	[97]
Pine wood	NM	600	5	30	0.368	0.099	[97]
Pine wood	NM	800	5	30	0.206	0.027	[97]
Rice straw	NM	400	5	30	0.768	0.267	[97]
Rice straw	NM	600	5	30	0.409	0.168	[97]
Rice straw	NM	800	5	30	0.215	0.145	[97]

produced at a higher pyrolysis temperature show a higher surface area compared to those produced at lower temperatures. In a study by Kim et al. [72], surface areas of biochars produced from pitch pine wood chips showed low surface areas below 500 °C (2.9-4.8 m^2/g from 300-400 °C and 175.4 m^2/g at 500 °C). Biochars with higher surface areas are correlated to a higher capacity for CO_2 capture [100]. The pore volume of the biochar, specifically micropores, affects CO_2 adsorption capacity as higher pore volume means a more defined interconnected porous structure and subsequently more space for adsorption [101]. Porosity analysis showed pore volume increases with pyrolysis temperature from 500-900 °C in a study done by Zubbri et al. [101]. As for the feedstock, the biochars produced from woody biomass typically show higher surface area and a better-developed pore structure compared to the biochars from non-woody biomass such as manures [102, 103]. Table 2.4 is a summary of the surface areas of biochars produced at different temperatures and their CO_2 capacities.

Data in Table 2.4 shows that for most of the feedstocks, surface area of the biochar increases with the pyrolysis temperature. Furthermore, there is a positive correlation between the surface area and CO_2 adsorption capacity of biochars for all the feedstocks in the reported studies.

Although biochar surface area plays a vital role in its CO_2 adsorption capacity, the nature and density of surface functional groups are also important [100]. For instance, basic nitrogen functional groups such as amines are attractive for slightly acidic CO_2 molecules and can enhance CO_2 adsorption capacity [100, 109]. Func-

Table 2.4: Surface areas, pore volumes, and CO_2 capacities of biochars produced from different feedstocks at different temperatures

Feedstock	Temperature (°C)	Surface area (m^2/g)	Total Pore Volume (cm^3/g)	CO_2 capacity (mg/g)	Ref.
Rambutan peel	500	7.80	0.011	27.83	[101]
Rambutan peel	700	175.84	0.111	56.61	[101]
Rambutan peel	900	569.64	0.313	68.74	[101]
Hickory wood	300	0.10	NA	34.48	[100]
Hickory wood	450	12.90	NA	44.96	[100]
Hickory wood	600	401.00	NA	61.00	[100]
Sugarcane baggasse	300	5.20	NA	38.72	[100]
Sugarcane baggasse	450	13.60	NA	53.83	[100]
Sugarcane baggasse	600	388.30	NA	73.55	[100]
Perilla leaf	700	473.4	0.1	101.728	[104]
Soybean stover	700	420.3	0.2	31.108	[104]
Korean oak	400	270.8	0.1	26.268	[104]
Japanese oak	500	475.6	0.2	16.676	[104]
Spent coffee grounds	400	539	0.32	123.2	[94]
Spent coffee grounds	500	311	0.24	57.2	[94]
Spent coffee grounds	600	179	0.13	30.8	[94]
Pine sawdust	550	315.59	0.17	29.48	[105]
Pig manure	500	31.57	0.044	23.5	[106]
Wheat straw	500	20.20	0.041	34.4	[106]
Sewage sludge	500	10.12	0.022	18.2	[106]
Softwood	500	95.58	NA	105.6	[107]
Sargassum seaweed	400	5.8	0.03	16.28	[41] [a]
Sargassum seaweed	600	220.0	0.17	38.28	[41] [a]
Sargassum seaweed	800	291.8	0.24	46.2	[41] [a]
Enteromorpha seaweed	400	12	0.06	16.28	[41] [a]
Enteromorpha seaweed	600	30.6	0.09	21.56	[41] [a]
Enteromorpha seaweed	800	60.2	0.16	22.88	[41] [a]
Vine shoots	600	405	0.27	43.648	[108][b]
Wheat straw	500	459	0.324	39.38	[108][b]

[a] KOH activated biochar

[b] CO_2 activated biochar

tional groups are affected by the pyrolysis temperature [110]. Zhao et al. [111] compared the functional groups of four biochars produced from apple tree branches at 300, 400, 500, and 600 °C using FTIR. It was reported that O-H stretching at 3200-3500 cm^{-1} decreases with increases in temperature due to dehydration, while aromatic C=C (1440 cm^{-1}) and C-H (885 cm^{-1}) increase due to the increase in the formation of the aromatic rings. The C-O (1030-1110 cm^{-1}) group which is related to cellulose, hemicellulose, and lignin structure almost disappears as the temperature increases to 500-600 °C. In a study of Usman et al. [95], FTIR of biochars produced at different temperatures (300-800 °C) from date palm waste were compared with their feedstock. Similar to the previous study, the intense O-H stretch related to the bonded water and volatiles in the feedstock is reduced in the biochar as the production temperature is increased. The aliphatic C-H (2855-2920 cm^{-1}), found in cellulose and hemicellulose, was noticeable in the feedstock (due to cellulose and hemicellulose) but intensity was reduced in the biochar and at temperatures greater than 500 °C, completely disappeared due to complete degradation of hemicellulose/cellulose. Different types of acids (quinine, lactone, and carboxylic acids) from hemicellulose are associated with the C=O bond (1755 cm^{-1}). This peak was not present in any biochars. The peak attributed to carboxylic acids (-COOH) is located at 1600 cm^{-1}. The intensity of this peak decreased as the pyrolysis temperature increased. The peak at 1430 cm^{-1} (aromatic and aliphatic O-H) decreased in intensity as temperature increased and completely disappeared at 800 °C as a result of the

elimination of O-H containing aliphatic groups. Suliman et al. [112] studied eighteen biochars surface oxygenated functional groups (phenolic, lactone, and carboxylic) by Boehm titration. The biochars were produced from three different feedstocks: douglas fir wood, douglas fir bark, and hybrid poplar wood at six different temperatures ranging between 350-600 °C). The results suggest that oxygenated functional groups (C=O, -COOH, and O-H) decrease linearly with temperature increase. Of the three feedstocks, douglas fir wood had the highest quantity of carboxylic groups. The basic functional groups (e.g., C=O (attached to amides) and C=N [113]) increased with temperature. Ash content of the biochar controls the fraction of the basic functional groups; biochars produced from hybrid poplar wood with the highest ash content had the highest portion of basic functional groups, while douglas fir wood biochars had the lowest ash and basic functional groups. Another common way to produce biochar is gasification [42, 114]. Gasification uses an oxidizing agent in biochar production [115]. This results in different biochar trends and properties.

2.2.2 Gasification

Gasification is a thermochemical process that converts biomass to a high heating value gaseous phase (syngas) and biochar [6]. Unlike pyrolysis, gasification requires a gasifying agent (oxygen, steam, or air). In contrast to combustion, where bonds are broken to release energy, gasification stores energy in the bonds of the compounds released in the gas phase [8]. Gasification has four stages: drying, pyrolysis, partial

oxidation of the gases/vapors/chars, and gasification of the previous stage products [8, 116]. The oxidation is exothermic, and the other three stages are endothermic. A summary of biochar yields at different gasification conditions and their atomic ratios are presented in Table 2.5.

Biochars produced from gasification typically have lower surface areas and pore volumes compared to pyrolysis-produced biochars. This is due to the high temperature of gasification, which induces pore blockage by ash melting and pore destruction and collapse. Although if oxygen or steam are used as the gasifying agent, they can somehow mimic the effect of physical activation and mitigate pore collapse. As such, the surface area and pore volume of gasification biochar might then be more comparable with that of the pyrolysis biochar [115]. Tay et al. [117] studied the effects that the gasifying agents have on the produced biochar by comparing the biochars produced at 800 °C using three different gasifying agents: steam, O_2/CO_2, and steam/CO_2/O_2 from brown coal. Steam is a reducing agent and CO_2 and O_2 are oxidizers. The results suggested that the ratio of the small to large aromatic groups in biochar decreased when steam was used as the gasifying agent. Liu et al. [118] studied the effect of the gasifying agents (steam, CO_2, and steam/CO_2) on biochar pore structure. For this study, biochars from mallee wood were produced at different temperatures (700, 800, and 900 °C). Micropore and mesopore formation occurred at lower temperatures (700 °C) when steam was used as the gasifying agent, while when CO_2 was used, the pore formation was negligible at the same temperature

Table 2.5: Yields and atomic ratios of biochars produced from gasification

Feedstock	Temperature (°C)	Gasification agent	Biochar yield(wt%)	H/C	O/C	Ref.
Woodchip/sawdust/wood shavings	850	Air	1.4	0.19	0.04	[119]
Woodchip/sawdust/wood shavings	836	Air/steam	3.7	0.09	0.02	[119]
Poultry	580-680	Air	15.6	0.048	0.01	[120]
Cotton residues	764	Air	14	0.004	0.117	[121]
Conifer wood	1000	NA	10	0.47	NA	[122]
Wood chips	800-900	Air	13.9	0.012	0.16	[123]
Wood chips/chicken manure	800-900	Air	7.2	0.029	0.37	[123]
Beech wood	700	CO_2	12.77	NA	NA	[124]
Beech wood	800	CO_2	7.26	NA	NA	[124]
Beech wood	700	steam	12.84	NA	NA	[124]
Beech wood	800	steam	5.92	NA	NA	[124]
Sawdust	750	Air	NA	0.011	0.016	[125]
Sawdust	850	Air	NA	0.014	0.056	[125]

(700 °C). In addition, the surface area of the biochar produced with steam/CO_2 as the gasifying agent was higher than the other two scenarios at 800 °C. The average diameter of the micropores was larger when steam was used as the gasifying agent, showing that steam can assist in micropore enlargement.

An additional physical chemical activation stage can improve biochar pore density, surface area, and properties in order to achieve a higher CO_2 adsorption capacity [126]. Dissanayake et al. [42] examined the activation effect on two biochars CO_2 adsorption capacities. The two biochars were produced from 100% wood chips and 70% wood chips/ 30% chicken manure at 800-900 °C, respectively. Biochars were

then activated with KOH with a 1:1 ratio between the biochar and KOH. Some of the activated biochars were further activated with an additional activation step using CO_2 at 550 °C for 1 hour. The surface areas, pore volumes, CO_2 adsorption capacities of the activated and non-activated biochars are reported in Table 2.6. The results suggested that the capacities of the biochars were significantly improved after the activation owing to the notable increase of the surface areas and micropore volume of the activated biochars. However, a balance must be struck between additional processing steps (which would increase energy demands and potentially greenhouse gas (GHG) emissions) and any marginal increase in adsorption capacity. In addition, harsh or toxic chemicals used in activation can reduce the overall environmental sustainability of the activation process.

In general, slow pyrolysis biochar has a higher aromaticity compared to fast pyrolysis and gasification chars due to longer solid residence time [127]. FTIR analysis of biochars from slow pyrolysis, fast pyrolysis and gasification has shown that fast pyrolysis biochar has the highest amount of oxygen-containing functional groups compared to slow pyrolysis and gasification biochars [128]. Comparison of gasification and pyrolysis biochars FTIR spectra also shows that gasification biochars have less structured surface functionalities compared to pyrolysis biochars with a lower number of visible peaks [128, 129]. In a study by Brewer et al. [127], the FTIR spectra of switchgrass feedstock were compared to the biochars produced from this feedstock via slow and fast pyrolysis (both at 500 °C) and gasification (at 760 °C).

It was noted that the O-H stretch at around 3400 cm^{-1} had completely disappeared in the gasification biochar while it was visible in all the other spectra. The peaks notable in the gasification biochars, as well as other biochars, were 3000-2860 cm^{-1} for aliphatic C-H and the one around 3060 cm^{-1} for aromatic C-H. The peaks around 1590 and 1515 cm^{-1} attributed to aromatic rings were also noted.

The oxidation results in higher ash content and pH and lower carbon content compared to pyrolysis biochars. This is due to carbon conversion to CO_2 with oxygen present [115]. Azargohar et al. [130] compared gasification and pyrolysis biochars from canola hall and canola meal pellet and observed gasification biochars have the same level of O/C as the pyrolysis biochars but higher H/C (indicative of aromaticity). Some gasification biochar surface areas and CO_2 capacities are summarized in Table 2.6.

Another thermochemical conversion method where the primary product is a solid carbon material is hydrothermal carbonization (HTC). HTC is performed in the presence of water [131] and produces hydrochar, an aqueous organic mixture, and small amounts of gas [132]. Hydrothermal carbonization is performed at temperatures lower than that of pyrolysis ($\sim$ 150-250 °C) [133], and high pressures (up to 50 bars) [134] for a reaction time that can vary from 1 to 16 hours [131]. The properties of the produced hydrochar are dependent on the temperature, pressure, reaction time, and biomass/water ratio of the hydrothermal process [131].

The main advantage of hydrothermal carbonization compared to the other men-

Table 2.6: Gasification biochar CO_2 capture performance

Feedstock	Temperature (°C)	Gasification agent	Surface area m^2/g)	Total Pore Volume (cm^3/g)	CO_2 capacity (mg/g)	Ref.
Sawdust	450	Air	8.76	0.015	19.7	[125]
Sawdust	450	Air	0.61	0.009	19.1	[125][a]
Sawdust	750	Air	11.36	0.016	45.2	[125]
Sawdust	750	Air	0.15	0.005	39.7	[125][a]
Sawdust	850	Air	182.04	0.0036	47.5	[125]
Sawdust	850	Air	3.17	0.007	44.8	[125][a]
Wood chips	700-1500	NM	125.7	0.07	84.5	[42]
Wood chips	700-1500	NM	1281.6	0.71	115.5	[42][b]
Wood chips	700-1500	NM	1012.6	0.56	113.8	[42][c]
Wood chips/chicken manure (70/30)	700-1500	NM	255.6	0.15	70.5	[42]
Wood chips/chicken manure (70/30)	700-1500	NM	1408.8	0.83	128.5	[42][b]
Wood chips/chicken manure (70/30)	700-1500	NM	1403.9	0.85	107.3	[42][c]

[a] Amine treated

[b] KOH activated

[c] KOH and CO_2 activated

tioned thermochemical processes is that it does not require a drying step which can be both cost and energy-effective, especially when the biomass has a high moisture content [131, 132]. Some studies indicate up to 50% lower energy consumption compared to pyrolysis for biomass with over 50% moisture level [134]. The disadvantage of the hydrochars versus biochars is that they have notably lower surface area compared to biochars and may have limited application in adsorption without an activation step [133]. There is limited work on hydrochars and gas adsorption, as such, this review was limited to biochars.

Biochar properties, and hence CO_2 adsorption capacity, are driven by its feedstock and production conditions; however, the adsorption is also a function of the gas matrix or competing/inhibiting gases in the gas mixture. In the next section, the effect of biochar CO_2 adsorption from gas mixtures is studied.

2.3 Biochar CO_2 adsorption in gas mixtures

The bulk of CO_2 removal from gas streams have focused on adsorption of CO_2 from pure CO_2 or mixed CO_2 and N_2 streams [33, 105, 107, 135]. However, flue gas from power plants and other industries is a mixture of different gases; therefore, studying the effect of these components on CO_2 adsorption is required to determine the feasibility of an adsorbent [136]. Typical flue gas from a coal-fired power plant is 68-77% N_2, 10-16% CO_2, 5-10% H_2O, 2-5% O_2, and small traces of NOx and SOx gases [137, 138]. NOx and SOx in the gas flow can react with or adsorb on the

adsorption sites reducing the number of the sites available for the adsorption of CO_2 molecules [50]. As noted above, syngas, from gasification, is a mixture of H_2, CO, CO_2, CH_4, N_2, and other light hydrocarbons [139] (Table 2.4). Biogas produced during anaerobic digestion of organic materials in sewage digesters is 55-65% CH_4, 35-45% CO_2, <1% N_2 and traces of O_2, H_2S, and aromatics [140]. The conventional solution proposed for impurities is pre-treatment prior to CO_2 adsorption stage [50].

Sethupathi et al. [104] investigated the adsorption of CO_2, H_2S, and CH_4 using four different biochars in pure and gas mixtures for CH_4 production. Biochars were produced from perilla leaf, soybean stover, Korean oak, and Japanese oak. The perilla and soybean biochars were produced at 700 °C with a heating rate of 7 °C/min while the oak biochars were produced at 400 °C (Korean) and 500 °C (Japanese) (purchased as commercial biochars). The surface areas for the perilla leaf, soybean stover, and Japanese oak were between 420-476 m^2/g, while the Korean oak biochar was 270.8 m^2/g. Adsorption experiments were performed in a continuous fixed bed. The gas mixture was 0.3% H_2S, 40% CO_2, and 59.7% CH_4 at a relative humidity of 20%. The biochars showed negligible adsorption of CH_4 even in the absence of the other gases. Pore sizes of the biochars in this study were estimated to be larger than 1 nm, allowing CH_4 molecules to slip. Based on this result, studying the adsorbate molecule sizes and biochar pore size distribution will be useful as it can inform the potential of molecules slipping through biochar pores.

All four biochars adsorbed CO_2 and H_2S well. The adsorption capacities were

2.312, 0.707, 0.597, and 0.379 mmol/g for pure CO_2 for perilla leaf, soybean stover, Korean oak, and Japanese oak, respectively. Perilla leaf and soybean stover biochars contained more nitrogen functional groups compared to the oak biochars; hence, the higher adsorption of pure CO_2. The CO_2 capacities decreased by 90-95% when the gas mixture was used. This was due to adsorption competition between CO_2 and H_2S, where H_2S was preferred. Acidic gases such as H_2S can inhibit CO_2 adsorption on the biochar surface. However, the extent that the CO_2 adsorption capacity may decrease for each individual biochar is certainly different, and that needs to be considered if the mixed gas contains gases such as H_2S.

Ding et al. [41] produced non-activated and activated biochars (using KOH) from seaweed biomass (sargassum and enteromorpha) at 400, 600, and 800 °C in a tubular furnace for two hours. The biomass powder and solid KOH were mixed prior to entering the furnace for a single-step activation. Activated sargassum seaweed had a surface area 11 times higher than the non-activated form. The surface areas for the activated biochars from sargassum seaweed produced at 400-800 °C and 1:1 ratio between KOH and biomass varied from 5.8-291.8 m^2/g and 12.0-60.2 m^2/g for enteromorpha seaweed biochars. The CO_2 adsorption experiments were performed in a fixed bed column. Biochars had a higher CO_2 adsorption capacity when operating at lower temperatures (25 °C > 50 °C > 75 °C > 100 °C) and higher inlet CO_2 concentration (3% < 8% < 12% <18%). The maximum CO_2 capacity was achieved using the activated biochar produced at 800 °C and with inlet CO_2 concentration

of 18% (88% N_2) (max capacity of 1.05 mmol/g for sargassum and 0.52 mmol/g for enteromorpha). The biochars were then tested with a gas mixture of O_2, SO_2, or NO. The O_2 was varied from 0-8%. NO varied from 0-800 ppm and 0-1500 ppm for SO_2. The O_2 and NO had little to no effect on CO_2 adsorption capacity. However, SO_2 in the gas decreased CO_2 adsorption capacity by approximately 3.8% for sargassum biochar and 9.6% for enteromorpha. This result agrees with the results of the previous article discussed as the competition over the adsorption sites was better noted between the acidic gases, CO_2 and SO_2. This could also explain the lack of impact of NO on CO_2 adsorption capacity since NO is not an acidic gas. A summary of CO_2 adsorption from gas mixtures by biochar is presented in Table 2.7.

Table 2.7: Biochar CO_2 adsorption from gas mixtures

Feedstock	Temperature (°C)	Gas Mixture	Results	Ref.
Perilla leaf	700	$CO_2/H_2S/CH_4$	CO_2 adsorption capacity decreased 90-95% due to H_2S and CO_2 competition over active sites	[104]
Soybean stover	700	$CO_2/H_2S/CH_4$	CO_2 adsorption capacity decreased 90-95% due to H_2S and CO_2 competition over active sites	[104]
Korean oak	400	$CO_2/H_2S/CH_4$	CO_2 adsorption capacity decreased 90-95% due to H_2S and CO_2 competition over active sites	[104]
Japanese	500	$CO_2/H_2S/CH_4$	CO_2 adsorption capacity decreased 90-95% due to H_2S and CO_2 competition over active sites	[104]
Sargassum seaweed[a]	800	$CO_2/N_2/O_2$	O_2 did not have a notable impact on CO_2 adsorption capacity	[41]
Sargassum seaweed[a]	800	$CO_2/N_2/NO$	NO did not have a notable impact on CO_2 adsorption capacity	[41]
Sargassum seaweed[a]	800	$CO_2/N_2/SO_2$	CO_2 adsorption capacity decreased around 3.8%	[41]
Enteromorpha seaweed[a]	800	$CO_2/N_2/O_2$	O_2 did not have a notable impact on CO_2 adsorption capacity	[41]
Enteromorpha seaweed[a]	800	$CO_2/N_2/NO$	NO did not have a notable impact on CO_2 adsorption capacity	[41]
Enteromorpha seaweed[a]	800	$CO_2/N_2/SO_2$	CO_2 adsorption capacity decreased around 9.6%	[41]

[a] KOH activated biochar

Although there are limited studies of CO_2/mixed gas adsorption, there are studies of biochar adsorption of gases other than CO_2. These studies are useful in that they can identify the properties of biochar, which may indicate an affinity for gases that may be present in CO_2 mixed gas streams. Khan et al. [141] investigated different types of biochars in the adsorption of benzene from the air. The results from this study suggested that KOH-activated biochar from mixed feed gasification showed performance as good as that of granular activated carbon. Ro et al. [142] examined NH_3 adsorption using red oak and chicken litter biochars (steam-activated and non-activated) produced at different temperatures (250-500 °C) and residence times (1.3-2.1 minutes). Steam activation enhanced biochar surface area but had little impact on NH_3 adsorption. Activation with phosphoric acid did improve biochar NH_3 adsorption confirming that surface acidic oxygen functional groups are the controlling factor in NH_3 adsorption rather than the adsorbent surface area. In addition, biochar adsorption capacity of NH_3 was proved to be comparable to that of the common adsorbents.

It was already discussed that H_2S had shown competition with CO_2 over biochar adsorption sites in one of the articles mentioned earlier. There is published work studying biochars for H_2S adsorption [143–145]. Shang et al. [144] produced biochar from three different forestry wastes (camphor, rice hull, and bamboo) in a furnace at 400 °C with a heating rate of 10 °C/min and residence time of 5 hours. The biochars were then used in a column to adsorb H_2S from a H_2S and H_2O mixture.

The breakthrough capacity of the biochars were compared with that of a commercial activated carbon and the results suggested that the biochars showed a higher H_2S adsorption due to their higher fraction of oxygen-containing functional groups. Among the biochars, rice hull biochar had the highest pH and showed the highest H_2S capacity (382.7 mg/g). Sun et al. [143] produced biochar from potato peel wastes by fast pyrolysis (5 solid minutes residence time) at 500 °C. A H_2S capacity of 53 mg/g was reported for this biochar. The dynamic experiments were conducted both in dry and wet conditions. The H_2S breakthrough time was higher for the wet experiment indicating H_2S adsorption was enhanced in wet condition. Ma et al. [145] produced sawdust biochars in a furnace at different temperatures (600-900 °C) with residence time of 2 hours. They examined the activated (with urea phosphate) and non-activated biochars H_2S adsorption capacities. The non-activated biochar showed a low H_2S adsorption capacity (0.24 mg/g) while activation enhanced the adsorption, increasing it to 54.8 mg/g for activated biochar produced at 700 °C. The results from these articles suggest that higher pH and the existence of some functional groups, such as oxygen-containing ones, would result in higher adsorption of H_2S. This is expected to be the same for CO_2 as well since both gases have shown acidic nature and competition over the same adsorption sites.

Another gas that showed competition with CO_2 over biochar adsorption sites in the discussed articles was SO_2. A study by Shao et al. [146] examined biochar adsorption of pure SO_2. The corncobs biochar from this study was produced at 600 °C

with 60 minutes residence time (10 °C/min) and showed a 57.8 mg/g capacity for SO_2. The capacity increased to 156.2 mg/g after the biochar was impregnated with Methyl diethanolamine (MDEA). Braghiroli et al. [147] produced biochars from black spruce and white birch by fast pyrolysis at 454 °C. The biochars were then activated by either KOH, CO_2, or steam. Higher SO_2 capacity was reported for the steam-activated white birch biochar (76.9 mg/g), and in general, activated biochars showed higher capacities than the non-activated biochars. While the gas stream composition varies considerably, all these streams contain water and can impact biochar performance. However, the bulk of the work on the impact of moisture is in adsorption and activated carbon.

2.4 Biochar gas adsorption in the presence of water vapor

For gas streams containing water vapor, such as post-combustion flue gas, carbon-based materials may be a better adsorbent compared to common adsorbents, such as zeolite, due to their rather hydrophobic surfaces. Other than hydrophobicity and high stability in water containing gases, characteristics such as lower cost and lower energy requirements for regeneration make the carbonaceous materials an attractive choice of adsorbent [148–150]. However, water vapor can adversely affect CO_2 adsorption and potentially complicate regeneration (desorption). Typically, water is removed

prior to adsorption, which adds to operational and capital costs [137, 148, 151]. As noted above, carbon adsorbents contain both hydrophobic and hydrophilic sites. Unlike water adsorption, which mainly occurs on hydrophilic sites by hydrogen bonding, CO_2 adsorption can take place on both hydrophobic and hydrophilic sites.

Water desorption from carbon is comparatively easier than other adsorbents and can be accomplished by lowering its partial pressure [151]. Water molecules can form clusters after being adsorbed on biochar polar hydrophilic sites and contribute to micropore filling within the adsorbent, potentially completely occupying the micropores. Therefore, investigating the impact of humidity influence on the adsorption of specific gases is essential as the water can compete with the target gas [151–153].

The biochar surface functionality in terms of hydrophobicity and hydrophilicity is a determining factor in water adsorption. Although there are several studies in this area, there is conflicting data on how biochar surface hydrophobicity changes with feedstock type and operating conditions. There are several studies proposing biochar hydrophobicity decreases with an increase in production temperature [153–155], the details of which are discussed below.

Gray et al. [153] studied biochar's hydrophobicity impact on water uptake as a function of biomass type (hazelnut shells and Douglas fir chips) and temperature (370, 500, and 620 °C). Specific surface areas for the hazelnut shell biochars varied from 58.7-211 m^2/g, and 153-280 m^2/g for the douglas fir. The biochar porosities varied from 62.5-69.2% (volume fraction) for the hazelnut shell biochar and

from 83-85.1% for the fir. Production temperature impacted surface hydrophobicity. The low-temperature biochars from both feedstocks showed lower water uptake (higher hydrophobicity). The mean water uptake increased with temperature from 53.8-64.1 vol.% for hazelnut biochar and from 71.5-78.8 vol.% for fir biochars. The decrease in aliphatic functional groups due to volatilization at higher temperatures was proposed as the primary reason for the hydrophobicity reduction. Longer resident times and smaller particle sizes can decrease the hydrophobicity, again through aliphatic functional groups volatilization.

Kameyama et al. [155] studied the hydrophobic nature of 21 different biochars produced from cedar wood chips, cypress wood chips, moso bamboo, rice husk, sugarcane bagasse, poultry manure, and agricultural wastewater sludge at different temperatures and a residence time of 2 hours. Biochars produced at 400 °C were found to be extremely or strongly hydrophobic, while biochars produced at 600 °C and 800 °C were characterized as either hydrophobic or hydrophilic. Both of the mentioned articles pointed out that the hydrophobicity of biochar is inversely correlated with its pyrolysis temperature due to the loss of aliphatic functional groups at higher production temperatures.

Contrary to the studies by Gray et al. and Kameyama et al. [153, 155], there are some other published works that have shown different results, where the hydrophobicity increased with an increase in production temperature. These studies measure hydrophobicity using atomic ratios such as H/C, O/C, and (O+N)/C of biochars

[89, 156]. As mentioned before, atomic ratios are widely used in biochar stability studies as well [130, 157, 158]. Looking at the H/C and O/C of biochars presented in Table 2.3, it can be concluded that raising pyrolysis temperature would result in the reduction of both ratios [159] Ahmad et al. [89] suggested that there is a decrease in char aromaticity (H/C) and polarity (O/C and (O+N)/C) with an increase in pyrolysis temperature, which means a subsequent increase in hydrophobicity. This is due to the loss of the polar functional groups, which are attractive sites for water molecules to form strong hydrogen bonds. Therefore, loss of oxygen from the biochar during the production process results in higher hydrophobicity. Figure 2.1 shows biochar CO_2 adsorption capacities for different biochars with different O/C atomic ratios. It can be observed that generally, with the decrease of O/C atomic ratio with the increase of production temperature for a specific biochar, the CO_2 adsorption would increase.

Biochar hydrophobicity can be increased post-production using heat treatment in either hydrogen or inert atmospheres. This removes hydrophilic functional groups from the surface [160]. Chemical activation methods can also be used for increasing hydrophobicity by removing certain functional groups. For instance, acid activation with nitric or hydrochloric acid at low temperatures can produce strong acidic groups such as carboxylic acids, thereby increasing the hydrophobicity of the surface. However, this treatment would negatively impact the adsorbent affinity toward CO_2 as CO_2 molecules are slightly acidic and are more attracted to basic surfaces [161].

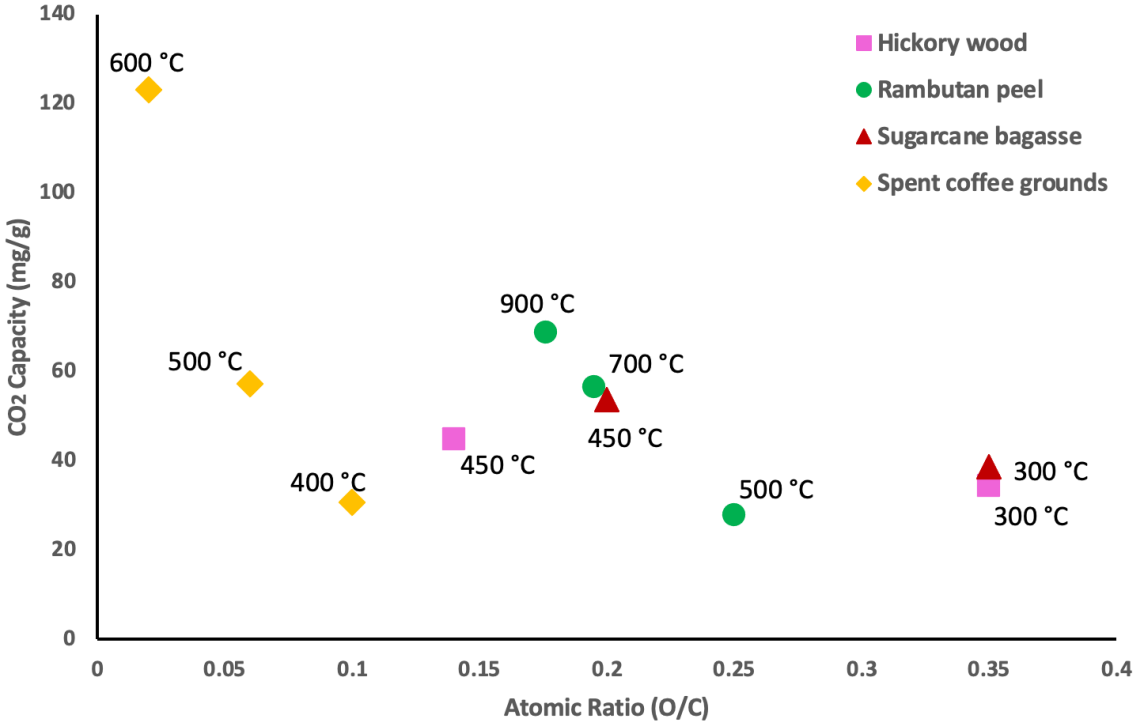

Figure 2.1: CO_2 adsorption capacities for biochars with different O/C atomic ratios. Data were obtained from [94, 100, 101]

Wang et al. [162] did a series of experiments on CO_2 and CH_4 adsorption at 275 K using activated carbon made from bamboo chips (produced at 700 °C in 4 hours) comparing adsorption in dry conditions and in the presence of water. Unlike CH_4, water did not affect CO_2 adsorption capacity (36 mmol/g). The only notable difference was an inflection point appearing in the CO_2 adsorption isotherm curve in wet experiments due to CO_2 condensation and reaction between water and CO_2 to form HCO_3^-. Therefore, for some adsorbents, CO_2 adsorption capacity might stay the same in dry and wet conditions, but the shape of the isotherm curve may be different for the wet condition compared to the dry one.

Plaza et al. [163] evaluated the presence of water vapor on CO_2 adsorption from post-combustion flue gas under dry and wet conditions (65% humidity) using biochar produced from olive stones. The breakthrough curves were evaluated to measure the effect of humidity on the gas adsorption process. In the first 11 minutes of the experiment, the CO_2 capacity was 1.1 mmol/g which is approximately the same capacity reported for the adsorption from pure CO_2 stream. The H_2O adsorption capacity was 0.2 mmol/g which is approximately 3-4% of the capacity reported for the pure H_2O adsorption. Therefore, the water vapor does not impact the CO_2 adsorption capacity if the adsorption-desorption cycles are short enough. This is due to the slower adsorption kinetics of H_2O. However, if the process continues for a longer time, H_2O can hinder CO_2 adsorption by displacing adsorbed CO_2 molecules. Biochars used in this set of experiments could regain full adsorption capacity after

regeneration. In subsequent work by Plaza et al. [164], a feed containing 84% N_2, 14% CO_2, and 2% H_2O to the same biochars showed CO_2 breakthrough time does not change in the presence of H_2O when the adsorbent is initially completely free from any CO_2 and H_2O. Again, this is due to slower adsorption kinetics of H_2O. The breakthrough time was 4-5 minutes for CO_2 and 127 minutes for H_2O. The CO_2 concentration in the feed was 7 times higher than H_2O and the adsorbent pure H_2O capacity is approximately 11 times higher than its capacity for pure CO_2. In order to study the effect of the water adsorbed, a separate set of experiments were done in which the adsorbents were saturated with H_2O prior to the adsorption process. These experiments showed that the CO_2 breakthrough time decreases when the adsorbent is saturated with water relative to unsaturated biochar. The decrease in capacity depends on the amount of water adsorbed on the adsorbent at the beginning of the process. The decrease in the capacity depends on the amount of water adsorbed at the beginning of the process. CO_2 adsorption can be reduced up to 64% if the gas stream has a relative humidity of approximately 95%.

Manyà et al. [108] performed adsorption experiments in dry and humid conditions for biochars produced from vine shoots (at 600 °C) and wheat straw pellets (at 500 °C). The heating rate for the pyrolysis process was 5 °C/min and the residence time was 60 minutes (slow pyrolysis). The biochars were physically activated using CO_2 at 800 °C and atmospheric pressure. The dry experiment was performed with 13.75-14.25% CO_2 feed (balance N_2). For the wet experiments, 0.0226 cm^3/min

of water vapor was added to the stream to achieve a relative humidity of 100% (11.2 vol.% H_2O). The results from dynamic experiments suggest that vine biochar showed similar results in both dry and wet conditions, whereas the wheat straw biochar showed a decrease in CO_2 uptake in wet conditions compared to the dry. The CO_2 capacity for the vine biochars at 50 °C and dry conditions was 0.543 mmol/g, relatively the same as wet conditions at 0.542 mmol/g. The wheat straw biochar capacity was 0.624 mmol/g for the dry condition and decreased to 0.486 mmol/g when water vapor was added. Comparing adsorbed CO_2 during ten cycles of adsorption-desorption experiments for the wheat straw biochar showed that more H_2O was adsorbed on the adsorbent during the cycles; thus, less CO_2 adsorption occurred. The amount of CO_2 adsorption remained the same after a few cycles for wheat straw biochar, while it had little impact on the vine shoots biochar. The differences in experiments with these two biochars compared to carbon-based adsorbents were because of pore size distribution, pore connectivity, and surface functional groups. Biochars with a hierarchical structure and high fraction of ultra-micropore volume showed better CO_2 adsorption capability. The differences in the impact of water were related to polar sites and oxygen-containing functional groups such as carboxylic groups. The adsorbed H_2O molecules were able to come together later, form a cluster, and move within the adsorbent to fill the pores. From this set of experiments, it can be concluded that biochar selectivity between CO_2 and N_2 does not change in wet conditions. The presence of water in the feed or in the adsorbent material can lower

the amount of bed available for adsorption.

Sadasivam et al. [165] studied wood pellet biochars produced from gasification adsorption of CH_4 from biogas under dry and wet conditions (50% and 75% of the packed column water holding capacity). The biochars were produced in an updraft gasifier at 500 °C. The feed gas was 5% CH_4, 5% CO_2, and 90% N_2. The adsorption was compared with granular activated carbon. Although there were decreases in both of the adsorbents CH_4 adsorption capacities as the water increased, the reduction was higher for the granular activated carbon. The wood pellet biochar capacity decreased from 0.00542 to 0.00213 mmol/g as the moisture level increased from 0% to 70%, while for the activated carbon, the capacity decreased from 0.00546 to 0.000644 mmol/g. It can be concluded that water molecules establish stronger bonds with oxygenated sites on activated carbon compared to the biochar sites. Some of the oxygenated functional groups on biochar surface are phenolic, lactonic, carboxylic, hydroxyl, and carbonyl groups [166].

La et al. [167] used mixtures of biochar and compost as an adsorbent for CH_4 under both dry and humid conditions. Sawdust biochar was produced at 550 °C over approximately 30 minutes. The adsorption experiments for dry and humid conditions (15% and 30% saturation) were performed in both a batch and a fixed-packed column using different ratios of biochar and compost. Pure CH_4 (99% (v/v)) was used. A fraction of the adsorbent mixture was mixed with water to reach the desired water-holding capacity. Batch experiments showed the highest adsorption

capacity at 100% biochar and dry conditions (17.10 mg/g).

Removing CO_2 from some gas mixtures may be used to purify certain gases. For instance, syngas from gasification contains valuable H_2 among other gases. Removing CO_2 can work in the purification of H_2. If biochar, which is the by-product of gasification, can be used for this purpose, it can work as a closed-loop system. The CO_2 adsorption performance of some biochars and activated carbons in wet conditions are summarized in Table 2.8.

Table 2.8: Biochar and activated carbon performance in wet conditions

Adsorbent	RH[a](%)	CO_2 capacity (mg/g)		Impact of water vapor presence	Ref.
		dry	wet		
Air-activated olive stone biochar	65	48.4	48.4	No differences were observed between dry and wet conditions for CO_2 adsorption in short time scale (around 11 mins) (due to H_2O delayed adsorption)	[163]
Pine sawdust AC [b]	55	91.52	61.16	Decreased CO_2 capacity in wet condition compared to the dry condition	[148]
CO_2-activated vine shoot biochars	100	23.892	23.848	CO_2 adsorption capacity was not impacted	[108]
CO_2-activated wheat straw biochars	100	27.456	21.384	Decreased CO_2 capacity in wet condition compared to the dry condition	[108]
Activated carbon fibers (ACFs)	55	30.170	30.193	CO_2 adsorption capacity was not impacted	[168]
KOH-activated ACFs	55	36.68	36.784	CO_2 adsorption capacity was not impacted	[168]
TEPA[c]functionalized ACFs	55	22.067	22.069	CO_2 adsorption capacity was not impacted	[168]

[a] Relative humidity

[b] Activated carbon

[c] Tetraethylenepentamine

2.5 H_2 Separation Using Biochar

Production of hydrogen from biomass is a growing research area [169–172] The two most conventional methods to produce H_2 from biomass are thermochemical (gasification) and biological. [173]. Gasification offers the synergy of producing biochar that could remove CO_2 and other gases to treat the syngas and recover H_2 [172]. To favor the production of H_2, a mixture of air and steam has been proposed as the gasifying agent. Pure steam gasification produces higher amounts of H_2 but is endothermic and requires energy. Air gasification produces less H_2 but is exothermic [173]. H_2 gas can also be produced from bio-oil, a by-product of gasification and the main product of pyrolysis, through processes such as steam reforming [173, 174]. Chemical looping gasification can also produce H_2 from biomass through a series of reduction and oxidation reactions occurring over a metal oxide [175]. Hu et al. [176] used chemical looping gasification to produce H_2 from biochars produced from camellia shell at 550 °C by using Fe/Ca as their oxygen carrier.

Regardless of the method used, pure H_2 is not produced but rather a gas mixture (syngas) of CO, CO_2, CH_4, H_2S, N_2, and H_2O. The water-gas shift reaction converts CO to CO_2 and as such the focus is on the separation of H_2 and CO_2 [177]. Shamsudin et al. [55] studied H_2 purification from a mixture of H_2 and CO_2 stream using activated carbon from dried palm kernel shell. The carbon was produced at 550 °C for 1 hour under a pure 200 mL/min N_2 stream. It was then chemically activated using cerium chloride at 750 °C for 1 hour in a N_2 atmosphere. The surface area of

the adsorbent was 698 m^2/g. Breakthrough curve analysis was done by adsorption experiment with 100 mL/min feed stream (85% H_2 and 15% CO_2). The breakthrough for H_2 was 4 and the bed saturation occurred at 10 minutes, while CO_2 breakthrough occurred at 21 minutes and saturation at 45 minutes. The gas produced was 100% H_2 with 88.43% recovery using a pressure swing adsorption unit.

Lopes et al. [178] used a fixed bed adsorption system to separate H_2 from binary mixtures of H_2 and CO_2, a ternary mixture of 70% H_2, 26% CO_2, and 4% CO, and five component feed streams of 79% H_2, 17% CO_2, 1.2% CO, 2.1% CH_4, and 0.7% N_2). A commercial activated carbon was physically activated to enhance its microporosity. The binary experiments were performed with 10%, 30%, and 80% CO_2 (balanced with H_2) at 50 °C and 5 bar and a total flow rate of 50 mL/s. As H_2 is not well adsorbed, the breakthrough time was fast.

The order of breakthrough times from lowest to highest was N_2, CO, CH_4, and CO_2. A ten PSA (pressure swing adsorption) cycle adsorption was performed at 30 °C and 5 bar with a flow rate of 50 mL/s. The resulting H_2 purity was 99.981% with a recovery of 81.6%. The Virial model extension for mixtures was used to predict adsorption and indicated increasing the pressure of the feed stream would increase H_2 production rate from 101 mol kg^{-1} day^{-1} to 160 mol kg^{-1} day^{-1} for the current unit without altering the high H_2 purity (with recovery higher than 75%). The carbon-based adsorbents in both of the mentioned articles showed a low affinity for H_2 gas. H_2 broke through fastest among all components in the gas stream resulting in a high

purity H_2 gas stream (above 99%). This shows the great potential of carbon-based materials in purifying H_2.

Delgado et al. [179] used a model simulation to predict the ability of a two-layer adsorption bed to purify H_2 from a gas mixture containing CO_2, CO, CH_4, and H_2. Adsorbents used in this research were BPL activated carbon (BPL 4X10) and 13X zeolite. It was assumed that the water in the steam reforming process would be removed in the initial layer of hydrophilic adsorbent (silica gel), the activated carbon would adsorb the CO_2 molecules, and the zeolite layer would separate the lighter CO and CH_4. The simulated feed gas had 76% H_2, 4% CO, 17% CO_2, 3% CH_4 at temperature of 25 °C. The simulations indicate a H_2 purity of 99.99% with 90% recovery. Both adsorbents showed the highest affinity toward CO_2 and the lowest affinity toward H_2. BPL activated carbon showed a higher affinity toward CH_4 than CO, while the 13X zeolite showed a higher affinity to CO. This was due to the strong electrostatic force between Na cations in zeolites and CO molecules. Yavary et al. [180] performed adsorption experiments for the same four gases with two adsorbents (activated carbon and 5A zeolite) separately to design a two-layer pressure swing adsorption system. The experiments were done at different pressures and temperatures, and the results pointed to the same affinity order as the study by Delgado et al. [179]. The activated carbon layer would ideally adsorb all the CO_2 before the gas stream reaches the zeolite layer as the zeolite affinity for CO_2 at lower pressures is high. This would result in CO_2 occupying zeolite activated sites and

hindering CO and CH_4 from being adsorbed.

Situmorang et al. [173] proposed producing H_2 from both the bio-oil and biochar (from pyrolysis of woody biomass in an auger reactor at 500 °C). H_2 was produced using a combination of catalytic steam reforming of the bio-oil and a chemical looping using biochar. The simulation of these processes predicted 6.9 kg/h production of H_2 with a 100 kg/h inlet biomass rate. Jordal et al. [181] studied the recovery of H_2 from coal gasification syngas which has gone through a water-shift reaction. The water-gas shift reaction converts CO to CO_2 and is crucial in this H_2 recovery process as CO molecules can adsorb on the Pd-alloy membrane sites, which will subsequently result in H_2 reduced permeability in the membrane. This process was followed by a low-temperature condensation process for capturing CO_2. The simulated membranes in this study showed recovery of 75% for H_2. Many of the discussed articles have analyzed the possibility of purifying H_2 by carbon-based adsorbents using simulations and got satisfactory results. However, experimental research is necessary for making further progress in purifying H_2 using carbon-based adsorbents and biochars. Purities and recovery percentages of some H_2 purification processes using different adsorbents are summarized in Table 2.9.

Table 2.9: H2 purification using different adsorbents

Adsorbent	Process	Gas mixture	H_2 Purity(%)	H_2 Recovery(%)	Ref.
CuBTC (MOFs)	PSA [a]	CO_2/H_2	99.99+	48.05	[182]
CuBTC (MOFs)	PSA	$CO_2/H_2/CH_4$	99.97	45.76	[182]
CuBTC (MOFs)	PSA	$CO_2/H_2/CO$	99.99	37.99	[182]
CuBTC (MOFs)	PSA	$CO_2/H_2/N_2$	94.66	51.44	[182]
BPL AC [b]	PSA	$H_2/CO_2/CH_4/CO$	99.99+	25.1	[183]
UTSA-16 (MOFs)	PSA	$H_2/CO_2/CH_4/CO$	99.88	16.7	[183]
MIL-125(Ti)_NH_2 (MOFs)	PSA	CO_2/H_2	100	23.5	[184]
AC-zeolite 13X	parallel two layered bed PSA	$H_2/CO_2/N_2/CO$	94.6-98.3	33.5-63.2	[185]
Modified AC (AC5-KS)	10 step Vacuum PSA	$H_2/CO_2/CH_4/CO/N_2$	99.981	81.6	[178]
AC (2GA-H2J)	2-bed PSA	$H_2/CO/N_2/CO_2/Ar$	99.78	73.04	[186]
AC (2GA-H2J)-zeolite LiX	2 layered bed PSA	$H_2/CO/N_2/CO_2/Ar$	99.95	73.30	[186]
AC (2GA-H2J)-zeolite LiX	4 layered bed PSA	$H_2/CO/N_2/CO_2/Ar$	99.95	79.25	[186]
AC (2GA-H2J)-zeolite LiX	8 layered bed PSA	$H_2/CO/N_2/CO_2/Ar$	99.991	86.58	[187]
AC	6 step 2-bed PSA	$H_2/CO/CO_2$	96.48	83.91	[188]
AC-zeolite 13X	Pd-Cu CMR [c]with 4 bed PSA	$H_2/CO/CO_2$	99.9991	91.37	[189]

[a] Pressure swing adsorption

[b] Activated carbon

[c] Catalytic membrane reactor

Biochar can also be used in methane purification from biogas, which is produced from biowaste anaerobic digestion [190, 191]. Biogas is a mixture of 35-70% CH_4, 15-45% CO_2, and other gases such as H_2S, NH_3, N_2, O_2 [190]. Low CH_4 production and high percentages of CO_2 are among the challenges of using biogas [191]. If the methane from biogas is purified over 97% (biomethane), it can have the same applications as natural gas [190]. Shen et al. [192] used corn stover biochar for biogas methane purification in batch anaerobic adsorption units. Biochar removed a good amount of CO_2 and H_2S from the biogas. The released biogases from this set of experiments all had high CH_4 concentrations (above 90%), and the H_2S was lower than 5 ppb showing biochar excellent capability for biomethane purification.

2.6 Conclusion

Processing residues from biomass offers the advantage of producing valuable products such as biochar and decreasing disposal and treatment costs. The economics of producing biochar instead of landfilling and incineration of waste is a function of the location, feedstock, biochar production process, regulations, and policy. However, the increased potential applications of pyrolysis (or other methods) products (bio-oil, syngas, and biochar), potential to both capture and sequester carbon, and increased regulations in the disposal of organic wastes, thermochemical conversion of biomass has the advantage of decreased environmental costs and potentially attractive economics [193]. In this work, we reviewed biochar as an adsorbent for CO_2,

focusing on biochar surface properties and the challenges ahead of biochar to become a commercial adsorbent. As for the surface properties, the biochar elemental ratios (H/C and O/C), which are indicative of its aromaticity and polarity, decrease with the increase of production temperature. Decrease of O/C translates into decrease of polarity and generally results in an increase of CO_2 adsorption capacity. Surface area of biochars generally increase with temperature (depending on residence time); however, the biochar feedstock also affects the surface area as biochars from woody biomass generally show a higher surface area. CO_2 adsorption capacity of biochar increases with biochar surface area. However, functional groups play a key role in CO_2 adsorption as well, potentially compensating for lower surface areas. Basic functional groups are generally attractive sites for slightly acidic CO_2 gas. The fraction of basic functional groups such as C=N and C=O increases with the increase of biochar production temperature. Increasing biochar production temperature also results in the loss of volatiles and acidic groups such as carboxylic acids and the increase of aromatic groups such as aromatic C=C and C-H.

There are challenges that should be addressed before the industrial application of biochar as CO_2 adsorbent. Biochar CO_2 adsorption performance can be impacted by the presence of other gases. According to the research done in this area, acidic gases such as H_2S and SO_2 do compete with CO_2 molecules over adsorption sites and reduce the adsorption capacity, while non-acidic gases do not impact adsorption capacity to the same extent. However, due to limited studies in this area, there is still

room for research to better understand the impact of other gases on CO_2 adsorption.

Another challenge is to see how biochar CO_2 adsorption would change in wet conditions. As noted in the review, water is typically co-produced with CO_2 and its impact on its adsorption is more complex. Typically, water is removed prior to the CO_2 adsorption process by adding a pre-treatment step. However, this adds significant capital and operational costs. Carbon-based adsorbents such as activated carbons have generally shown a steady performance when operating in wet conditions due to the hydrophobic surface. Breakthrough curves of the CO_2 and H_2O in biochars, indicate that CO_2 adsorption would not be impacted over short adsorption times (approximately 10 minutes) due to the water delayed breakthrough time compared to CO_2. However, there is disagreement in the literature on the impact of biochar production temperature on its hydrophobicity, longer adsorption cycles (typical in the industry), and impact of water on CO_2 adsorption capacity and rate of adsorption. Therefore, more research is required in this area to better compare the biochar CO_2 adsorption in dry and wet conditions.

Biochar performance for CO_2 capture from gas mixtures can also indicate if it can assist the purification of certain gases. For instance, syngas from gasification contains a notable amount of H_2 along with other gases such as CO, CO_2, and CH_4. H_2 is a valuable gas, especially when it is ultra-pure. If the biochar which is produced along syngas during gasification can be applied to separate the CO_2 and possibly other gases, it can an efficient way to produce H_2 at a rather low cost. Hence, doing

research in this area can assist in coming up with an efficient, cost-effective way of producing H_2.

Acknowledgment

The authors thank the NSERC (Natural Science and Engineering Research Council of Canada) and SGS (School of Graduate Studies of Memorial University) for their contributions in funding this project.

Bibliography

[1] D. Were, F. Kansiime, T. Fetahi, A. Cooper, and C. Jjuuko, "Carbon sequestration by wetlands: A critical review of enhancement measures for climate change mitigation," *Earth Systems and Environment*, vol. 3, no. 2, pp. 327–340, 2019.

[2] D. A. Ussiri and R. Lal, *Carbon sequestration for climate change mitigation and adaptation*. Springer, 2017.

[3] K. Ramasubramanian, Y. Zhao, and W. Winston Ho, "Co2 capture and h2 purification: Prospects for co2-selective membrane processes," *AIChE Journal*, vol. 59, no. 4, pp. 1033–1045, 2013.

[4] D. M. D'Alessandro, B. Smit, and J. R. Long, "Carbon dioxide capture: prospects for new materials," *Angewandte Chemie International Edition*, vol. 49, no. 35, pp. 6058–6082, 2010.

[5] T. L. T. Nguyen, J. E. Hermansen, and R. G. Nielsen, "Environmental assessment of gasification technology for biomass conversion to energy in comparison with other alternatives: the case of wheat straw," *Journal of cleaner production*, vol. 53, pp. 138–148, 2013.

[6] A. Molino, S. Chianese, and D. Musmarra, "Biomass gasification technology:

The state of the art overview," *Journal of Energy Chemistry*, vol. 25, no. 1, pp. 10–25, 2016.

[7] C. Ciliberti, A. Biundo, R. Albergo, G. Agrimi, G. Braccio, I. de Bari, and I. Pisano, "Syngas derived from lignocellulosic biomass gasification as an alternative resource for innovative bioprocesses," *Processes*, vol. 8, no. 12, p. 1567, 2020.

[8] P. Basu, *Biomass gasification, pyrolysis and torrefaction: practical design and theory*. Academic press, 2018.

[9] Y. Li, C. P. Alaimo, M. Kim, N. Y. Kado, J. Peppers, J. Xue, C. Wan, P. G. Green, R. Zhang, B. M. Jenkins, *et al.*, "Composition and toxicity of biogas produced from different feedstocks in california," *Environmental science & technology*, vol. 53, no. 19, pp. 11569–11579, 2019.

[10] J. George, P. Arun, and C. Muraleedharan, "Experimental investigation on co-gasification of coffee husk and sawdust in a bubbling fluidised bed gasifier," *Journal of the Energy Institute*, vol. 92, no. 6, pp. 1977–1986, 2019.

[11] Y.-S. Jeong, Y.-K. Choi, K.-B. Park, and J.-S. Kim, "Air co-gasification of coal and dried sewage sludge in a two-stage gasifier: Effect of blending ratio on the producer gas composition and tar removal," *Energy*, vol. 185, pp. 708–716, 2019.

[12] N. B. Rasmussen and N. Aryal, "Syngas production using straw pellet gasification in fluidized bed allothermal reactor under different temperature conditions," *Fuel*, vol. 263, p. 116706, 2020.

[13] Z. Ong, Y. Cheng, T. Maneerung, Z. Yao, Y. W. Tong, C.-H. Wang, and Y. Dai, "Co-gasification of woody biomass and sewage sludge in a fixed-bed downdraft gasifier," *AIChE Journal*, vol. 61, no. 8, pp. 2508–2521, 2015.

[14] L. Liu, Y. Huang, J. Cao, C. Liu, L. Dong, L. Xu, and J. Zha, "Experimental study of biomass gasification with oxygen-enriched air in fluidized bed gasifier," *Science of the Total Environment*, vol. 626, pp. 423–433, 2018.

[15] E. S. Aydin, O. Yucel, and H. Sadikoglu, "Experimental study on hydrogen-rich syngas production via gasification of pine cone particles and wood pellets in a fixed bed downdraft gasifier," *International Journal of Hydrogen Energy*, vol. 44, no. 32, pp. 17389–17396, 2019.

[16] S. Maisano, F. Urbani, F. Cipitì, F. Freni, and V. Chiodo, "Syngas production by bfb gasification: experimental comparison of different biomasses," *International Journal of Hydrogen Energy*, vol. 44, no. 9, pp. 4414–4422, 2019.

[17] V. Arora, R. K. Saran, R. Kumar, and S. Yadav, "Separation and sequestration of co2 in geological formations," *Materials Science for Energy Technologies*, vol. 2, no. 3, pp. 647–656, 2019.

[18] G. Avci, S. Velioglu, and S. Keskin, "High-throughput screening of mof adsorbents and membranes for h2 purification and co2 capture," *ACS applied materials & interfaces*, vol. 10, no. 39, pp. 33693–33706, 2018.

[19] M. K. Mondal, H. K. Balsora, and P. Varshney, "Progress and trends in co2 capture/separation technologies: A review," *Energy*, vol. 46, no. 1, pp. 431–441, 2012.

[20] G. Xu, F. Liang, Y. Yang, Y. Hu, K. Zhang, and W. Liu, "An improved co2 separation and purification system based on cryogenic separation and distillation theory," *Energies*, vol. 7, no. 5, pp. 3484–3502, 2014.

[21] H. Yang, Z. Xu, M. Fan, R. Gupta, R. B. Slimane, A. E. Bland, and I. Wright, "Progress in carbon dioxide separation and capture: A review," *Journal of environmental sciences*, vol. 20, no. 1, pp. 14–27, 2008.

[22] H. Jilvero, F. Normann, K. Andersson, and F. Johnsson, "The rate of co2 absorption in ammonia implications on absorber design," *Industrial & Engineering Chemistry Research*, vol. 53, no. 16, pp. 6750–6758, 2014.

[23] C.-H. Yu, C.-H. Huang, C.-S. Tan, *et al.*, "A review of co2 capture by absorption and adsorption," *Aerosol and Air Quality Research*, vol. 12, no. 5, pp. 745–769, 2012.

[24] D. Dortmundt and K. Doshi, "Recent developments in co2 removal membrane technology," *UOP LLC*, vol. 1, 1999.

[25] P. Bernardo, E. Drioli, and G. Golemme, "Membrane gas separation: a review/state of the art," *Industrial & engineering chemistry research*, vol. 48, no. 10, pp. 4638–4663, 2009.

[26] A. Chakma, "Separation of co2 and so2 from flue gas streams by liquid membranes," *Energy conversion and management*, vol. 36, no. 6-9, pp. 405–410, 1995.

[27] D. Nikolaeva and P. Luis, "Top-down polyelectrolytes for membrane-based post-combustion co2 capture," *Molecules*, vol. 25, no. 2, p. 323, 2020.

[28] M. Mofarahi, Y. Khojasteh, H. Khaledi, and A. Farahnak, "Design of co2 absorption plant for recovery of co2 from flue gases of gas turbine," *Energy*, vol. 33, no. 8, pp. 1311–1319, 2008.

[29] S. Shang, Z. Tao, C. Yang, A. Hanif, L. Li, D. C. Tsang, Q. Gu, and J. Shang, "Facile synthesis of cubtc and its graphene oxide composites as efficient adsorbents for co2 capture," *Chemical Engineering Journal*, vol. 393, p. 124666, 2020.

[30] Z. Zhang, J. A. Schott, M. Liu, H. Chen, X. Lu, B. G. Sumpter, J. Fu, and S. Dai, "Prediction of carbon dioxide adsorption via deep learning," *Angewandte Chemie*, vol. 131, no. 1, pp. 265–269, 2019.

[31] E. E. Ünveren, B. Ö. Monkul, Ş. Sarıoğlan, N. Karademir, and E. Alper, "Solid

amine sorbents for co2 capture by chemical adsorption: A review," *Petroleum*, vol. 3, no. 1, pp. 37–50, 2017.

[32] I. Hinkov, F. D. Lamari, P. Langlois, M. Dicko, C. Chilev, and I. Pentchev, "Carbon dioxide capture by adsorption," *Journal of Chemical Technology & Metallurgy*, vol. 51, no. 6, 2016.

[33] S.-H. Liu and Y.-Y. Huang, "Valorization of coffee grounds to biochar-derived adsorbents for co2 adsorption," *Journal of Cleaner Production*, vol. 175, pp. 354–360, 2018.

[34] E. M. Calvo-Munoz, F. J. Garcia-Mateos, J. M. Rosas, J. Rodriguez-Mirasol, and T. Cordero, "Biomass waste carbon materials as adsorbents for co2 capture under post-combustion conditions," *Frontiers in materials*, vol. 3, p. 23, 2016.

[35] A. González, M. Plaza, F. Rubiera, and C. Pevida, "Sustainable biomass-based carbon adsorbents for post-combustion co2 capture," *Chemical engineering journal*, vol. 230, pp. 456–465, 2013.

[36] M.-V. Nguyen and B.-K. Lee, "A novel removal of co2 using nitrogen doped biochar beads as a green adsorbent," *Process Safety and Environmental Protection*, vol. 104, pp. 490–498, 2016.

[37] V. Gargiulo, A. Gomis-Berenguer, P. Giudicianni, C. O. Ania, R. Ragucci, and M. Alfe, "Assessing the potential of biochars prepared by steam-assisted slow

pyrolysis for co2 adsorption and separation," *Energy & fuels*, vol. 32, no. 10, pp. 10218–10227, 2018.

[38] T. M. Abdel-Fattah, M. E. Mahmoud, S. B. Ahmed, M. D. Huff, J. W. Lee, and S. Kumar, "Biochar from woody biomass for removing metal contaminants and carbon sequestration," *Journal of Industrial and Engineering Chemistry*, vol. 22, pp. 103–109, 2015.

[39] N. Liu, A. B. Charrua, C.-H. Weng, X. Yuan, and F. Ding, "Characterization of biochars derived from agriculture wastes and their adsorptive removal of atrazine from aqueous solution: a comparative study," *Bioresource technology*, vol. 198, pp. 55–62, 2015.

[40] M.-M. Fu, C.-H. Mo, H. Li, Y.-N. Zhang, W.-X. Huang, and M. H. Wong, "Comparison of physicochemical properties of biochars and hydrochars produced from food wastes," *Journal of Cleaner Production*, vol. 236, p. 117637, 2019.

[41] S. Ding and Y. Liu, "Adsorption of co2 from flue gas by novel seaweed-based koh-activated porous biochars," *Fuel*, vol. 260, p. 116382, 2020.

[42] P. D. Dissanayake, S. W. Choi, A. D. Igalavithana, X. Yang, D. C. Tsang, C.-H. Wang, H. W. Kua, K. B. Lee, and Y. S. Ok, "Sustainable gasification biochar as a high efficiency adsorbent for co2 capture: A facile method to designer biochar

fabrication," *Renewable and Sustainable Energy Reviews*, vol. 124, p. 109785, 2020.

[43] Y.-F. Huang, P.-T. Chiueh, C.-H. Shih, S.-L. Lo, L. Sun, Y. Zhong, and C. Qiu, "Microwave pyrolysis of rice straw to produce biochar as an adsorbent for co2 capture," *Energy*, vol. 84, pp. 75–82, 2015.

[44] L. Cao, X. Zhang, Y. Xu, W. Xiang, R. Wang, F. Ding, P. Hong, and B. Gao, "Straw and wood based biochar for co2 capture: Adsorption performance and governing mechanisms," *Separation and Purification Technology*, vol. 287, p. 120592, 2022.

[45] R. Chatterjee, B. Sajjadi, W.-Y. Chen, D. L. Mattern, N. Hammer, V. Raman, and A. Dorris, "Effect of pyrolysis temperature on physicochemical properties and acoustic-based amination of biochar for efficient co2 adsorption," *Frontiers in Energy Research*, vol. 8, p. 85, 2020.

[46] F. Dreisbach, R. Staudt, and J. Keller, "High pressure adsorption data of methane, nitrogen, carbon dioxide and their binary and ternary mixtures on activated carbon," *Adsorption*, vol. 5, no. 3, pp. 215–227, 1999.

[47] D. T. Tefera, Z. Hashisho, J. H. Philips, J. E. Anderson, and M. Nichols, "Modeling competitive adsorption of mixtures of volatile organic compounds in a fixed-bed of beaded activated carbon," *Environmental science & technology*, vol. 48, no. 9, pp. 5108–5117, 2014.

[48] J. Wilcox, R. Haghpanah, E. C. Rupp, J. He, and K. Lee, "Advancing adsorption and membrane separation processes for the gigaton carbon capture challenge," *Annual review of chemical and biomolecular engineering*, vol. 5, pp. 479–505, 2014.

[49] R. L. Siegelman, P. J. Milner, E. J. Kim, S. C. Weston, and J. R. Long, "Challenges and opportunities for adsorption-based co 2 capture from natural gas combined cycle emissions," *Energy & environmental science*, vol. 12, no. 7, pp. 2161–2173, 2019.

[50] J. Zhang, P. Xiao, G. Li, and P. A. Webley, "Effect of flue gas impurities on co2 capture performance from flue gas at coal-fired power stations by vacuum swing adsorption," *Energy Procedia*, vol. 1, no. 1, pp. 1115–1122, 2009.

[51] G. Li, P. Xiao, P. A. Webley, J. Zhang, and R. Singh, "Competition of co2/h2o in adsorption based co2 capture," *Energy Procedia*, vol. 1, no. 1, pp. 1123–1130, 2009.

[52] A. Qader, B. Hooper, T. Innocenzi, G. Stevens, S. Kentish, C. Scholes, K. Mumford, K. Smith, P. A. Webley, and J. Zhang, "Novel post-combustion capture technologies on a lignite fired power plant-results of the co2crc/h3 capture project," *Energy Procedia*, vol. 4, pp. 1668–1675, 2011.

[53] M. G Plaza, A. S. González, F. Rubiera, and C. Pevida, "Water vapour ad-

sorption by a coffee-based microporous carbon: effect on co2 capture," *Journal of Chemical Technology & Biotechnology*, vol. 90, no. 9, pp. 1592–1600, 2015.

[54] S.-I. Yang, D.-Y. Choi, S.-C. Jang, S.-H. Kim, and D.-K. Choi, "Hydrogen separation by multi-bed pressure swing adsorption of synthesis gas," *Adsorption*, vol. 14, no. 4, pp. 583–590, 2008.

[55] I. Shamsudin, A. Abdullah, I. Idris, S. Gobi, and M. Othman, "Hydrogen purification from binary syngas by psa with pressure equalization using microporous palm kernel shell activated carbon," *Fuel*, vol. 253, pp. 722–730, 2019.

[56] C. Zhang, L. Liu, M. Zhao, H. Rong, and Y. Xu, "The environmental characteristics and applications of biochar," *Environmental Science and Pollution Research*, vol. 25, no. 22, pp. 21525–21534, 2018.

[57] P. Lucchini, R. Quilliam, T. H. DeLuca, T. Vamerali, and D. L. Jones, "Increased bioavailability of metals in two contrasting agricultural soils treated with waste wood-derived biochar and ash," *Environmental Science and Pollution Research*, vol. 21, pp. 3230–3240, 2014.

[58] J. S. Cha, S. H. Park, S.-C. Jung, C. Ryu, J.-K. Jeon, M.-C. Shin, and Y.-K. Park, "Production and utilization of biochar: A review," *Journal of Industrial and Engineering Chemistry*, vol. 40, pp. 1–15, 2016.

[59] N. A. Qambrani, M. M. Rahman, S. Won, S. Shim, and C. Ra, "Biochar properties and eco-friendly applications for climate change mitigation, waste management, and wastewater treatment: A review," *Renewable and Sustainable Energy Reviews*, vol. 79, pp. 255–273, 2017.

[60] S. Rangabhashiyam, P. Balasubramanian, *et al.*, "The potential of lignocellulosic biomass precursors for biochar production: performance, mechanism and wastewater application-a review.," *Industrial Crops and Products*, vol. 128, pp. 405–423, 2019.

[61] H. W. Kua, C. Pedapati, R. V. Lee, and S. Kawi, "Effect of indoor contamination on carbon dioxide adsorption of wood-based biochar–lessons for direct air capture," *Journal of Cleaner Production*, vol. 210, pp. 860–871, 2019.

[62] R. Ibarrola, S. Shackley, and J. Hammond, "Pyrolysis biochar systems for recovering biodegradable materials: A life cycle carbon assessment," *Waste Management*, vol. 32, no. 5, pp. 859–868, 2012.

[63] R. C. Brown, "The role of pyrolysis and gasification in a carbon negative economy," *Processes*, vol. 9, no. 5, p. 882, 2021.

[64] O. Mašek, "Biochar in thermal and thermochemical biorefineries—production of biochar as a coproduct," in *Handbook of biofuels production*, pp. 655–671, Elsevier, 2016.

[65] D. A. Laird, R. C. Brown, J. E. Amonette, and J. Lehmann, "Review of the pyrolysis platform for coproducing bio-oil and biochar," *Biofuels, bioproducts and biorefining*, vol. 3, no. 5, pp. 547–562, 2009.

[66] Z. Liu and G. Han, "Production of solid fuel biochar from waste biomass by low temperature pyrolysis," *Fuel*, vol. 158, pp. 159–165, 2015.

[67] D. Wang, P. Jiang, H. Zhang, and W. Yuan, "Biochar production and applications in agro and forestry systems: A review," *Science of The Total Environment*, vol. 723, p. 137775, 2020.

[68] H. Tan, C. Lee, P. Ong, K. Wong, C. Bong, C. Li, and Y. Gao, "A review on the comparison between slow pyrolysis and fast pyrolysis on the quality of lignocellulosic and lignin-based biochar," in *IOP Conference Series: Materials Science and Engineering*, vol. 1051, p. 012075, IOP Publishing, 2021.

[69] T. Yuan, W. He, G. Yin, and S. Xu, "Comparison of bio-chars formation derived from fast and slow pyrolysis of walnut shell," *Fuel*, vol. 261, p. 116450, 2020.

[70] A. Shaaban, S.-M. Se, N. M. M. Mitan, and M. Dimin, "Characterization of biochar derived from rubber wood sawdust through slow pyrolysis on surface porosities and functional groups," *Procedia Engineering*, vol. 68, pp. 365–371, 2013.

[71] K. B. Cantrell, P. G. Hunt, M. Uchimiya, J. M. Novak, and K. S. Ro, "Impact of pyrolysis temperature and manure source on physicochemical characteristics of biochar," *Bioresource technology*, vol. 107, pp. 419–428, 2012.

[72] K. H. Kim, J.-Y. Kim, T.-S. Cho, and J. W. Choi, "Influence of pyrolysis temperature on physicochemical properties of biochar obtained from the fast pyrolysis of pitch pine (pinus rigida)," *Bioresource technology*, vol. 118, pp. 158–162, 2012.

[73] F. Sotoudehniakarani, A. Alayat, and A. G. McDonald, "Characterization and comparison of pyrolysis products from fast pyrolysis of commercial chlorella vulgaris and cultivated microalgae," *Journal of Analytical and Applied Pyrolysis*, vol. 139, pp. 258–273, 2019.

[74] E. W. Bruun, H. Hauggaard-Nielsen, N. Ibrahim, H. Egsgaard, P. Ambus, P. A. Jensen, and K. Dam-Johansen, "Influence of fast pyrolysis temperature on biochar labile fraction and short-term carbon loss in a loamy soil," *Biomass and Bioenergy*, vol. 35, no. 3, pp. 1182–1189, 2011.

[75] M. Laghari, Z. Hu, M. S. Mirjat, B. Xiao, A. A. Tagar, and M. Hu, "Fast pyrolysis biochar from sawdust improves the quality of desert soils and enhances plant growth," *Journal of the Science of Food and Agriculture*, vol. 96, no. 1, pp. 199–206, 2016.

[76] K. Wang, R. C. Brown, S. Homsy, L. Martinez, and S. S. Sidhu, "Fast pyrol-

ysis of microalgae remnants in a fluidized bed reactor for bio-oil and biochar production," *Bioresource technology*, vol. 127, pp. 494–499, 2013.

[77] C. Guizani, S. Valin, J. Billaud, M. Peyrot, and S. Salvador, "Biomass fast pyrolysis in a drop tube reactor for bio oil production: Experiments and modeling," *Fuel*, vol. 207, pp. 71–84, 2017.

[78] A. K. Varma, L. S. Thakur, R. Shankar, and P. Mondal, "Pyrolysis of wood sawdust: Effects of process parameters on products yield and characterization of products," *Waste Management*, vol. 89, pp. 224–235, 2019.

[79] W. Cai and R. Liu, "Performance of a commercial-scale biomass fast pyrolysis plant for bio-oil production," *Fuel*, vol. 182, pp. 677–686, 2016.

[80] K. H. Kim, T.-S. Kim, S.-M. Lee, D. Choi, H. Yeo, I.-G. Choi, and J. W. Choi, "Comparison of physicochemical features of biooils and biochars produced from various woody biomasses by fast pyrolysis," *Renewable Energy*, vol. 50, pp. 188–195, 2013.

[81] K. H. Kim, I. Y. Eom, S. M. Lee, D. Choi, H. Yeo, I.-G. Choi, and J. W. Choi, "Investigation of physicochemical properties of biooils produced from yellow poplar wood (liriodendron tulipifera) at various temperatures and residence times," *Journal of Analytical and Applied Pyrolysis*, vol. 92, no. 1, pp. 2–9, 2011.

[82] M. Irfan, Q. Chen, Y. Yue, R. Pang, Q. Lin, X. Zhao, and H. Chen, "Co-production of biochar, bio-oil and syngas from halophyte grass (achnatherum splendens l.) under three different pyrolysis temperatures," *Bioresource technology*, vol. 211, pp. 457–463, 2016.

[83] R. Moreira, R. dos Reis Orsini, J. M. Vaz, J. C. Penteado, and E. V. Spinacé, "Production of biochar, bio-oil and synthesis gas from cashew nut shell by slow pyrolysis," *Waste and biomass valorization*, vol. 8, no. 1, pp. 217–224, 2017.

[84] S. Liang, Y. Han, L. Wei, and A. G. McDonald, "Production and characterization of bio-oil and bio-char from pyrolysis of potato peel wastes," *Biomass Conversion and Biorefinery*, vol. 5, no. 3, pp. 237–246, 2015.

[85] A. E. Pütün, E. Önal, B. B. Uzun, and N. Özbay, "Comparison between the "slow" and "fast" pyrolysis of tobacco residue," *Industrial Crops and Products*, vol. 26, no. 3, pp. 307–314, 2007.

[86] S. Papari, K. Hawboldt, and R. Helleur, "Production and characterization of pyrolysis oil from sawmill residues in an auger reactor," *Industrial & Engineering Chemistry Research*, vol. 56, no. 8, pp. 1920–1925, 2017.

[87] K. Crombie, O. Mašek, S. P. Sohi, P. Brownsort, and A. Cross, "The effect of pyrolysis conditions on biochar stability as determined by three methods," *Gcb Bioenergy*, vol. 5, no. 2, pp. 122–131, 2013.

[88] M. Ji, L. Zhou, S. Zhang, G. Luo, and W. Sang, "Effects of biochar on methane emission from paddy soil: Focusing on dom and microbial communities," *Science of The Total Environment*, vol. 743, p. 140725, 2020.

[89] M. Ahmad, S. S. Lee, X. Dou, D. Mohan, J.-K. Sung, J. E. Yang, and Y. S. Ok, "Effects of pyrolysis temperature on soybean stover-and peanut shell-derived biochar properties and tce adsorption in water," *Bioresource technology*, vol. 118, pp. 536–544, 2012.

[90] Z. Wang, L. Han, K. Sun, J. Jin, K. S. Ro, J. A. Libra, X. Liu, and B. Xing, "Sorption of four hydrophobic organic contaminants by biochars derived from maize straw, wood dust and swine manure at different pyrolytic temperatures," *Chemosphere*, vol. 144, pp. 285–291, 2016.

[91] P. D. Dissanayake, S. You, A. D. Igalavithana, Y. Xia, A. Bhatnagar, S. Gupta, H. W. Kua, S. Kim, J.-H. Kwon, D. C. Tsang, *et al.*, "Biochar-based adsorbents for carbon dioxide capture: A critical review," *Renewable and Sustainable Energy Reviews*, vol. 119, p. 109582, 2020.

[92] D. Chen, X. Yu, C. Song, X. Pang, J. Huang, and Y. Li, "Effect of pyrolysis temperature on the chemical oxidation stability of bamboo biochar," *Bioresource technology*, vol. 218, pp. 1303–1306, 2016.

[93] Z. Zhao, T. Nie, and W. Zhou, "Enhanced biochar stabilities and adsorption

properties for tetracycline by synthesizing silica-composited biochar," *Environmental Pollution*, vol. 254, p. 113015, 2019.

[94] A. Mukherjee, V. B. Borugadda, J. J. Dynes, C. Niu, and A. Dalai, "Carbon dioxide capture from flue gas in biochar produced from spent coffee grounds: Effect of surface chemistry and porous structure," *Journal of Environmental Chemical Engineering*, p. 106049, 2021.

[95] A. R. Usman, A. Abduljabbar, M. Vithanage, Y. S. Ok, M. Ahmad, M. Ahmad, J. Elfaki, S. S. Abdulazeem, and M. I. Al-Wabel, "Biochar production from date palm waste: charring temperature induced changes in composition and surface chemistry," *Journal of Analytical and Applied Pyrolysis*, vol. 115, pp. 392–400, 2015.

[96] Y. Wang and R. Liu, "Comparison of characteristics of twenty-one types of biochar and their ability to remove multi-heavy metals and methylene blue in solution," *Fuel Processing Technology*, vol. 160, pp. 55–63, 2017.

[97] J. Xu, J. Liu, P. Ling, X. Zhang, K. Xu, L. He, Y. Wang, S. Su, S. Hu, and J. Xiang, "Raman spectroscopy of biochar from the pyrolysis of three typical chinese biomasses: A novel method for rapidly evaluating the biochar property," *Energy*, vol. 202, p. 117644, 2020.

[98] S. Gupta, H. W. Kua, and C. Y. Low, "Use of biochar as carbon sequestering

additive in cement mortar," *Cement and concrete composites*, vol. 87, pp. 110–129, 2018.

[99] G. Sigmund, T. Hüffer, T. Hofmann, and M. Kah, "Biochar total surface area and total pore volume determined by n2 and co2 physisorption are strongly influenced by degassing temperature," *Science of the Total Environment*, vol. 580, pp. 770–775, 2017.

[100] A. E. Creamer, B. Gao, and M. Zhang, "Carbon dioxide capture using biochar produced from sugarcane bagasse and hickory wood," *Chemical Engineering Journal*, vol. 249, pp. 174–179, 2014.

[101] N. A. Zubbri, A. R. Mohamed, N. Kamiuchi, and M. Mohammadi, "Enhancement of co 2 adsorption on biochar sorbent modified by metal incorporation," *Environmental Science and Pollution Research*, pp. 1–21, 2020.

[102] A. Tomczyk, Z. Sokołowska, and P. Boguta, "Biochar physicochemical properties: pyrolysis temperature and feedstock kind effects," *Reviews in Environmental Science and Bio/Technology*, vol. 19, pp. 191–215, 2020.

[103] J. A. Ippolito, L. Cui, C. Kammann, N. Wrage-Mönnig, J. M. Estavillo, T. Fuertes-Mendizabal, M. L. Cayuela, G. Sigua, J. Novak, K. Spokas, *et al.*, "Feedstock choice, pyrolysis temperature and type influence biochar characteristics: a comprehensive meta-data analysis review," *Biochar*, vol. 2, pp. 421–438, 2020.

[104] S. Sethupathi, M. Zhang, A. U. Rajapaksha, S. R. Lee, N. Mohamad Nor, A. R. Mohamed, M. Al-Wabel, S. S. Lee, and Y. S. Ok, "Biochars as potential adsorbers of ch4, co2 and h2s," *Sustainability*, vol. 9, no. 1, p. 121, 2017.

[105] A. D. Igalavithana, S. W. Choi, J. Shang, A. Hanif, P. D. Dissanayake, D. C. Tsang, J.-H. Kwon, K. B. Lee, and Y. S. Ok, "Carbon dioxide capture in biochar produced from pine sawdust and paper mill sludge: Effect of porous structure and surface chemistry," *Science of the Total Environment*, vol. 739, p. 139845, 2020.

[106] X. Xu, Y. Kan, L. Zhao, and X. Cao, "Chemical transformation of co2 during its capture by waste biomass derived biochars," *Environmental pollution*, vol. 213, pp. 533–540, 2016.

[107] H. Bamdad, K. Hawboldt, S. MacQuarrie, and S. Papari, "Application of biochar for acid gas removal: experimental and statistical analysis using co 2," *Environmental Science and Pollution Research*, vol. 26, no. 11, pp. 10902–10915, 2019.

[108] J. J. Manyà, D. García-Morcate, and B. González, "Adsorption performance of physically activated biochars for postcombustion co2 capture from dry and humid flue gas," *Applied Sciences*, vol. 10, no. 1, p. 376, 2020.

[109] C. Zhang, W. Song, G. Sun, L. Xie, J. Wang, K. Li, C. Sun, H. Liu, C. E. Snape,

and T. Drage, "Co2 capture with activated carbon grafted by nitrogenous functional groups," *Energy & fuels*, vol. 27, no. 8, pp. 4818–4823, 2013.

[110] L. Zhao, Z. Wang, H.-Y. Ren, C. Chen, J. Nan, G.-L. Cao, S.-S. Yang, and N.-Q. Ren, "Residue cornstalk derived biochar promotes direct bio-hydrogen production from anaerobic fermentation of cornstalk," *Bioresource Technology*, vol. 320, p. 124338, 2021.

[111] S.-X. Zhao, N. Ta, and X.-D. Wang, "Effect of temperature on the structural and physicochemical properties of biochar with apple tree branches as feedstock material," *Energies*, vol. 10, no. 9, p. 1293, 2017.

[112] W. Suliman, J. B. Harsh, N. I. Abu-Lail, A.-M. Fortuna, I. Dallmeyer, and M. Garcia-Perez, "Influence of feedstock source and pyrolysis temperature on biochar bulk and surface properties," *Biomass and Bioenergy*, vol. 84, pp. 37–48, 2016.

[113] L.-Y. Gao, J.-H. Deng, G.-F. Huang, K. Li, K.-Z. Cai, Y. Liu, and F. Huang, "Relative distribution of cd2+ adsorption mechanisms on biochars derived from rice straw and sewage sludge," *Bioresource technology*, vol. 272, pp. 114–122, 2019.

[114] A. D. Igalavithana, S. W. Choi, P. D. Dissanayake, J. Shang, C.-H. Wang, X. Yang, S. Kim, D. C. Tsang, K. B. Lee, and Y. S. Ok, "Gasification biochar

from biowaste (food waste and wood waste) for effective co2 adsorption," *Journal of hazardous materials*, vol. 391, p. 121147, 2020.

[115] S. You, Y. S. Ok, S. S. Chen, D. C. Tsang, E. E. Kwon, J. Lee, and C.-H. Wang, "A critical review on sustainable biochar system through gasification: energy and environmental applications," *Bioresource technology*, vol. 246, pp. 242–253, 2017.

[116] V. S. Sikarwar, M. Zhao, P. Clough, J. Yao, X. Zhong, M. Z. Memon, N. Shah, E. J. Anthony, and P. S. Fennell, "An overview of advances in biomass gasification," *Energy & Environmental Science*, vol. 9, no. 10, pp. 2939–2977, 2016.

[117] H.-L. Tay, S. Kajitani, S. Zhang, and C.-Z. Li, "Effects of gasifying agent on the evolution of char structure during the gasification of victorian brown coal," *Fuel*, vol. 103, pp. 22–28, 2013.

[118] Y. Liu, M. Paskevicius, M. V. Sofianos, G. Parkinson, and C.-Z. Li, "In situ saxs studies of the pore development in biochar during gasification," *Carbon*, vol. 172, pp. 454–462, 2021.

[119] M. Del Grosso, L. Cutz, U. Tiringer, C. Tsekos, P. Taheri, and W. de Jong, "Influence of indirectly heated steam-blown gasification process conditions on biochar physico-chemical properties," *Fuel Processing Technology*, vol. 235, p. 107347, 2022.

[120] N. Taupe, D. Lynch, R. Wnetrzak, M. Kwapinska, W. Kwapinski, and J. Leahy, "Updraft gasification of poultry litter at farm-scale–a case study," *Waste Management*, vol. 50, pp. 324–333, 2016.

[121] G. Allesina, S. Pedrazzi, F. Allegretti, N. Morselli, M. Puglia, G. Santunione, and P. Tartarini, "Gasification of cotton crop residues for combined power and biochar production in mozambique," *Applied Thermal Engineering*, vol. 139, pp. 387–394, 2018.

[122] E. Lugato, F. P. Vaccari, L. Genesio, S. Baronti, A. Pozzi, M. Rack, J. Woods, G. Simonetti, L. Montanarella, and F. Miglietta, "An energy-biochar chain involving biomass gasification and rice cultivation in northern italy," *Gcb Bioenergy*, vol. 5, no. 2, pp. 192–201, 2013.

[123] W. C. Ng, S. You, R. Ling, K. Y.-H. Gin, Y. Dai, and C.-H. Wang, "Co-gasification of woody biomass and chicken manure: Syngas production, biochar reutilization, and cost-benefit analysis," *Energy*, vol. 139, pp. 732–742, 2017.

[124] L. Reyes, L. Abdelouahed, B. Campusano, J.-C. Buvat, and B. Taouk, "Exergetic study of beech wood gasification in fluidized bed reactor using co2 or steam as gasification agents," *Fuel Processing Technology*, vol. 213, p. 106664, 2021.

[125] H. Madzaki, W. A. W. A. KarimGhani, *et al.*, "Carbon dioxide adsorption on sawdust biochar," *Procedia engineering*, vol. 148, pp. 718–725, 2016.

[126] F. L. Braghiroli, H. Bouafif, N. Hamza, B. Bouslimi, C. M. Neculita, and A. Koubaa, "The influence of pilot-scale pyro-gasification and activation conditions on porosity development in activated biochars," *Biomass and bioenergy*, vol. 118, pp. 105–114, 2018.

[127] C. E. Brewer, K. Schmidt-Rohr, J. A. Satrio, and R. C. Brown, "Characterization of biochar from fast pyrolysis and gasification systems," *Environmental Progress & Sustainable Energy: An Official Publication of the American Institute of Chemical Engineers*, vol. 28, no. 3, pp. 386–396, 2009.

[128] C. E. Brewer, R. Unger, K. Schmidt-Rohr, and R. C. Brown, "Criteria to select biochars for field studies based on biochar chemical properties," *Bioenergy Research*, vol. 4, pp. 312–323, 2011.

[129] M. Ilić, F.-H. Haegel, A. Lolić, Z. Nedić, T. Tosti, I. S. Ignjatović, A. Linden, N. D. Jablonowski, and H. Hartmann, "Surface functional groups and degree of carbonization of selected chars from different processes and feedstock," *Plos one*, vol. 17, no. 11, p. e0277365, 2022.

[130] R. Azargohar, S. Nanda, A. K. Dalai, and J. A. Kozinski, "Physico-chemistry of biochars produced through steam gasification and hydro-thermal gasification of canola hull and canola meal pellets," *Biomass and Bioenergy*, vol. 120, pp. 458–470, 2019.

[131] M. Cavali, N. L. Junior, J. D. de Sena, A. L. Woiciechowski, C. R. Soccol,

P. Belli Filho, R. Bayard, H. Benbelkacem, and A. B. de Castilhos Junior, "A review on hydrothermal carbonization of potential biomass wastes, characterization and environmental applications of hydrochar, and biorefinery perspectives of the process," *Science of The Total Environment*, p. 159627, 2022.

[132] C. Goel, S. Mohan, and P. Dinesha, "Co2 capture by adsorption on biomass-derived activated char: A review," *Science of The Total Environment*, vol. 798, p. 149296, 2021.

[133] H. M. Fagnani, C. T. da Silva, M. M. Pereira, A. W. Rinaldi, P. A. Arroyo, and M. A. de Barros, "Co 2 adsorption in hydrochar produced from waste biomass," *SN Applied Sciences*, vol. 1, pp. 1–10, 2019.

[134] E. Atallah, J. Zeaiter, M. N. Ahmad, J. J. Leahy, and W. Kwapinski, "Hydrothermal carbonization of spent mushroom compost waste compared against torrefaction and pyrolysis," *Fuel Processing Technology*, vol. 216, p. 106795, 2021.

[135] S. Shi, F. O. Ochedi, J. Yu, and Y. Liu, "Porous biochars derived from microalgae pyrolysis for co2 adsorption," *Energy & Fuels*, vol. 35, no. 9, pp. 7646–7656, 2021.

[136] J. Hu, Y. Liu, J. Liu, and C. Gu, "Effects of water vapor and trace gas impurities in flue gas on co2 capture in zeolitic imidazolate frameworks: The significant role of functional groups," *Fuel*, vol. 200, pp. 244–251, 2017.

[137] X. Dong, J. Zhang, L. Gang, P. Xiao, P. Webley, and Y.-c. ZHAI, "Effect of water vapor from power station flue gas on co2 capture by vacuum swing adsorption with activated carbon," *Journal of Fuel Chemistry and Technology*, vol. 39, no. 3, pp. 169–174, 2011.

[138] Y. Liu, J. Liu, Y. Lin, and M. Chang, "Effects of water vapor and trace gas impurities in flue gas on co2/n2 separation using zif-68," *The Journal of Physical Chemistry C*, vol. 118, no. 13, pp. 6744–6751, 2014.

[139] N. Couto, A. Rouboa, V. Silva, E. Monteiro, and K. Bouziane, "Influence of the biomass gasification processes on the final composition of syngas," *Energy Procedia*, vol. 36, pp. 596–606, 2013.

[140] S. Rasi, A. Veijanen, and J. Rintala, "Trace compounds of biogas from different biogas production plants," *Energy*, vol. 32, no. 8, pp. 1375–1380, 2007.

[141] A. Khan, J. E. Szulejko, P. Samaddar, K.-H. Kim, B. Liu, H. A. Maitlo, X. Yang, and Y. S. Ok, "The potential of biochar as sorptive media for removal of hazardous benzene in air," *Chemical Engineering Journal*, vol. 361, pp. 1576–1585, 2019.

[142] K. S. Ro, I. M. Lima, G. B. Reddy, M. A. Jackson, and B. Gao, "Removing gaseous nh3 using biochar as an adsorbent," *Agriculture*, vol. 5, no. 4, pp. 991–1002, 2015.

[143] Y. Sun, G. Yang, L. Zhang, and Z. Sun, "Preparation of high performance h2s removal biochar by direct fluidized bed carbonization using potato peel waste," *Process Safety and Environmental Protection*, vol. 107, pp. 281–288, 2017.

[144] G. Shang, G. Shen, L. Liu, Q. Chen, and Z. Xu, "Kinetics and mechanisms of hydrogen sulfide adsorption by biochars," *Bioresource technology*, vol. 133, pp. 495–499, 2013.

[145] Q. Ma, W. Chen, Z. Jin, L. Chen, Q. Zhou, and X. Jiang, "One-step synthesis of microporous nitrogen-doped biochar for efficient removal of co2 and h2s," *Fuel*, vol. 289, p. 119932, 2021.

[146] J. Shao, J. Zhang, X. Zhang, Y. Feng, H. Zhang, S. Zhang, and H. Chen, "Enhance so2 adsorption performance of biochar modified by co2 activation and amine impregnation," *Fuel*, vol. 224, pp. 138–146, 2018.

[147] F. L. Braghiroli, H. Bouafif, and A. Koubaa, "Enhanced so2 adsorption and desorption on chemically and physically activated biochar made from wood residues," *Industrial Crops and Products*, vol. 138, p. 111456, 2019.

[148] I. Durán, N. Álvarez-Gutiérrez, F. Rubiera, and C. Pevida, "Biogas purification by means of adsorption on pine sawdust-based activated carbon: Impact of water vapor," *Chemical Engineering Journal*, vol. 353, pp. 197–207, 2018.

[149] M. Plaza, S. García, F. Rubiera, J. Pis, and C. Pevida, "Post-combustion co2

capture with a commercial activated carbon: comparison of different regeneration strategies," *Chemical Engineering Journal*, vol. 163, no. 1-2, pp. 41–47, 2010.

[150] N. Querejeta, M. G. Plaza, F. Rubiera, and C. Pevida, "Water vapor adsorption on biomass based carbons under post-combustion co2 capture conditions: Effect of post-treatment," *Materials*, vol. 9, no. 5, p. 359, 2016.

[151] D. Xu, P. Xiao, J. Zhang, G. Li, G. Xiao, P. A. Webley, and Y. Zhai, "boneffects of water vapour on co2 capture with vacuum swing adsorption using activated car," *Chemical engineering journal*, vol. 230, pp. 64–72, 2013.

[152] P. D. Sullivan, B. R. Stone, Z. Hashisho, and M. J. Rood, "Water adsorption with hysteresis effect onto microporous activated carbon fabrics," *Adsorption*, vol. 13, no. 3-4, pp. 173–189, 2007.

[153] M. Gray, M. G. Johnson, M. I. Dragila, and M. Kleber, "Water uptake in biochars: The roles of porosity and hydrophobicity," *Biomass and Bioenergy*, vol. 61, pp. 196–205, 2014.

[154] T. Kinney, C. Masiello, B. Dugan, W. Hockaday, M. Dean, K. Zygourakis, and R. Barnes, "Hydrologic properties of biochars produced at different temperatures," *Biomass and Bioenergy*, vol. 41, pp. 34–43, 2012.

[155] K. Kameyama, T. Miyamoto, and Y. Iwata, "The preliminary study of water-

retention related properties of biochar produced from various feedstock at different pyrolysis temperatures," *Materials*, vol. 12, no. 11, p. 1732, 2019.

[156] Q. Fang, B. Chen, Y. Lin, and Y. Guan, "Aromatic and hydrophobic surfaces of wood-derived biochar enhance perchlorate adsorption via hydrogen bonding to oxygen-containing organic groups," *Environmental science & technology*, vol. 48, no. 1, pp. 279–288, 2014.

[157] L. Leng, H. Huang, H. Li, J. Li, and W. Zhou, "Biochar stability assessment methods: a review," *Science of the total environment*, vol. 647, pp. 210–222, 2019.

[158] M. F. Aller, "Biochar properties: Transport, fate, and impact," *Critical reviews in environmental science and technology*, vol. 46, no. 14-15, pp. 1183–1296, 2016.

[159] M. Ahmad, A. U. Rajapaksha, J. E. Lim, M. Zhang, N. Bolan, D. Mohan, M. Vithanage, S. S. Lee, and Y. S. Ok, "Biochar as a sorbent for contaminant management in soil and water: a review," *Chemosphere*, vol. 99, pp. 19–33, 2014.

[160] M. S. Shafeeyan, W. M. A. W. Daud, A. Houshmand, and A. Shamiri, "A review on surface modification of activated carbon for carbon dioxide adsorption," *Journal of Analytical and Applied Pyrolysis*, vol. 89, no. 2, pp. 143–151, 2010.

[161] A. E. Creamer and B. Gao, "Carbon-based adsorbents for postcombustion co2 capture: a critical review," *Environmental science & technology*, vol. 50, no. 14, pp. 7276–7289, 2016.

[162] Y. Wang, Y. Zhou, C. Liu, and L. Zhou, "Comparative studies of co2 and ch4 sorption on activated carbon in presence of water," *Colloids and Surfaces A: Physicochemical and Engineering Aspects*, vol. 322, no. 1-3, pp. 14–18, 2008.

[163] M. Plaza, A. González, F. Rubiera, and C. Pevida, "Evaluation of microporous biochars produced by single-step oxidation for postcombustion co2 capture under humid conditions," *Energy Procedia*, vol. 63, pp. 693–702, 2014.

[164] M. G. Plaza, I. Duran, N. Querejeta, F. Rubiera, and C. Pevida, "Experimental and simulation study of adsorption in postcombustion conditions using a microporous biochar. 2. h2o, co2, and n2 adsorption," *Industrial & Engineering Chemistry Research*, vol. 55, no. 24, pp. 6854–6865, 2016.

[165] B. Y. Sadasivam and K. R. Reddy, "Quantifying the effects of moisture content on transport and adsorption of methane through biochar in landfills," in *Geoenvironmental Engineering*, pp. 191–200, 2014.

[166] J. K. Brennan, K. T. Thomson, and K. E. Gubbins, "Adsorption of water in activated carbons: effects of pore blocking and connectivity," *Langmuir*, vol. 18, no. 14, pp. 5438–5447, 2002.

[167] H. La, J. P. A. Hettiaratchi, and G. Achari, "The influence of biochar and compost mixtures, water content, and gas flow rate, on the continuous adsorption of methane in a fixed bed column," *Journal of environmental management*, vol. 233, pp. 175–183, 2019.

[168] Y.-C. Chiang, Y.-J. Chen, and C.-Y. Wu, "Effect of relative humidity on adsorption breakthrough of co2 on activated carbon fibers," *Materials*, vol. 10, no. 11, p. 1296, 2017.

[169] E. Shayan, V. Zare, and I. Mirzaee, "Hydrogen production from biomass gasification; a theoretical comparison of using different gasification agents," *Energy Conversion and management*, vol. 159, pp. 30–41, 2018.

[170] M. A. Salam, K. Ahmed, N. Akter, T. Hossain, and B. Abdullah, "A review of hydrogen production via biomass gasification and its prospect in bangladesh," *International journal of hydrogen energy*, vol. 43, no. 32, pp. 14944–14973, 2018.

[171] A. Arregi, M. Amutio, G. Lopez, J. Bilbao, and M. Olazar, "Evaluation of thermochemical routes for hydrogen production from biomass: A review," *Energy conversion and management*, vol. 165, pp. 696–719, 2018.

[172] I. N. Zaini, Y. Gomez-Rueda, C. G. López, D. K. Ratnasari, L. Helsen, T. Pretz, P. G. Jönsson, and W. Yang, "Production of h2-rich syngas from

excavated landfill waste through steam co-gasification with biochar," *Energy*, vol. 207, p. 118208, 2020.

[173] Y. A. Situmorang, Z. Zhao, P. An, T. Yu, J. Rizkiana, A. Abudula, and G. Guan, "A novel system of biomass-based hydrogen production by combining steam bio-oil reforming and chemical looping process," *Applied Energy*, vol. 268, p. 115122, 2020.

[174] B. Pandey, Y. K. Prajapati, and P. N. Sheth, "Recent progress in thermochemical techniques to produce hydrogen gas from biomass: a state of the art review," *International Journal of Hydrogen Energy*, vol. 44, no. 47, pp. 25384–25415, 2019.

[175] Q. Hu and C.-H. Wang, "Insight into the fe2o3/cao-based chemical looping process for biomass conversion," *Bioresource technology*, vol. 310, p. 123384, 2020.

[176] Z. Hu, Z. Miao, H. Chen, J. Wu, W. Wu, Y. Ren, and E. Jiang, "Chemical looping gasification of biochar to produce hydrogen-rich syngas using fe/ca-based oxygen carrier prepared by coprecipitation," *Journal of the Energy Institute*, vol. 94, pp. 157–166, 2021.

[177] S. Doong, "Membranes, adsorbent materials and solvent-based materials for syngas and hydrogen separation," in *Functional Materials for Sustainable Energy Applications*, pp. 179–216, Elsevier, 2012.

[178] F. V. Lopes, C. A. Grande, and A. E. Rodrigues, "Activated carbon for hydrogen purification by pressure swing adsorption: Multicomponent breakthrough curves and psa performance," *Chemical Engineering Science*, vol. 66, no. 3, pp. 303–317, 2011.

[179] J. A. Delgado, V. Águeda, M. Uguina, J. Sotelo, P. Brea, and C. A. Grande, "Adsorption and diffusion of h2, co, ch4, and co2 in bpl activated carbon and 13x zeolite: evaluation of performance in pressure swing adsorption hydrogen purification by simulation," *Industrial & Engineering Chemistry Research*, vol. 53, no. 40, pp. 15414–15426, 2014.

[180] M. Yavary, H. Ale Ebrahim, and C. Falamaki, "Competitive adsorption equilibrium isotherms of co, co2, ch4, and h2 on activated carbon and zeolite 5a for hydrogen purification," *Journal of Chemical & Engineering Data*, vol. 61, no. 10, pp. 3420–3427, 2016.

[181] K. Jordal, R. Anantharaman, T. A. Peters, D. Berstad, J. Morud, P. Nekså, and R. Bredesen, "High-purity h2 production with co2 capture based on coal gasification," *Energy*, vol. 88, pp. 9–17, 2015.

[182] B. Silva, I. Solomon, A. M. Ribeiro, U.-H. Lee, Y. K. Hwang, J.-S. Chang, J. M. Loureiro, and A. E. Rodrigues, "H2 purification by pressure swing adsorption using cubtc," *Separation and Purification Technology*, vol. 118, pp. 744–756, 2013.

[183] P. Brea, J. Delgado, V. I. Águeda, and M. A. Uguina, "Comparison between mof utsa-16 and bpl activated carbon in hydrogen purification by psa," *Chemical Engineering Journal*, vol. 355, pp. 279–289, 2019.

[184] M. J. Regufe, J. Tamajon, A. M. Ribeiro, A. Ferreira, U.-H. Lee, Y. K. Hwang, J.-S. Chang, C. Serre, J. M. Loureiro, and A. E. Rodrigues, "Syngas purification by porous amino-functionalized titanium terephthalate mil-125," *Energy & Fuels*, vol. 29, no. 7, pp. 4654–4664, 2015.

[185] Y. Park, J.-H. Kang, D.-K. Moon, Y. S. Jo, and C.-H. Lee, "Parallel and series multi-bed pressure swing adsorption processes for h2 recovery from a lean hydrogen mixture," *Chemical Engineering Journal*, vol. 408, p. 127299, 2021.

[186] D.-K. Moon, D.-G. Lee, and C.-H. Lee, "H2 pressure swing adsorption for high pressure syngas from an integrated gasification combined cycle with a carbon capture process," *Applied Energy*, vol. 183, pp. 760–774, 2016.

[187] D.-K. Moon, Y. Park, H.-T. Oh, S.-H. Kim, M. Oh, and C.-H. Lee, "Performance analysis of an eight-layered bed psa process for h2 recovery from igcc with pre-combustion carbon capture," *Energy Conversion and Management*, vol. 156, pp. 202–214, 2018.

[188] D.-K. Moon, Y.-H. Kim, H. Ahn, and C.-H. Lee, "Pressure swing adsorption process for recovering h2 from the effluent gas of a melting incinerator," *In-*

dustrial & Engineering Chemistry Research, vol. 53, no. 40, pp. 15447–15455, 2014.

[189] G. Bang, D.-K. Moon, J.-H. Kang, Y.-J. Han, K.-M. Kim, and C.-H. Lee, "High-purity hydrogen production via a water-gas-shift reaction in a palladium-copper catalytic membrane reactor integrated with pressure swing adsorption," *Chemical Engineering Journal*, vol. 411, p. 128473, 2021.

[190] M. Cavali, N. L. Junior, R. de Almeida Mohedano, P. Belli Filho, R. H. R. da Costa, and A. B. de Castilhos Junior, "Biochar and hydrochar in the context of anaerobic digestion for a circular approach: An overview," *Science of The Total Environment*, p. 153614, 2022.

[191] W. Zhao, H. Yang, S. He, Q. Zhao, and L. Wei, "A review of biochar in anaerobic digestion to improve biogas production: performances, mechanisms and economic assessments," *Bioresource Technology*, vol. 341, p. 125797, 2021.

[192] Y. Shen, J. L. Linville, M. Urgun-Demirtas, R. P. Schoene, and S. W. Snyder, "Producing pipeline-quality biomethane via anaerobic digestion of sludge amended with corn stover biochar with in-situ co2 removal," *Applied energy*, vol. 158, pp. 300–309, 2015.

[193] O. Ławińska, A. Korombel, and M. Zajemska, "Pyrolysis-based municipal solid waste management in poland—swot analysis," *Energies*, vol. 15, no. 2, p. 510, 2022.

.

Chapter 3

Wood biochar as a point source CO_2 adsorbent-impact of humidity on performance

A modified version of this chapter has been submitted for publication; Z.Ghanbarpour Mamaghani, K. Hawboldt, S. MacQuarrie, M. Katz. Wood biochar as a point source CO_2 adsorbent-impact of humidity on performance.

Abstract

Adsorption of carbon using biobased materials is a sustainable approach to point source carbon capture and storage, particularly if the biomass is a "waste" and the adsorbent can then be re-used in soils. In this work, biochar derived from fast pyrolysis of softwood residues (sawdust) was investigated as a CO_2 adsorbent under humid conditions to determine the effect of water on biochar adsorption performance. Dry and wet adsorption experiments were run at concentrations of CO_2 between 20-80 vol.% (balanced with N_2) at 20 °C. Water concentrations were set by saturating the N_2 stream and resulted in 0.5-1.8 vol.% (relative humidity of 20-80%). For the dry gas experiments, the adsorption capacities doubled (0.83-1.98 mmol/g) as the CO_2 concentration increased from 20% to 80%. The capacity did not change between wet and dry experiments for 20, 40, and 60 vol.% CO_2; however, at 80 vol.% CO_2, the adsorption capacity increased by 38% for the "wet" gas from the dry gas. This is potentially due to carbonates formed due to CO_2 dissolution/reaction in water. The adsorption time was not impacted by the range of water concentrations studied. The Avrami kinetic model best represented the rate of adsorption in both dry and wet conditions. The fact that neither the biochar adsorption capacity nor its adsorption rate was negatively impacted by water shows that biochar can be a promising option for stack gases, which contain water vapor. However, more experiments at higher temperatures are required.

Keywords: CO_2 capture; Biomass-based adsorbents; Biochar; Humid conditions;

Breakthrough analysis; Adsorption kinetics

3.1 Introduction

Stationary (point) sources of CO_2, including flue gas from power plants, gasification, and other types of stacks, are contributors to climate change [1]. These flue gases contain water, which can impact the removal performance of the physical adsorbent used in carbon capture [2, 3]. For instance, zeolites show a high affinity toward water; therefore, CO_2 adsorption capacity decreases when water is present [3]. Adding a pre-treatment step to remove the water before CO_2 adsorption is an option, but it increases the costs. Another option is using adsorbents that are not negatively affected by water [2]. Carbon-based adsorbents are generally hydrophobic [3, 4]. Given this, it may be possible to create opportunistic cooperative effects between water vapor and CO_2 gas by forming carbonates that might lead to improvement of CO_2 adsorption on biochar [3].

Biochar is a carbon-based material produced by the thermochemical conversion of biomass [5–7]. Biochar characteristics can differ depending on its feedstock and production conditions resulting in variation in adsorption ability [5]. For instance, in a study by Manyà et al. [8], CO_2 adsorptions on biochars produced from pyrolysis of vine shoots and wheat straw (at 600 and 500 °C, respectively) were tested in dry and wet conditions. The CO_2 adsorption capacity did not change for the vine shoot biochars, but the capacity reduced for the wheat straw biochar in wet conditions.

The water content of the feed gas was 11.2 vol.% in feed gas (100% relative humidity). In a related study, CO_2 capacity was almost doubled when the adsorbent was wetted beforehand (ratio of water to the solid particles=1.65). In addition, the adsorption isotherm changed from a type I isotherm with a plateau to an S-shaped isotherm with an inflection point. The behavior was attributed to the formation of HCO_3^- from the dissolution of CO_2 in water [9]. Another study on olive stone biochars showed that CO_2 adsorption capacity did not change in wet conditions when the adsorption test was less than eleven minutes. This was attributed to the slow water rate of adsorption relative to CO_2. However, beyond eleven minutes, the CO_2 adsorption decreased [10].

The importance of producing an adsorbent that performs well in both wet and dry conditions is evident; however, limited study has been done in this area [5]. To address this data gap, in this work, biochar was first produced from softwood biomass in an auger reactor via fast pyrolysis. Pyrolysis was performed at 500 °C and a feed flow of approximately 1 kg/hr under a slight vacuum. Biochar and softwood characterization were performed to gather information on the elemental composition, surface properties, functional groups, and thermal stability. To examine the CO_2 adsorption performance of the biochar in the presence of water, a series of dynamic adsorption experiments were performed under both dry and wet conditions using an automated breakthrough analyzer (ABR) at 20 °C and 1.2 bar. Dry adsorption experiments were performed with different mixtures of CO_2 and N_2 (20-80 vol.% of

CO_2 balanced with N_2). For the wet experiments, the N_2 gas was first saturated with water at 20 °C in a water bath before being mixed with CO_2 and entering the adsorption column resulting in relative humidity of 20-80 vol.% or water concentrations of 0.5-1.8 vol.%. The breakthrough curves were collected, and the adsorption capacities and rates were compared for the dry and wet experiments to understand the impact of water vapor on CO_2 adsorption on biochar.

3.2 Materials and Methods

3.2.1 Preparation of biochar

Softwood shavings were supplied by Sexton Lumber Co sawmill, Bloomfield, NL, Canada. The shavings were grounded to <2 mm and dried at 75 °C overnight prior to pyrolysis. The ground and dried softwood was then pyrolyzed in an auger reactor (Figure 3.1) at 500 °C. The softwood was fed to the auger reactor at a flow rate of 1 kg/hr (Figure 3.1: 100 and 101). The woody biomass went through fast pyrolysis inside the reactor and biochar was collected (Figure 3.1: 305). The gases produced were cooled down in two condensers and the condensable portion was collected as bio-oil (Figure 3.1: 405). A detailed explanation of the auger reactor operation is presented elsewhere [11].

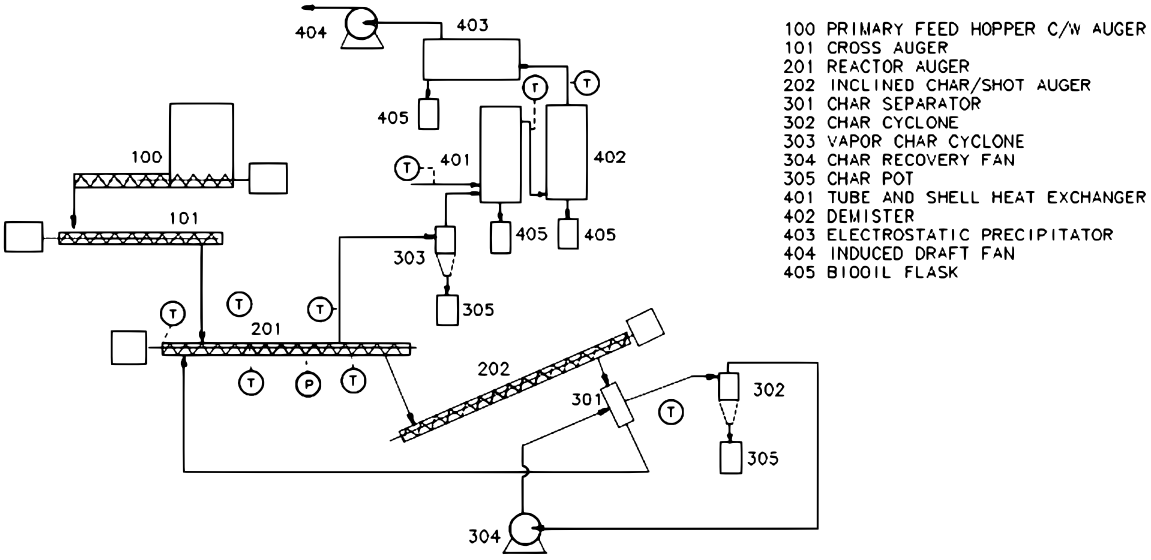

Figure 3.1: Process flow diagram (PFD) of the auger reactor

3.2.2 Characterisation of the biochar

The produced biochar and its softwood feedstock were characterized by different characterization techniques. Elemental analysis was conducted using a Perkin-Elmer 2400 Series II CHN/O analyzer at the Aquatic Research Cluster (ARC) at Memorial University of Newfoundland. The samples were placed in an oven at 60 °C for 24 hours to remove any moisture. Samples were then weighed using a Mettler Toledo UMT 2 balance into tin capsules (Isomass, Calgary, AB), folded to ensure there was no sample loss, and placed into a 96-well plate. The plate was stored in a desiccator until the samples could be run on the Perkin Elmer 2400 Series II CHN/O analyzer. The carbon, nitrogen, and hydrogen weight fractions were determined and the oxygen portion of the biochar was then calculated by deducting the wt.% of C, N, and H

from the total elements.

A Micrometrics Tristar II plus device was used to assess the surface properties of the biochar and the softwood by measuring the N_2 accessible adsorption isotherm at 77 K. Approximately 0.3 g of samples were put into a sample tube and degassed at 120 °C for 24 hours under N_2 gas flow. The Brunauer–Emmett–Teller (BET) theory [12] was applied to determine the biochar and softwood specific surface areas. The desorption data were analyzed using Barrett-Joyner-Halenda (BJH) [13] method to gather information on the total pore volume and average pore width of the biochar and softwood.

Fourier-Transform Infrared Spectroscopy (FTIR) was conducted at Cape Breton University, Sydney, NS, Canada, using a Nicolet Summit Mid-infrared FTIR spectrometer (KBr method). The FTIR diagrams show the percentage of transmittance for the wavenumber of 4000-600 cm^{-1} with a resolution of 4 cm^{-1}. This analysis was performed to collect data on biochar and softwood functional groups.

Thermogravimetric analysis (TGA) was performed at Cape Breton University using an Sdt Q600 V20 9 Build 20 Thermal Gravimetric Analyzer. TGA and Derivative Thermogravimetry (DTG) plots from this analysis were used to analyze the thermal stability via mass reduction as a function of temperature. Approximately 18 mg of the biochar was heated from 30 to 800 °C with a heating rate of 10 °C under a constant 20 mL/min flow of N_2 gas. The mass was recorded as temperature increased. The TGA diagram shows the decomposition profiles of the biochar and sawdust at

the temperature range of 30-800 °C, while the DTG diagram shows the rate of mass loss at different temperatures.

3.2.3 Molecular modeling

In this work, the adsorption behavior of CO_2 on the biochar surface was studied by computational methods by calculating the binding energy. The purpose was to use the molecular model as a tool in assessing the impact of water on CO_2 adsorption in an effort to optimize the approach to experiments. Gaussian 09 [14] software (on ACENET) was used to calculate the binding energy of CO_2 on biochar both under dry condition and when water was present.

The molecules were first drawn using Avogadro software [15] and the geometries were optimized using the Avogadro built-in optimization tool. DFT simulations in Gaussian 09 were done based on B3LYP theory and 6-31G(d) basis set as the previous research with our setup (same feedstock and production conditions) has shown that the calculations with this theory had great accuracy for our biochar and shorter running time compared to other theories [16]. The Gaussian 09 input file was generated in Avogadro software. The first set of calculations run by Gaussian was Geometry optimization for each molecule. This was a more thorough optimization calculation compared to the optimization conducted in Avogadro software. After securing the optimized geometry, the frequency calculation was run in the Gaussian 09 software using the keywords opt and freq. The energy of the structure was then

derived from the results. For calculating the binding energy, the same procedure was performed for CO_2 molecule, and the adsorbent/CO_2 molecules close to each other. The initial distance of the CO_2 molecule to the adsorbent molecule was approximately set to the summation of the Van der Waals radius of the carbon atom (1.85 Å) of CO_2 and the atom on the surface of the biochar that was closest to the CO_2 [16] (This was the initial assumption as the distances changed during the geometry optimization).

The binding energy was calculated using the equation below [17]:

$$E_{\text{ads}} = E_{\text{biochar-adsorbate}} - (E_{\text{biochar}} + E_{\text{adsorbate}}) \tag{3.1}$$

E_{ads} is the adsorption energy, and $E_{\text{biochar-adsorbate}}$, E_{biochar}, and $E_{\text{adsorbate}}$ are the energies of the adsorbate adsorbed on biochar, biochar, and adsorbate, respectively (kJ/mol). The lower (more negative) number indicates a higher affinity between adsorbent and adsorbate [17].

To calculate the binding energy in wet experiments, the same calculations were reperformed in the Gaussian 09 software. However, this time the keyword SCRF was added to the Gaussian 09 input file. This keyword requests the calculations to be done in the presence of a solvent. The solvent is determined by adding the following phrase to the input file: "SCRF=(Solvent=Water)". Therefore, the amount of water and the specification of the feed stream could not be specified. Still, it could provide a rough estimation of how the water presence can impact the binding energy.

The binding energies for CO_2 and biochar calculated with and without the pres-

ence of water as a solvent were then compared to study the possible increase/ decrease of the affinity of the biochar toward CO_2 in the presence of water.

A second set of simulations was performed to study the impact of carbonates, which could potentially form due to the water. As noted above, CO_2 dissolves in water could form HCO_3^- [18]. Therefore, the binding energy calculations were also performed for HCO_3^- and biochar functional groups, and the results were compared with that of the CO_2.

3.2.4 Adsorption experiments

Adsorption experiments were performed using an automated breakthrough analyzer (ABR) supplied by Hiden Isochema, Warrington, U.K. (Figure 3.2). Approximately 0.5 g of the biochar sample was placed in the fixed bed column (2 cc). Before each run, the samples were degassed using helium through valve B at 10 mL/min at 120 °C and 1.2 bar for 2 hours. The system was then cooled to 20 °C before the CO_2 mixtures (20-80 vol.% CO_2 balanced with N_2) were fed to the bed (the overall flow of the feed gas was 5 mL/min in all experiments). The experiments were performed at 20 °C and 1.2 bar. In the wet experiments, the N_2 flow first traveled through a water bath (at 20 °C) to saturate the N_2 with water. CO_2 and N_2 were then mixed and fed to the adsorption bed, and the composition of the effluent gas was determined using the mass spectrometer. All the experiments were performed twice.

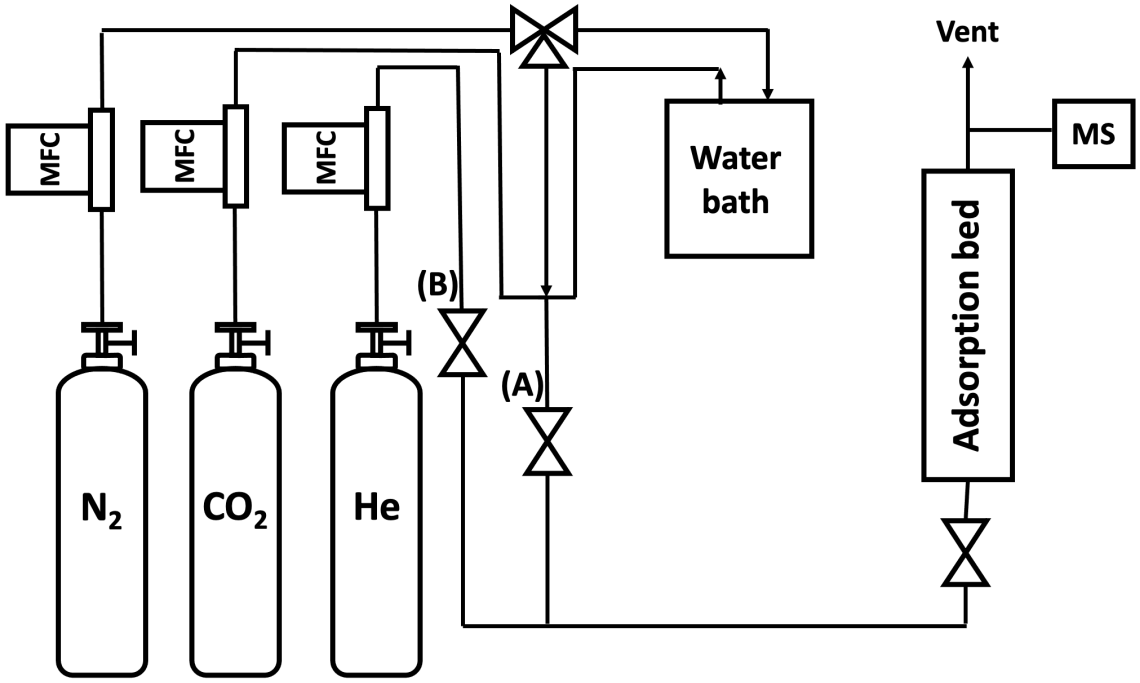

Figure 3.2: A schematic diagram of the adsorption experiment setup

3.2.4.1 Adsorption breakthrough and capacity

Breakthrough curves are created by plotting the normalized outlet concentration of an adsorption system against time. The time at which the ratio of the outlet concentration to the initial concentration is at 0.05 is considered the breakthrough time [19]. Capacity at any time (t) can be calculated using the area above the breakthrough curve by the following equation:

$$q = \frac{F \times C_0 \times \int_0^t (1 - \frac{C}{C_0})\, dt}{m} \tag{3.2}$$

Where q is the adsorption capacity (mmol/g), F is the volumetric flowrate of the feed gas (mL/min), C/C_0 is the ratio of the outlet to inlet concentration at time t (min), and m is the biochar mass (g).

3.2.4.2 Adsorption kinetic

In the design and scale-up of adsorption systems, the rate of adsorption must be established. Different kinetic models are available in the literature for analyzing the rate behavior of CO_2 adsorption on biochar. Three kinetics models, the pseudo-first-order, the pseudo-second-order, and the Avrami model, were tested to describe the rate of CO_2 adsorption under dry and wet conditions.

The pseudo-first-order kinetic model assumes that the adsorption rate is proportional to the free active adsorption sites on the adsorbent and is typically suitable to describe the physical adsorptions (physisorption) [20]. The equation is written as

[21]:

$$q = q_e[1 - exp(-k_1 t)] \tag{3.3}$$

Where q and q_e are the capacity at each time (t) and the capacity at the equilibrium, respectively (mmol/g). k_1 is the pseudo-first-order kinetic rate constant (min^{-1}).

The pseudo-second-order kinetic model assumes that the adsorption rate is proportional to the square of the number of adsorption sites and is mostly used to describe the chemical adsorption process (chemisorption) [22]. The equation is written as:

$$q = \frac{q_e^2 k_2 t}{1 + q_e k_2 t} \tag{3.4}$$

Where q and q_e are the capacity at each time (t) and the capacity at the equilibrium, respectively (mmol/g). k_2 is the pseudo-second-order kinetic rate constant (g $mmol^{-1}min^{-1}$).

The Avrami model [23] is able to predict rates under hybrid physisorption/chemisorption adsorption [20], and is written as:

$$q = q_e[1 - exp(-(k_A t)^n] \tag{3.5}$$

Where q and q_e are the capacity at each time (t) and the capacity at the equilibrium, respectively (mmol/g). k_A is the Avrami kinetic constant (min^{-1}), and n is

the Avrami exponent. The Avrami exponent is proposed to allow the model to be used under adsorption processes where phase changes may be occurring [22].

3.3 Results and discussions

3.3.1 Characterization of the absorbent

3.3.1.1 Elemental analysis

The elemental analyses for biochar and its softwood feedstock are presented in Table 3.1. As expected, hydrogen and oxygen fractions have decreased from feedstock to biochar, resulting in carbonization. Elemental ratios of biochar relative to the feedstock can be used to evaluate quality. A decrease in the H/C ratio is an indicator of an increase in aromaticity, while a decrease in O/C ratio indicates an increase in stability due to the loss of oxygen-containing functional groups [24]. Both the H/C and O/C ratios are lower in biochar compared to softwood. This confirms that a more stable aromatic structure is produced as the softwood decomposes during pyrolysis [25]. The elemental composition and other physicochemical properties of the biochar in this work are compared to published works in Table 3.2. It can be noted that all the woody biochars have a notable fraction of carbon atoms, which is resulted from the hydrogen and oxygen lost during the thermochemical degradation process.

Table 3.1: Biochar and softwood surface area, pore volume, pore width, elemental compositions and ratios

Sample	Surface area[a]	Total pore volume[b]	Average pore width[c]	Elemental composition (wt%)				Elemental ratios	
	m^2/g	cm^3/g	nm	C	H	N	O[d]	H/C	O/C
Biochar	48.852	0.026	7.092	73.176	2.919	0.184	23.721	0.040	0.324
Softwood	1.313	0.005	5.922	47.70	5.68	0.01	46.62	0.12	0.98

[a] BET surface area

[b] BJH desorption cumulative pore volume

[c] BJH desorption average pore width

[d] Calculated by difference

Table 3.2: Physicochemical properties of woody biochars produced at different temperatures

Feedstock	Temperature	Pyrolysis	Surface area[a]	Total pore volume[b]	Elemental composition (wt%)			Ref.
	°C	type	m^2/g	cm^3/g	C	H	N	
Softwood	500	Fast	48.852	0.026	73.176	2.919	0.184	This work
Hickory wood	450	Slow	12.90	NA	83.62	3.24	0.17	[26]
Gliricidia sepium tree	500	Slow	76.30	0.010	73.29	3.55	0.84	[27]
Mix softwood	600-700	NA	25.2	NA	68.2	3.66	0.51	[28]
Pine softwood	500-650	NA	4.9	NA	71.2	2.88	0.91	[28]
Eucalyptus sawdust	550	Slow	23.1	NA	83.80	2.75	0.82	[29]
Mixed wood sawdust	550	Fast	4.30	NA	49.81	2.57	0.53	[29]
Peach branch	550	Fast	1.72	NA	63.87	3.03	1.30	[29]
Wood bark	500	Slow	13.6	NA	84.84	3.13	1.83	[30]

[a] BET surface area

[b] BJH desorption cumulative pore volume

3.3.1.2 Surface area analysis

Biochar and softwood surface area, pore volume, and average pore size are presented in Table 3.1. The loss of the volatiles and the decomposition during pyrolysis has left biochar with a higher surface area and pore volume than its softwood precursor. The surface area increased from 1.313 to 48.852 m^2/g. Comparing the surface area of the biochar studied in this work to other woody biochars in Table 3.2 show that biochars surface areas vary depending on the feed source and production process; however, the biochar produced in this study is in the same range as the other woody biochars.

3.3.1.3 FTIR analysis

FTIR analyses for the biochar and its softwood feedstock are presented in Figure 3.3. The wide peak at 3600-3000 cm^{-1} region in the softwood FTIR corresponds to O-H stretching [31]. The notable O-H stretching in the sawdust is mostly due to water. The peak is not that visible in biochar plot, due to the loss of moisture at high temperatures of biochar production. Also, the presence of other O-H containing functional groups, such as phenol and hydroxyl, are probably too low compared to other functional groups to be detected by the FTIR, considering the heterogeneity and non-transparency of the biochar [32]. The peak at 2950-2800 cm^{-1} represents alkyl C-H [33]. The disappearance of this peak in the biochar FTIR diagram is likely due to the loss of alkyl groups as a result of aromatization. The peak at

approximately 1020 cm^{-1} in the softwood FTIR plot corresponds to aliphatic ether C-O stretching. The peaks at approximately 1500 cm^{-1} and 1260 cm^{-1} are due to aromatic C=C ring stretching and aromatic C-H stretching, respectively. The small peaks in the regions of 1400-1300 cm^{-1} are due to aliphatic CH_3 and CH_2 deformations. The peaks at approximately 800 and 860 cm^{-1}, noted in both softwood and biochar plots, represent aromatic C-H deformation. The peak at the 630 cm^{-1} of the softwood FTIR diagram corresponds to phenol O-H deformation, and its absence in the biochar IR confirms the lack of O-H stretching in the 3000 cm^{-1} region. The peaks at 1570 cm^{-1} and 1700 cm^{-1}, present in both biochar and softwood diagram, correspond to C=C stretching and aromatic carbonyl/carboxyl C=O stretching, respectively [34]. The overall comparison of the biochar and softwood FTIR suggests that most of the aliphatic function groups are lost during the pyrolysis resulting in a biochar structure with a higher density of aromatic groups.

3.3.1.4 TGA analysis

TGA and DTG plots for the biochar and the softwood feedstock, are presented in Figure 3.4. Thermal degradation of woody biomass generally shows three major stages [35]. The first step, initiating at approximately 200 °C, represents moisture and light volatiles loss [35]. The dried softwood mass loss was 1.96% up to 200 °C. The second step in woody biomass decomposition is devolatilization in the temperature range of 200-600 °C [35]. The main carbohydrates associated with woody biomass

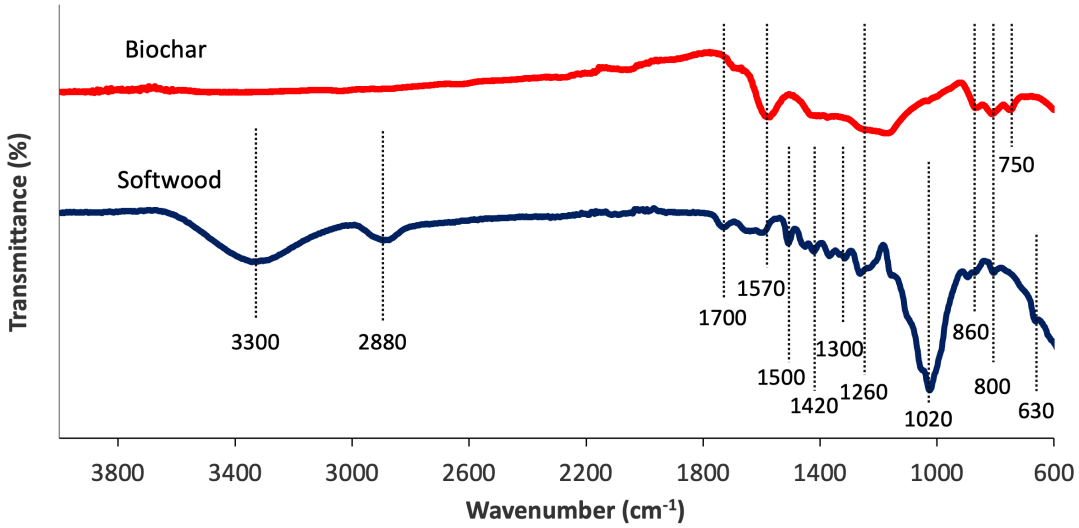

Figure 3.3: FTIR plots for the biochar and the softwood feedstock

degrade during this step. Hemicellulose decomposition initiates at approximately 220 °C and is completed by approximately 315 °C, and cellulose decomposition occurs from 315-400 °C. Lignin degrades over a wide range of temperatures from 160 °C up to 900 °C [31]. The softwood lost 87.4% of its mass during this step. The last step of woody biomass degradation is the stabilization stage, in which the rate of mass loss is lowered, and the mass becomes almost constant [35]. Toward the end of the TGA process ($\sim$ 800 °C), the softwood lost approximately 92.83%. Over the same ranges, biochar behavior is quite different, losing approximately double the mass up to 200 °C (2.39%). The cellulose and hemicellulose were already degraded in the pyrolysis process; therefore, biochar mass loss was approximately 13% from 200-600 °C. The biochar lost approximately 17% of its mass in the temperature range of

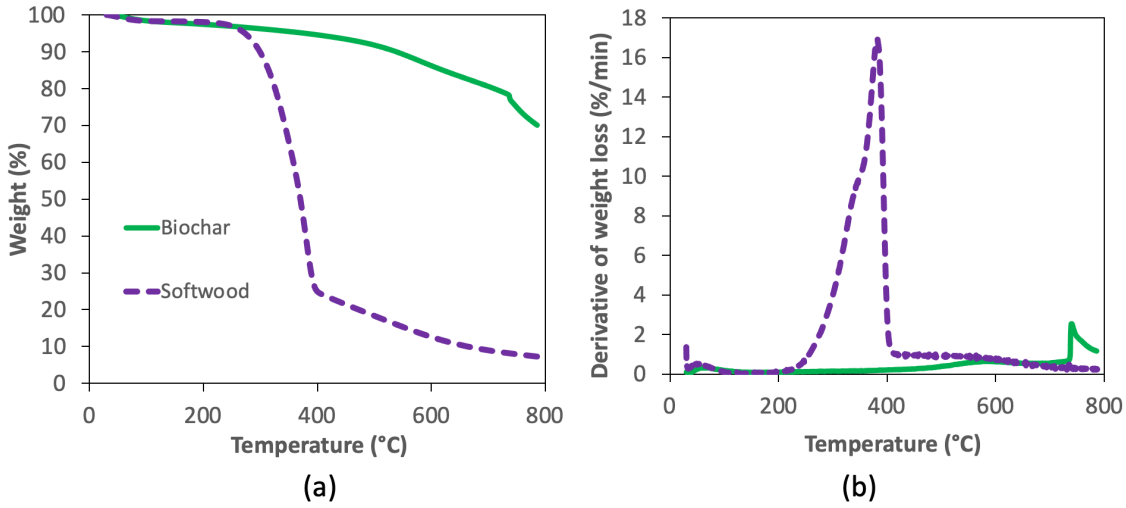

Figure 3.4: TGA (a) and DTG (b) plots for the biochar and the softwood feedstock

600-800 °C leading to a total mass loss of approximately 30% up to 800 °C. From the DTG plot, it can be noted that the rate of mass loss for the biochar increased after 500 °C, peaking at approximately 750 °C due to the degradation of lignin fraction that decomposes at temperatures higher than the biochar production temperature (500 °C).

3.3.2 Molecular Modeling

Previous work in our lab (the same feedstock and production conditions) established a biochar molecule structure based on work by Zhao et al. [36]. The structure was validated as a suitable representation of the biochar produced in our lab by comparing the elemental composition and the surface functional groups [32]. Figure 3.5 shows the biochar molecular structure based on the model presented by Zhao et al. [36].

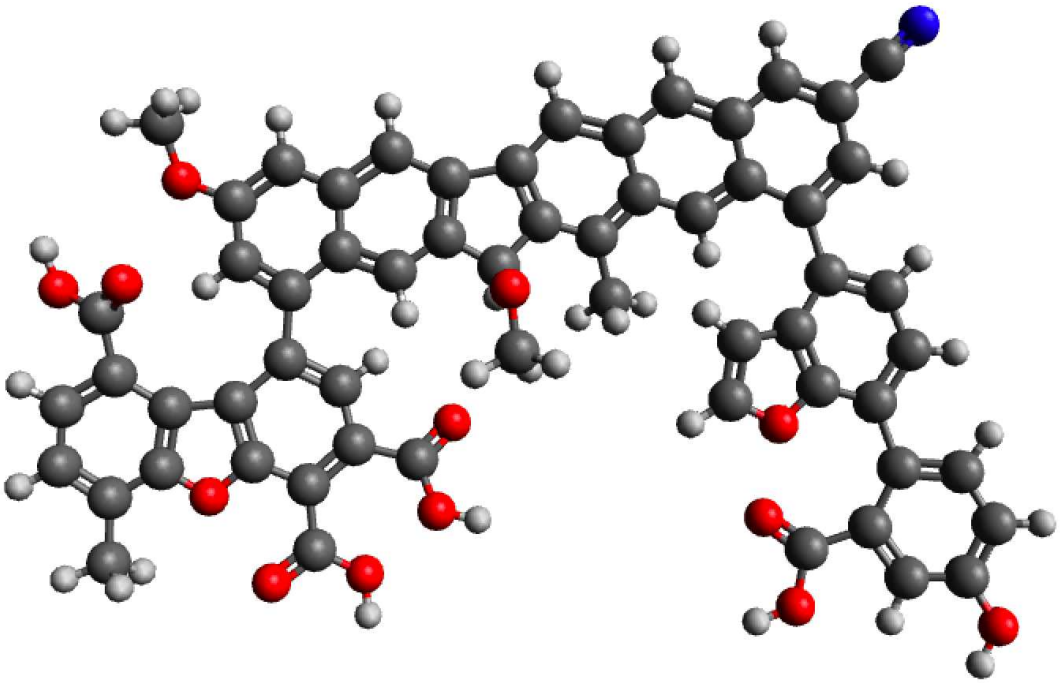

Figure 3.5: Biochar molecular structure based on the model presented by Zhao et al. [36]

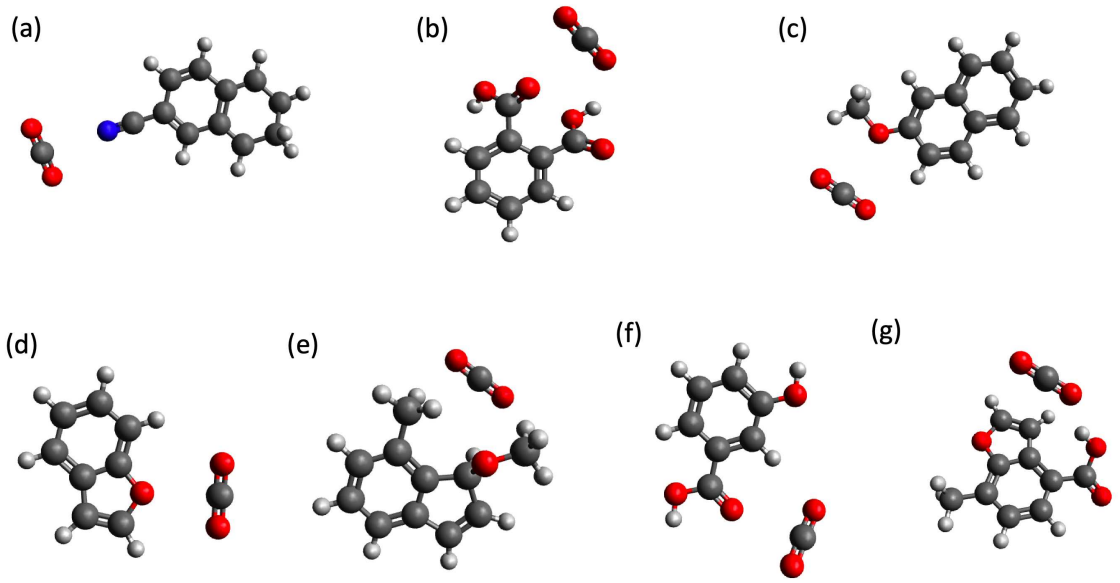

Figure 3.6: Seven functional groups put close to CO_2 as a part of binding energy calculations: (a) nitrile (b) carboxyl (c) ether (d) furan (e) methyl ether (f) carboxyl hydroxyl (g) carboxyl furan. Nitrogen atoms are colored blue, oxygen atoms are colored red, carbon atoms are colored dark gray, and hydrogen atoms are colored light gray

Calculating the binding energy using the whole biochar structure and CO_2 was not feasible due to the excessive calculation time and memory required for convergence. As such, seven different functional groups of the biochar surface were selected, based on occurrence in multiple biochar samples tested, to examine the binding energies in dry and wet conditions. The seven functional groups (near CO_2 molecules) are shown in Figure 3.6.

The results from the energy calculations for CO_2 adsorption in dry, saturated

conditions (in the presence of solvent), and HCO_3^- (formed as the result of CO_2 dissolution/reaction with water) adsorption energy calculations are presented in Table 3.3. Negative binding energy indicates that the energy is released as the result of the adsorption. A lower (more negative) value, therefore, indicates the molecules higher affinity toward one another and stronger adsorption. It can be noted that binding energies with carboxyl are the most negative among functional groups for all three studied structures, meaning that carboxyl had the strongest adsorptions. Comparing dry and wet binding energies indicates that all of the functional groups other than carboxyl had higher binding energies and stronger adsorptions with CO_2 when water was present. The carboxyl group is extremely hydrophilic and highly polar, which is the reason the adsorption drops when water is present, i.e. water adsorbs or bonds to surface over CO_2 because of its hydrophilicity, causing its CO_2 binding energy to be higher in the presence of water (less affinity toward CO_2 in wet conditions). Functional groups such as ether and furan are hydrophobic and nonpolar, and Nitrile is hydro neutral [37]; therefore, water existence did not affect their affinity toward CO_2 negatively.

Comparing the adsorption energies of HCO_3^- and CO_2 with functional groups of biochar shows that the binding energy is much lower in value (higher energy) for HCO_3^-. This is due to the reactive nature of ions, where they are ready to donate their excess electrons and bond with other molecules. The modeling indicates CO_2 adsorption may increase when water is present, assuming HCO_3^- forms. It should be

Table 3.3: Calculated binding energies for different biochars functional groups in dry and wet conditions

Functional group	Binding energy (kJ/mol)		
	CO_2	CO_2 (wet)	HCO_3^-
Nitrile	-9.128	-10.533	-63.197
Carboxyl	-17.557	-15.296	-203.960
Ether	-12.410	-13.970	-44.186
Furan	-11.232	-13.122	-58.977
Methyl ether	-4.408	-9.932	-77.083
Carboxyl hydroxyl	-11.482	-13.428	-13.658
Carboxyl furan	-10.671	-14.308	-124.526

noted that this type of simulation is only a rough tool but can potentially reduce the number of experiments or focus of experiments.

3.3.3 Adsorption breakthrough and capacity

Breakthrough curves for the CO_2 adsorption under dry and partially saturated conditions are provided in Figure 3.7, and the breakthrough times are in Table 3.4. There was a 58% increase in the breakthrough time for 80 vol.% CO_2 under humid condi-

Table 3.4: Breakthrough times (C/C_0=0.05) for different dry and wet experiments

CO_2 (vol.%)	19.6	20	39.5	40	59.5	60	79.6	80
Relative humidity (%)	80	0	60	0	40	0	20	0
H_2O (vol.%)	1.8	0	1.4	0	0.9	0	0.5	0
Breakthrough time (min)	7.98	7.62	6.53	6.18	5.83	5.38	6.62	4.19

tions compared to dry conditions. Longer breakthrough time translates to a higher adsorption capacity [19]. Therefore, it would appear adsorption has been enhanced by wet conditions for 80 vol.% CO_2. This was not reflected at the lower CO_2 inlets.

The CO_2 adsorption capacities for the dry and wet experiments are presented in Table 4.3 (q_{exp}). The adsorption capacities mirror the breakthrough curves, where humid conditions did not impact capacity when inlet CO_2 is less than 80 vol.%. At 80 vol.% CO_2, the CO_2 adsorption capacity increased by 38% compared to the dry experiment.

As indicated above, the capacity increase for the CO_2 adsorption is potentially due to the formation of HCO_3^- as the result of the dissolution/reaction of CO_2 in water. The molecular modeling indicated a stronger potential for adsorption of HCO_3^- compared to CO_2. Carbonates (HCO_3^-) have a higher polarity compared to CO_2 molecules, which makes them attractive for polar sites on biochar, such as oxygen-containing functional groups (C-O/C=O) [38], resulting in a boost in the

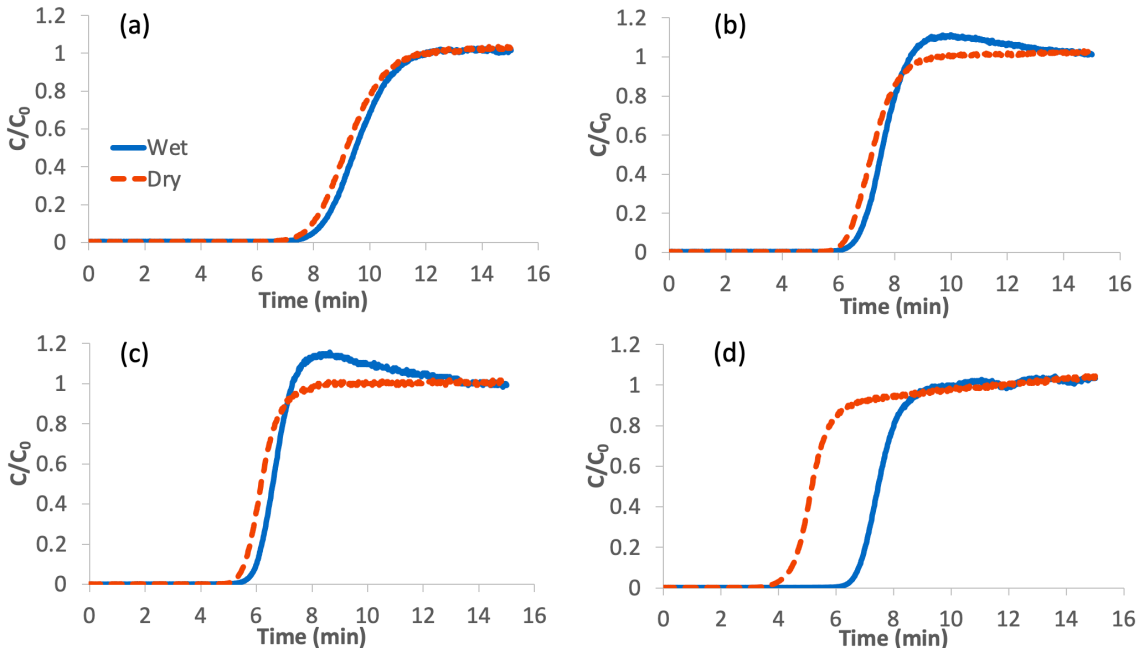

Figure 3.7: Breakthrough curves of biochar CO_2 adsorption under dry and wet conditions. Compositions (vol.%): (a) dry: CO_2/N_2:20%/80%; wet: $CO_2/N_2/H_2O$: 19.6%/78.6%/1.8%; (b) dry: CO_2/N_2: 40%/60%; wet: $CO_2/N_2/H_2O$: 39.5%/59.2%/1.4%; (c) dry: CO_2/N_2: 60%/40%; wet: $CO_2/N_2/H_2O$: 59.5%/39.6%/0.9%; (d) dry: CO_2/N_2: 80%/20%; wet: $CO_2/N_2/H_2O$: 79.6%/19.9%/0.5%.

adsorption capacity. The reason for the lack of impact at lower CO_2 inlets could be that even though carbonates could be forming, according to Henry's law, the higher the partial pressure of CO_2 in the feed gas would result in higher dissolved gas in the water. Therefore, at 80 vol.% CO_2 level, the concentration of HCO_3^- would be higher. From our results, it appears that for the HCO_3^- to have an observable impact on adsorption, a minimum CO_2 to water ratio (or partial pressure to water) is required. The minimum will vary depending on the system.

Although the capacities have approximately the same value for the first three experiments, a slight roll-up can be seen in the breakthrough curves of the experiments with 40% and 60% CO_2, which is more visible in the experiment with 60% of CO_2. Breakthrough curve roll-up happens when the outlet concentration exceeds the inlet concentration temporarily. The general cause for roll-up is when the initially adsorbed component is displaced by another component with a higher affinity to the adsorbent. Roll-ups can also happen during non-isothermal operations when the heat released during the adsorption of the heavier/ more strongly adsorbed component detaches the lighter/ more weakly adsorbed component [39]. In this work, the process was isothermal, so the second theory does not apply here. For the experiments with 40% and 60% CO_2 levels, initially, an additional amount of CO_2 may be adsorbed due to the formation of carbonates, but as the experiment proceeds the lower partial pressure in the gas phase (as CO_2 is adsorbed), results in water displacing the adsorbed CO_2, resulting in the same capacity as the dry tests. The

roll-up effect due to water has been reported in other works [40–42]. Due to the low concentration of CO_2 in the feed gas for the experiment with 20% CO_2 (lower partial pressure), the amount of CO_2 dissolved in the water was lower; therefore, if formed the carbonates were low enough not to influence the adsorption. In 80% CO_2, the higher partial pressure of CO_2 in the feed gas resulted in higher dissolved CO_2 in the water and the formation of enough carbonates to have an impact. The high partial pressure of CO_2 in the gas phase inhibited the evolution of adsorbed CO_2 back to the gas, which resulted in higher adsorption capacity compared to dry experiment.

Comparing the adsorption capacities for dry experiment and wet experiments separately (Table 4.3 and final capacities in Figure 3.9) indicates the impact of initial CO_2 initial concentration on the adsorption capacity. The adsorption capacity increased with the initial concentration of CO_2 under both dry and wet conditions as a result of a greater mass transfer driving force between the surface of the adsorbent and the gas flow.

3.3.4 Adsorption kinetics

The rate of adsorption capacity for dry and wet experiments at each CO_2 concentration level are presented in Figure 3.8. The adsorption rate is not affected by the presence of water. The adsorption rate plots for the first three experiments (20, 40, and 60 vol.%) are approximately the same. Small roll-ups can be noted in the kinetic plots of the wet experiments with 40 vol.% and 60 vol.% concentrations of

CO_2, which were also visible in their breakthrough curves as previously discussed. At 80 vol.% CO_2 inlet, there was a capacity increase during the wet experiments, which was discussed previously. However, the rate of adsorption was not impacted as noted by the slopes of the curves (Figure 3.8 (d)).

The adsorption rate plots of the (a) dry and (b) wet adsorption tests are presented in Figure 3.9. It can be noted that the increase in the initial concentration of CO_2 under both dry and wet conditions resulted in an increase in the driving force of the adsorption, and that caused an increase in the adsorption rate.

The fitted parameters of the three kinetic models tested are presented in Table 4.3. Judging from the correlation coefficient of the fitted models (Table 4.3), as well as the plots (Figure 3.10 and Figure 3.11), it is evident that the Avrami kinetic model fits the adsorption data for both dry and wet experiments the best. This shows that both physical and chemical interactions are involved in the adsorption of CO_2 on biochar under dry and wet conditions. The Avrami exponent (n) for all of the tests is higher than 1, which shows that CO_2 adsorption in both dry and wet experiments was heterogeneous, reflecting that the adsorption was not uniform over the surface [43]. This reflects the heterogeneous nature of the surface functional groups on the biochar.

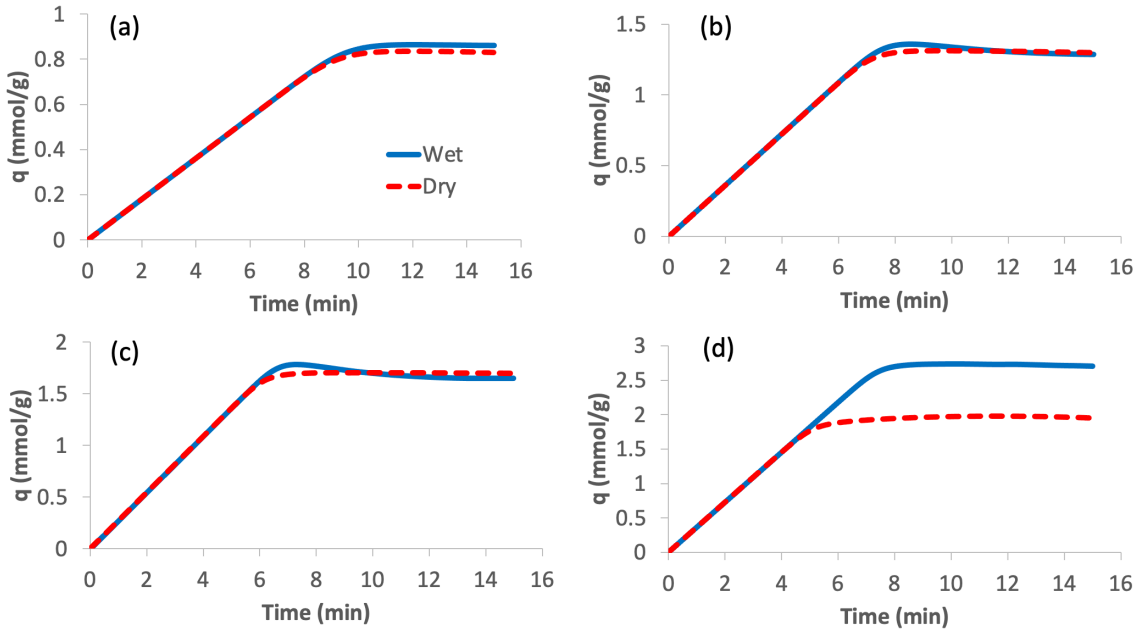

Figure 3.8: CO_2 adsorption rate plots of experiments under dry and wet conditions. Compositions (vol.%): (a) dry: CO_2/N_2:20%/80%; wet: $CO_2/N_2/H_2O$: 19.6%/78.6%/1.8%; (b) dry: CO_2/N_2: 40%/60%; wet: $CO_2/N_2/H_2O$: 39.5%/59.2%/1.4%; (c) dry: CO_2/N_2: 60%/40%; wet: $CO_2/N_2/H_2O$: 59.5%/39.6%/0.9%; (d) dry: CO_2/N_2: 80%/20%; wet: $CO_2/N_2/H_2O$: 79.6%/19.9%/0.5%.

Table 3.5: Fitted parameters of pseudo-first-order, pseudo-second-order, and Avrami kinetic models for the CO_2 adsorption on biochar in dry and wet conditions

CO_2	RH[a]	q_{exp}	Pseudo-first-order			Pseudo-second-order			Avrami			
(vol.%)	(%)	(mmol/g)	q_e	k_1	R^2	q_e	k_2	R^2	q_e	k_A	n	R^2
		±0.4 %	(mmol/g)	(min^{-1})		(mmol/g)	(g/mmol min)		(mmol/g)	(min^{-1})		
19.6	80	0.86	1.20	0.104	0.975	1.91	0.036	0.971	0.91	0.166	1.550	0.993
20	0	0.83	0.95	0.162	0.973	1.74	0.044	0.968	0.87	0.173	1.564	0.993
39.5	60	1.29	1.49	0.198	0.947	2.06	0.077	0.929	1.33	0.232	1.727	0.986
40	0	1.31	1.28	0.223	0.834	2.07	0.075	0.944	1.33	0.230	1.652	0.992
59.5	40	1.65	1.82	0.258	0.933	2.38	0.098	0.903	1.71	0.273	1.787	0.982
60	0	1.70	1.61	0.243	0.721	2.45	0.088	0.934	1.72	0.268	1.662	0.993
79.6	20	2.74	3.15	0.181	0.961	4.45	0.032	0.946	2.78	0.221	1.654	0.992
80	0	1.98	1.85	0.259	0.674	2.65	0.106	0.937	1.98	0.307	1.582	0.996

[a] Relative humidity

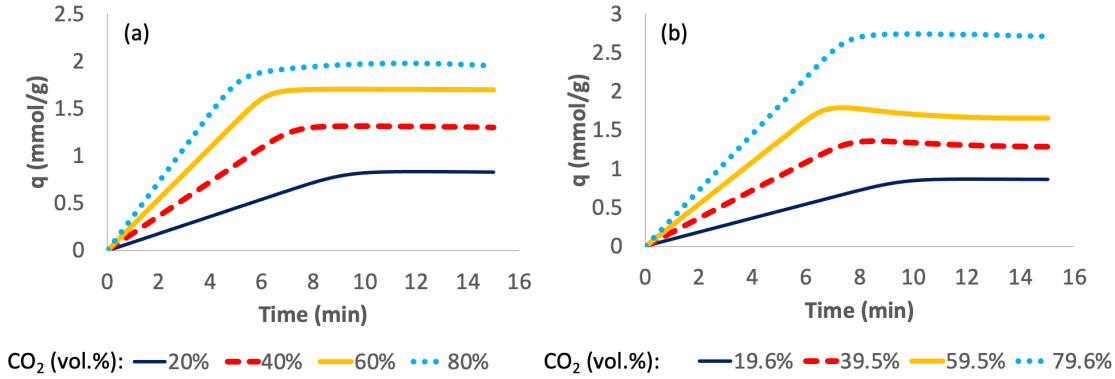

Figure 3.9: Adsorption rate plots of (a) dry and (b) wet experiments

3.4 Conclusions

The CO_2 capture capability of the biochars produced from softwood sawdust via fast pyrolysis at 500 °C was examined by performing dynamic adsorption tests using an automated breakthrough analyzer under dry and wet conditions. The adsorption capacities increased with an increase in the concentration of CO_2 in the feed gas for both dry and wet experiments, 0.83 mmol/g at 20 vol.% CO_2 to 1.98 mmol/g at 80 vol.% CO_2 for the dry experiments and 0.86 mmol/g at 19.6 vol.% CO_2 to 2.74 mmol/g at 79.6 vol.% CO_2 for the wet experiments. Comparing the adsorption capacities under dry and wet experiments, the water did not impact adsorption at CO_2 concentration between 20-60 vol.%. However, at 80 vol.% CO_2, the capacity increased by 38% when water was added to the system, which is attributed to carbonates formation from CO_2 dissolution/reaction in water. This result was also

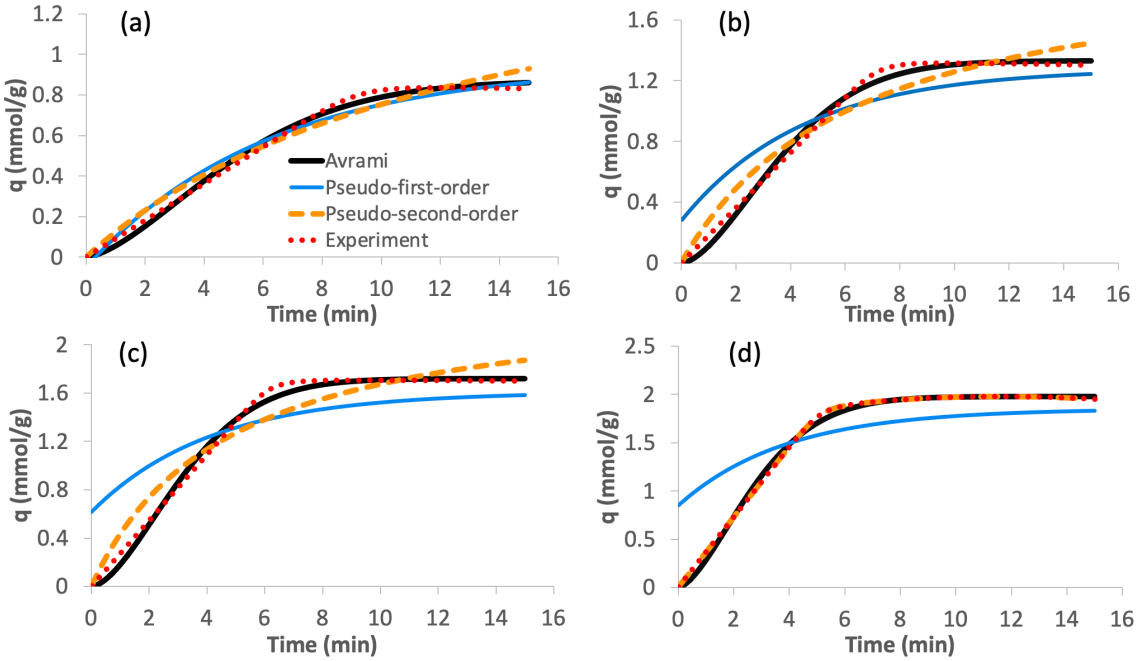

Figure 3.10: Experimental data and fitted kinetic models of CO_2 adsorption capacity over time on biochar under dry conditions. Compositions (vol.%): (a) CO_2/N_2:20%/80%; (b) CO_2/N_2: 40%/60%; (c) CO_2/N_2: 60%/40%; (d) CO_2/N_2: 80%/20%.

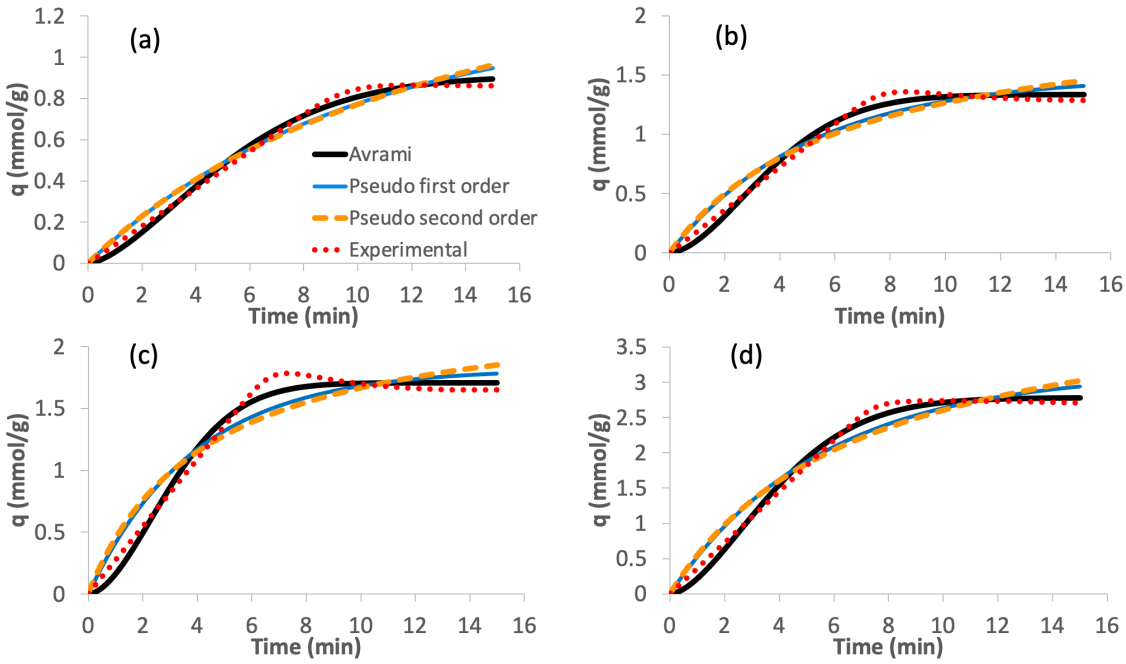

Figure 3.11: Experimental data and fitted kinetic models of CO_2 adsorption capacity over time on biochar under wet conditions. Compositions (vol.%): (a) $CO_2/N_2/H_2O$: 19.6%/78.6%/1.8%; (b) $CO_2/N_2/H_2O$: 39.5%/59.2%/1.4%; (c) $CO_2/N_2/H_2O$: 59.5%/39.6%/0.9%; (d) $CO_2/N_2/H_2O$: 79.6%/19.9%/0.5%.

confirmed by the approximation of binding energies using Gaussian software, where the binding energies of functional groups of biochar and HCO_3^- were much lower (higher energy released) than that of the CO_2.

The 80 vol.% CO_2 was the point of the increase in the adsorption capacity for this work; however, this minimum may be different for different biochars and water contents. It should be noted that the experiments in this work were performed at ambient temperature, whereas most stack gases are between 150-300 °C. Higher flue gas temperatures translate into higher water holding capacity. Flue gas from a natural gas-fired power plant and a coal-fired power plant contains approximately 18-20 vol.% and 8-10 vol.% H_2O, respectively [44]. Therefore, although this work has produced important baseline data on biochar CO_2 adsorption from wet gas streams, more research at higher temperatures where the gas can contain higher levels of water is necessary.

Adsorption kinetic is another parameter that needs to be studied to check the performance of biochar under dry and wet conditions. The adsorption rate study of dry and wet experiments separately showed that the adsorption rate increased with the increase of initial concentration of CO_2 in the feed gas as the result of the increase in the mass transfer driving force. Comparing the adsorption rate plots of CO_2 on biochar under dry and wet conditions showed that the presence of water did not impact the adsorption rate. Therefore, not only water presence did not have a negative impact on the adsorption capacity, but it also did not impact the

rate of adsorption. The Avrami kinetic model fits the adsorption data for both dry and wet experiments the best, which shows that both physical and chemical interactions are determining factors in the CO_2 adsorption on biochar. The Avrami exponent, which was above 1 for all of the tests, shows that the adsorption of CO_2 on the biochar was not homogeneous, meaning that CO_2 adsorption probability on different regions of biochar was not the same. This kinetic study in this work was on adsorption experiments at ambient temperature (20 °C). As the adsorption rate is highly dependent on the temperature, performing the dry and wet experiments at temperatures closer to that of real flue gas is necessary in future studies.

3.5 Acknowledgements

This research was funded by the Natural Science and Engineering Research Council of Canada (NSERC) and Memorial University of Newfoundland. The authors would like to express their deepest gratitude to Dr. Peter Franshman from ABRI-Tech Inc., Dr. Oliver Stueker and Dr. Serguei Vassiliev from ACENET, and Etienne Guinand and Dr. Mason Lawrence for their valuable contributions to this research work.

Bibliography

[1] G. Singh, J. Lee, A. Karakoti, R. Bahadur, J. Yi, D. Zhao, K. AlBahily, and A. Vinu, "Emerging trends in porous materials for co 2 capture and conversion," *Chemical Society Reviews*, vol. 49, no. 13, pp. 4360–4404, 2020.

[2] Y. Ji, X. Liu, H. Li, X. Jiao, X. Yu, and Y. Zhang, "Hydrophobic zif-8 covered active carbon for co2 capture from humid gas," *Journal of Industrial and Engineering Chemistry*, vol. 121, pp. 331–337, 2023.

[3] J. M. Kolle, M. Fayaz, and A. Sayari, "Understanding the effect of water on co2 adsorption," *Chemical Reviews*, vol. 121, no. 13, pp. 7280–7345, 2021.

[4] S. Sankaranarayanan, D. S. Lakshmi, S. Vivekanandhan, and C. Ngamcharussrivichai, "Biocarbons as emerging and sustainable hydrophobic/oleophilic sorbent materials for oil/water separation," *Sustainable Materials and Technologies*, vol. 28, p. e00268, 2021.

[5] Z. G. Mamaghani, K. A. Hawboldt, and S. MacQuarrie, "Adsorption of co2 using biochar-review of the impact of gas mixtures and water on adsorption," *Journal of Environmental Chemical Engineering*, p. 109643, 2023.

[6] J. Wang and S. Wang, "Preparation, modification and environmental application of biochar: A review," *Journal of Cleaner Production*, vol. 227, pp. 1002–1022, 2019.

[7] J. S. Cha, S. H. Park, S.-C. Jung, C. Ryu, J.-K. Jeon, M.-C. Shin, and Y.-K. Park, "Production and utilization of biochar: A review," *Journal of Industrial and Engineering Chemistry*, vol. 40, pp. 1–15, 2016.

[8] J. J. Manyà, D. García-Morcate, and B. González, "Adsorption performance of physically activated biochars for postcombustion co2 capture from dry and humid flue gas," *Applied Sciences*, vol. 10, no. 1, p. 376, 2020.

[9] Y. Sun, Y. Wang, Y. Zhang, Y. Zhou, and L. Zhou, "Co2 sorption in activated carbon in the presence of water," *Chemical physics letters*, vol. 437, no. 1-3, pp. 14–16, 2007.

[10] M. Plaza, A. González, F. Rubiera, and C. Pevida, "Evaluation of microporous biochars produced by single-step oxidation for postcombustion co2 capture under humid conditions," *Energy Procedia*, vol. 63, pp. 693–702, 2014.

[11] S. Papari, K. Hawboldt, and R. Helleur, "Production and characterization of pyrolysis oil from sawmill residues in an auger reactor," *Industrial & Engineering Chemistry Research*, vol. 56, no. 8, pp. 1920–1925, 2017.

[12] S. Brunauer, P. H. Emmett, and E. Teller, "Adsorption of gases in multimolecular layers," *Journal of the American chemical society*, vol. 60, no. 2, pp. 309–319, 1938.

[13] E. P. Barrett, L. G. Joyner, and P. P. Halenda, "The determination of pore

volume and area distributions in porous substances. i. computations from nitrogen isotherms," *Journal of the American Chemical society*, vol. 73, no. 1, pp. 373–380, 1951.

[14] M. J. Frisch, G. W. Trucks, H. B. Schlegel, G. E. Scuseria, M. A. Robb, J. R. Cheeseman, G. Scalmani, V. Barone, B. Mennucci, G. A. Petersson, H. Nakatsuji, M. Caricato, X. Li, H. P. Hratchian, A. F. Izmaylov, J. Bloino, G. Zheng, J. L. Sonnenberg, M. Hada, M. Ehara, K. Toyota, R. Fukuda, J. Hasegawa, M. Ishida, T. Nakajima, Y. Honda, O. Kitao, H. Nakai, T. Vreven, J. A. Montgomery, Jr., J. E. Peralta, F. Ogliaro, M. Bearpark, J. J. Heyd, E. Brothers, K. N. Kudin, V. N. Staroverov, R. Kobayashi, J. Normand, K. Raghavachari, A. Rendell, J. C. Burant, S. S. Iyengar, J. Tomasi, M. Cossi, N. Rega, J. M. Millam, M. Klene, J. E. Knox, J. B. Cross, V. Bakken, C. Adamo, J. Jaramillo, R. Gomperts, R. E. Stratmann, O. Yazyev, A. J. Austin, R. Cammi, C. Pomelli, J. W. Ochterski, R. L. Martin, K. Morokuma, V. G. Zakrzewski, G. A. Voth, P. Salvador, J. J. Dannenberg, S. Dapprich, A. D. Daniels, Farkas, J. B. Foresman, J. V. Ortiz, J. Cioslowski, and D. J. Fox, "Gaussian09 Revision E.01." Gaussian Inc. Wallingford CT 2009.

[15] M. D. Hanwell, D. E. Curtis, D. C. Lonie, T. Vandermeersch, E. Zurek, and G. R. Hutchison, "Avogadro: an advanced semantic chemical editor, visualization, and analysis platform," *Journal of cheminformatics*, vol. 4, no. 1, pp. 1–17, 2012.

[16] H. Bamdad, S. Papari, S. MacQuarrie, and K. Hawboldt, "Study of surface heterogeneity and nitrogen functionalizing of biochars: Molecular modeling approach," *Carbon*, vol. 171, pp. 161–170, 2021.

[17] C. Chen, K. Xu, X. Ji, L. Miao, and J. Jiang, "Enhanced adsorption of acidic gases (co 2, no 2 and so 2) on light metal decorated graphene oxide," *Physical Chemistry Chemical Physics*, vol. 16, no. 22, pp. 11031–11036, 2014.

[18] H. Wang, J. Zeuschner, M. Eremets, I. Troyan, and J. Willams, "Stable solid and aqueous h2co3 from co2 and h2o at high pressure and high temperature," *Scientific Reports*, vol. 6, no. 1, pp. 1–8, 2016.

[19] M. K. Al Mesfer and M. Danish, "Breakthrough adsorption study of activated carbons for co2 separation from flue gas," *Journal of Environmental Chemical Engineering*, vol. 6, no. 4, pp. 4514–4524, 2018.

[20] F. Raganati, M. Alfe, V. Gargiulo, R. Chirone, and P. Ammendola, "Kinetic study and breakthrough analysis of the hybrid physical/chemical co2 adsorption/desorption behavior of a magnetite-based sorbent," *Chemical Engineering Journal*, vol. 372, pp. 526–535, 2019.

[21] S. K. Lagergren, "About the theory of so-called adsorption of soluble substances," *Sven. Vetenskapsakad. Handingarl*, vol. 24, pp. 1–39, 1898.

[22] N. A. Zubbri, A. R. Mohamed, N. Kamiuchi, and M. Mohammadi, "Enhance-

ment of co 2 adsorption on biochar sorbent modified by metal incorporation," *Environmental Science and Pollution Research*, pp. 1–21, 2020.

[23] M. Avrami, "Kinetics of phase change. i general theory," *The Journal of chemical physics*, vol. 7, no. 12, pp. 1103–1112, 1939.

[24] D. Chen, X. Yu, C. Song, X. Pang, J. Huang, and Y. Li, "Effect of pyrolysis temperature on the chemical oxidation stability of bamboo biochar," *Bioresource technology*, vol. 218, pp. 1303–1306, 2016.

[25] M. Ahmad, A. U. Rajapaksha, J. E. Lim, M. Zhang, N. Bolan, D. Mohan, M. Vithanage, S. S. Lee, and Y. S. Ok, "Biochar as a sorbent for contaminant management in soil and water: a review," *Chemosphere*, vol. 99, pp. 19–33, 2014.

[26] A. E. Creamer, B. Gao, and M. Zhang, "Carbon dioxide capture using biochar produced from sugarcane bagasse and hickory wood," *Chemical Engineering Journal*, vol. 249, pp. 174–179, 2014.

[27] A. Wathukarage, I. Herath, M. Iqbal, and M. Vithanage, "Mechanistic understanding of crystal violet dye sorption by woody biochar: implications for wastewater treatment," *Environmental geochemistry and health*, vol. 41, pp. 1647–1661, 2019.

[28] F. N. Mukome, X. Zhang, L. C. Silva, J. Six, and S. J. Parikh, "Use of chemical

and physical characteristics to investigate trends in biochar feedstocks," *Journal of agricultural and food chemistry*, vol. 61, no. 9, pp. 2196–2204, 2013.

[29] Y. Wang and R. Liu, "Comparison of characteristics of twenty-one types of biochar and their ability to remove multi-heavy metals and methylene blue in solution," *Fuel Processing Technology*, vol. 160, pp. 55–63, 2017.

[30] Y. Lee, J. Park, C. Ryu, K. S. Gang, W. Yang, Y.-K. Park, J. Jung, and S. Hyun, "Comparison of biochar properties from biomass residues produced by slow pyrolysis at 500 c," *Bioresource technology*, vol. 148, pp. 196–201, 2013.

[31] H. Yang, R. Yan, H. Chen, D. H. Lee, and C. Zheng, "Characteristics of hemicellulose, cellulose and lignin pyrolysis," *Fuel*, vol. 86, no. 12-13, pp. 1781–1788, 2007.

[32] H. Bamdad, *A theoretical and experimental study on biochar as an adsorbent for removal of acid gases (CO and HS)*. PhD thesis, Memorial University of Newfoundland, 2019.

[33] A. Krutof, H. Bamdad, K. Hawboldt, and S. MacQuarrie, "Co-pyrolysis of softwood with waste mussel shells: Biochar analysis," *Fuel*, vol. 282, p. 118792, 2020.

[34] R. Yin, R. Liu, Y. Mei, W. Fei, and X. Sun, "Characterization of bio-oil and bio-char obtained from sweet sorghum bagasse fast pyrolysis with fractional condensers," *Fuel*, vol. 112, pp. 96–104, 2013.

[35] A. Mukherjee, V. B. Borugadda, J. J. Dynes, C. Niu, and A. Dalai, "Carbon dioxide capture from flue gas in biochar produced from spent coffee grounds: Effect of surface chemistry and porous structure," *Journal of Environmental Chemical Engineering*, p. 106049, 2021.

[36] N. Zhao, Y. Lv, and X. Yang, "A new 3d conceptual structure modeling of biochars by molecular mechanic and molecular dynamic simulation," *Journal of Soils and Sediments*, vol. 17, no. 3, pp. 641–655, 2017.

[37] N. Sagawa and T. Shikata, "Are all polar molecules hydrophilic? hydration numbers of nitro compounds and nitriles in aqueous solution," *Physical Chemistry Chemical Physics*, vol. 16, no. 26, pp. 13262–13270, 2014.

[38] W. Suliman, J. B. Harsh, N. I. Abu-Lail, A.-M. Fortuna, I. Dallmeyer, and M. Garcia-Pérez, "The role of biochar porosity and surface functionality in augmenting hydrologic properties of a sandy soil," *Science of the Total Environment*, vol. 574, pp. 139–147, 2017.

[39] G. Li, P. Xiao, D. Xu, and P. A. Webley, "Dual mode roll-up effect in multicomponent non-isothermal adsorption processes with multilayered bed packing," *Chemical engineering science*, vol. 66, no. 9, pp. 1825–1834, 2011.

[40] I. Durán, N. Álvarez-Gutiérrez, F. Rubiera, and C. Pevida, "Biogas purification by means of adsorption on pine sawdust-based activated carbon: Impact of water vapor," *Chemical Engineering Journal*, vol. 353, pp. 197–207, 2018.

[41] D. Xu, P. Xiao, J. Zhang, G. Li, G. Xiao, P. A. Webley, and Y. Zhai, "boneffects of water vapour on co2 capture with vacuum swing adsorption using activated car," *Chemical engineering journal*, vol. 230, pp. 64–72, 2013.

[42] C. Shen and W. Worek, "Cosorption characteristics of solid adsorbents," *International journal of heat and mass transfer*, vol. 37, no. 14, pp. 2123–2129, 1994.

[43] X. Zhang, L. Cao, W. Xiang, Y. Xu, and B. Gao, "Preparation and evaluation of fine-tuned micropore biochar by lignin impregnation for co2 and vocs adsorption," *Separation and Purification Technology*, vol. 295, p. 121295, 2022.

[44] C. Song, W. Pan, S. T. Srimat, J. Zheng, Y. Li, Y.-H. Wang, B.-Q. Xu, and Q.-M. Zhu, "Tri-reforming of methane over ni catalysts for co2 conversion to syngas with desired h2/co ratios using flue gas of power plants without co2 separation," *Stud. Surf. Sci. Catal*, vol. 153, pp. 315–322, 2004.

Chapter 4

Evaluating the impact of CO in the gas mixture on CO_2 adsorption on biochar

A modified version of this chapter has been submitted for publication; Z. Ghanbarpour Mamaghani, K. Hawboldt, S. MacQuarrie, M. Katz. Evaluating the impact of CO in the gas mixture on CO_2 adsorption on biochar.

4.1 Abstract

Biochar capability in CO_2 adsorption has already been confirmed by multiple research works. However, CO_2 is never emitted as a pure gas; therefore, studying the impact of other components in the gas mixture on CO_2 adsorption on biochar is necessary. One of the components that is always co-released with CO_2 is CO. In this work, the affinity of biochar for CO and CO_2 was first predicted using molecular modeling binding energy calculations. The results suggested that CO_2 would be favored over CO for adsorption on biochar because of its stronger adsorption (higher released adsorption energy). The biochar adsorption of pure CO and CO_2 were then studied using batch and dynamic experiments, where the isotherm and kinetic models of the pure gas adsorptions were derived. Dual-site Langmuir isotherm fitted both of the gases equilibrium adsorption data the best, confirming the non-homogeneous surface of biochar. The Avrami kinetic model was the best-fitted model for the adsorption rate of the gases, which showed that both chemical and physical interactions were involved in the adsorption processes.

The results from molecular modeling matched the results from pure CO and CO_2 adsorption on biochar, as the capacity of pure CO_2 was more than three times greater than that of pure CO. The dynamic binary CO/CO_2 adsorption experiments with 10-90 vol.% CO_2 (balanced with CO), carried out at 20 °C, showed that although both of the gases were adsorbed on biochar when the adsorption bed was fresh, some of the CO molecules were later removed by the more favored CO_2 molecules to the

extent that for up to 50 vol.% CO, all of the CO molecules were removed by the CO_2 molecules, and the CO overall capacity was 0.

For examining the impact of temperature on CO_2 and CO adsorption on biochar, the pure CO and CO_2 along with three selected binary CO/CO_2 adsorption tests were repeated at 100 °C. The pure adsorption tests of the two gases on biochar at 100 °C suggested that although CO_2 adsorption capacity was negatively impacted by the temperature increase, CO adsorption capacity was not altered by the temperature. Results from binary adsorption tests at 100 °C confirmed that at 100 °C, more CO would adsorb on biochar at the same input levels of the two gases compared to 20 °C due to CO_2 decreased adsorption at higher temperatures.

Key words: CO_2 capture; Biomass-based adsorbents; Biochar; Mixture adsorption; Breakthrough analysis; Temperature impact

4.2 Introduction

The capture/separation of CO_2 from stationary sources via adsorption is used widely [1]. Biochar, produced from the thermochemical conversion of biomass, has demonstrated good CO_2 adsorption capacities and, when sourced from renewable feedstock (biomass residues), is potentially a more sustainable process compared to other common adsorbents [2–4]. The bulk of the research in biochar and CO_2 adsorption is focused on pure CO_2 or binary CO_2/N_2 mixtures [5]. However, flue gas emissions from different sources are never pure, but a mixture of different gas components [5]

and the other gases in the mixture could inhibit/enhance CO_2 adsorption, resulting in a lower/higher adsorption capacity [6]. As such, before the application of biochar in industrial settings, the effect of gas mixture on CO_2 adsorption must be assessed. One of the most common gases present in combustion or gasification emission is CO [7]. Traces of CO are found in power plant flue gases (as high as 400 ppbV (parts per billion by volume), as the result of incomplete combustion of fuels) [7], and CO is one of the main products released in syngas from gasification (the composition varies based on the feedstock and the process conditions, but it can have values as high as 27 vol.%) [5].

There are limited publications on carbon-based adsorbents (especially biochar) involving CO and CO_2. Wilson et al. [8] examined the adsorption of pure CO and CO_2 on three different activated carbons (BPL, Xtrusorb A754, and Xtrusorb HP115). Based on the pure gas studies, it was proposed in the co-adsorption, CO_2 will be favored over CO as the adsorbents showed a higher adsorption capacity and heat of adsorption for pure CO_2 compared to pure CO. The adsorbents capacities for pure CO_2 at pressures greater than 1 atm were approximately 5 times greater than pure CO, and at approximately 10 atm, the adsorbents pure CO_2 capacities were over 3 times greater than pure CO. The affinity of activated carbon for CO and CO_2 was analyzed by Monte Carlo simulation in research by Lithoxoos et al. [9]. In this study, pure CO and CO_2 adsorption on activated carbon was compared using the simulation, showing higher uptake (adsorption) of CO_2 molecules compared to CO.

Based on a review of the literature, there are no published experimental studies on the co-adsorption of CO and CO_2 on biochar. In this work, aside from pure CO and CO_2 adsorption on wood biochar, the co-adsorption of CO and CO_2 were examined using computational and experimental approaches.

The adsorption experiments for pure CO and CO_2 were conducted in a batch setup to obtain the pure adsorption isotherms and predict the adsorption isotherm of the binary mixture. The computational study served as the foundational framework prior to the dynamic adsorption experiments. For the computational study, the adsorptions of CO and CO_2 on biochar were simulated using molecular modeling, and the binding energies were calculated and compared. The dynamic adsorption experiments were then performed for pure CO and CO_2 and binary mixtures containing different levels of these two gases. The breakthrough curves were collected, and capacities were calculated for different trials to study the co-adsorption of CO and CO_2 on the wood biochar.

4.3 Materials and Methods

4.3.1 Preparation and characterization of biochar

Softwood shavings were provided by Sexton Lumber Co sawmill, Bloomfield, NL, Canada. The softwood was grounded to <2 mm and dried overnight at 75 °C. Biochar was produced via fast pyrolysis in an auger reactor under a slight vacuum

at 500 °C at 1 kg/hr of feed rate. Detailed descriptions of the production process and characterization of biochar are presented elsewhere [10].

4.3.2 Molecular modeling

The molecular modeling of the adsorption was conducted for two purposes: The previous work with the biochar produced from the same feedstock, setup, and operation conditions has confirmed the biochar affinity toward CO_2 [11]. However, it was unclear if CO would also adsorb on biochar surface. Therefore, the first purpose was to figure out if biochar had an affinity for CO. In addition, in the case of biochar having an affinity for both of the gases, CO could compete for adsorption sites. Therefore, the second purpose of molecular modeling in this work was to compare the adsorption affinities of the two gases on the biochar surface.

The molecular modeling was performed using the Gaussian 09 [12] software. The adsorbent and adsorbate molecules were first drawn and optimized separately using the Avogadro software [13]. The Gaussian calculations were then performed using the input files from the Avogadro software. The first set of calculations conducted in Gaussian software is optimization, and after reaching the optimized structure, frequency calculations are conducted. The energy of the structure was derived from the Gaussian output file. The same calculation steps were performed for the adsorbent and adsorbate molecules put close to each other. The initial distance was set to the sum of the Van der Waals radius of the two atoms in each of the molecules

that were closer to each other. For instance, if carbon dioxide was put close to a nitrogen group, the initial distance of the carbon (in CO_2) and nitrogen (in the nitrogen group) would be 1.85 Å (Van der Waals radius of C) + 1.54 Å (Van der Waals radius of N). It should be noted the initial distance changed during the optimization process. The binding energy was calculated using the following equation [14]:

$$E_{\text{ads}} = E_{\text{biochar-adsorbate}} - (E_{\text{biochar}} + E_{\text{adsorbate}}) \tag{4.1}$$

E_{ads} is the adsorption energy, and $E_{\text{biochar-adsorbate}}$, E_{biochar}, and $E_{\text{adsorbate}}$ are the energies of the adsorbate adsorbed on biochar, biochar, and adsorbate, respectively (kJ/mol). The lower value (higher absolute value) of E_{ads} means that larger energy is released during adsorption; therefore, the stronger the adsorption [14]. The binding energies of CO and CO_2 on biochar were calculated and compared to have a rough estimation of the affinity of biochar for these two components.

4.3.3 Adsorption isotherm

Adsorption isotherm, which is determined based on the adsorption equilibrium data, represents the interaction mechanism of the adsorbate and the adsorbent [15, 16]. An understanding of the adsorption mechanism is required for designing the adsorption systems [16]. Pure isotherm data are typically used to study the gas mixture isotherms since collecting the equilibrium data for the gas mixture adsorption can be challenging and time-consuming [17]. Adsorption equilibrium data points for the

pure gas adsorption data in a batch system were collected using a Micromeritics 3flex device. Approximately 0.5 grams of biochar were put in the sample tubes and degassed at 150 °C overnight under vacuum conditions. The adsorption data were then collected with pure CO and CO_2 at 20 °C (in the pressure range of approximately 0 to 100 kPa). The data were fitted to the adsorption isotherms to find the best model for describing the adsorption behavior of the pure gases.

4.3.3.1 Pure gas isotherm

There are various pure gas isotherm models in the literature. The Langmuir isotherms that is commonly used [18]:

$$q = \frac{q_{\mathrm{m}} K_{\mathrm{L}} P}{1 + K_{\mathrm{L}} P} \tag{4.2}$$

Where q (mmol/g) is the adsorption capacity, q_m (mmol/g) is the maximum adsorption capacity, K_L (1/kPa) is the inverse of Langmuir constant (the actual Langmuir constant is based on desorption), which is dependent on the temperature, P (kPa) is the pressure of the adsorbate. Langmuir isotherm considers the adsorbent to be homogeneous with identical adsorption sites. According to this theory, the adsorption is monolayer, meaning that each adsorption site can only adsorb a single molecule at a time, and the adsorbed molecules do not have any interactions with each other [19].

Another common pure gas adsorption isotherm used is the Freundlich isotherm.

This isotherm is a two-parameter isotherm like Langmuir but is suitable for multi-layered adsorption on heterogeneous surfaces [20]:

$$q = K_{\mathrm{F}} P^{\frac{1}{n}} \tag{4.3}$$

Where q (mmol/g) is the adsorption capacity, K_F (mmol/(g $kPa^{1/n}$)) is the Freundlich constant, P (kPa) is the pressure of the adsorbate, and n is another Freundlich constant. 1/n value between 0 and 1 shows favorable adsorption, while 1/n>1 shows unfavorable adsorption, and 1/n=1 shows irreversible adsorption [20].

Langmuir-Freundlich (Sips) isotherm is derived from the combination of Langmuir and Freundlich isotherms [21]:

$$q = q_{\mathrm{m}} \frac{(K_{\mathrm{LF}} P)^n}{1 + (K_{\mathrm{LF}} P)^n} \tag{4.4}$$

Where q (mmol/g) is the adsorption capacity, q_m (mmol/g) is the maximum adsorption capacity, K_{LF} is the isotherm coefficient (1/kPa), and P (kPa) is the pressure of the adsorbate. This isotherm can represent both Langmuir and Freundlich isotherms behaviors at the same time. The "n" is the heterogeneity index and can be between 0 and 1. If n=1, the equation will turn into the Langmuir equation, which shows that the adsorbent was homogeneous, while an n value lower than 1 shows the heterogeneity of the adsorbent [22].

As addressed before, Langmuir assumes a homogeneous surface for the adsorbents; however, a perfect homogeneous surface is an unrealistic assumption for most

of the adsorbents, particularly biochar. The Dual-site Langmuir isotherm model has been established to compensate for the heterogeneity of the surfaces by considering two different adsorption sites on the adsorbent surfaces:

$$q = q_{\mathrm{m1}} \frac{K_{\mathrm{L1}} P}{1 + K_{\mathrm{L1}} P} + q_{\mathrm{m2}} \frac{K_{\mathrm{L2}} P}{1 + K_{\mathrm{L2}} P} \tag{4.5}$$

Where q (mmol/g) is the adsorption capacity, q_{m1} (mmol/g) and q_{m2} (mmol/g) are the maximum adsorption capacities for site type 1 and type 2, respectively. K_{L1} (1/kPa) and K_{L2} (1/kPa) are the inverse of Langmuir coefficients for the two types of sites. P (kPa) is the pressure of the adsorbate.

4.3.3.2 Gas mixture isotherm

The Ideal Adsorbed Solution Theory (IAST) [23] is used to integrate the mixed gas adsorption isotherm from the pure gas adsorption isotherms. This theory considers the equilibrium between the adsorbed phase and the gas phase to resemble the equilibrium between liquid and gas phases. As such, in this theory, the equilibrium between the adsorbed phase and the gas phase follows Raoult's Law [24]. This theory can use the pure gas isotherms to generate the mixed gas adsorption isotherm. The general equations of this equation can be written as [24]:

$$\frac{1}{q_{\mathrm{t}}} = \sum_{i=1}^{N} \frac{x_{\mathrm{i}}}{q_{\mathrm{i}}} \tag{4.6}$$

Where q_t (mmol/g) is the total adsorbed capacity of all the components, q_i (mmol/g)

is the adsorption capacity for component i, and x_i is the mole fraction of component i in the adsorbed phase. The component i capacity can be written as [24]:

$$q_i = x_i/q_t \tag{4.7}$$

The IAST++ software [25] was used for deriving the mixture adsorption isotherm based on the best-fitted pure gas adsorption models.

4.3.4 Adsorption experiments

Adsorption experiments were performed, and the breakthrough curves were collected using an automated breakthrough analyzer (ABR) supplied by Hiden Isochema, Warrington, U.K. A schematic diagram of the setup is shown in Figure **??**. Approximately 0.5 grams of the biochar sample was put in the adsorption fixed bed (2 cc volume). In order to degas the biochar, the adsorption bed was purged with helium gas (through valve B) with a flow of 10 mL/min at 120 °C and 1.2 bar for two hours. The system was then cooled down to 20 °C, and different compositions of CO/CO_2 mixture were fed to the adsorption column. The concentrations of CO and CO_2 were varied from 0-100 vol.% at 20 °C and 1 bar (100% CO_2, 90%/10% CO_2/CO, 70%/30% CO_2/CO, 50%/50% CO_2/CO, 30%/70% CO_2/CO, 10%/90% CO_2/CO, 100% CO). The adsorption column outlet gas composition was analyzed using a mass spectrometer.

4.3.5 Adsorption breakthrough curve and capacity

The adsorption breakthrough curves (outlet to inlet concentration of the adsorbate vs time) were plotted. The adsorption capacity (at time t) of the dynamic adsorption experiments can be calculated using the area above the breakthrough curves using the equation below:

$$q = \frac{F \times C_0 \times \int_0^t (1 - \frac{C}{C_0})\, dt}{m} \tag{4.8}$$

Where q is the adsorption capacity (mmol/g), F is the volumetric flowrate of the feed gas (mL/min), C/ C_0 is the ratio of the outlet to inlet concentration at time t, and m is the biochar mass (g). The capacities from dynamic experiments of pure CO and CO_2, along with their various binary mixtures, were calculated and compared to study the co-adsorption of these two gases on the biochar surface.

4.3.6 Adsorption rate

The rate of the adsorption system is important as a suitable adsorbent needs to show an adequate adsorption rate to be feasible [26]. The rate of the adsorption is a determining factor in system sizing (capital cost) [27]. In this work, the adsorption data of CO and CO_2 were fitted to three different rate models: pseudo-first-order, pseudo-second-order, and Avrami to determine the model that best describes the adsorption rate.

The pseudo-first-order kinetic model can be written as [28]:

$$q = q_e[1 - exp(-k_1 t)] \tag{4.9}$$

Where q and q_e are the capacity at each time (t) and the capacity at the equilibrium, respectively (mmol/g). k_1 is the pseudo-first-order kinetic rate constant (min^{-1}). The pseudo-first-order theory assumes reversible adsorption [27], where the adsorption rate is proportional to the availability of the vacant sites [26].

The pseudo-second-order kinetic model considers the adsorption rate to be proportional to the square of the number of vacant sites on the adsorbent [26] and can be written as:

$$q = \frac{q_e^2 k_2 t}{1 + q_e k_2 t} \tag{4.10}$$

Where q and q_e are the capacity at each time (t) and the capacity at the equilibrium, respectively (mmol/g). k_2 is the pseudo-second-order kinetic rate constant (g mmol $^{-1}min^{-1}$). The pseudo-second-order kinetic model considers the chemical interactions to be the governing force in the adsorption [27].

Avrami kinetic model can be written as [29]:

$$q = q_e[1 - exp(-(k_A t)^n] \tag{4.11}$$

Where q and q_e are the capacity at each time (t) and the capacity at the equilibrium, respectively (mmol/g). k_A is the Avrami kinetic constant (min^{-1}), and n is the

Avrami exponent. The significant advantage of this kinetic model is that it can take both physical and chemical interactions in an adsorption system into account [30].

4.3.7 Impact of temperature on adsorption

The temperature at CO_2 emission sources are generally higher than ambient temperatures. For instance, the typical temperature of flue gas leaving a coal-fired power plant is in the range of 120-130 °C [31]. Adsorption temperature is an important factor that needs to be considered when designing the adsorption process [32]. For most gases, the adsorption capacity decreases with temperature increase due to the higher adsorbate vapor pressure and higher energy of the adsorbed phase molecules. This results in the adsorbed molecules to overcome the Van der Waals force between the adsorbent and the adsorbate and be released [33]. For this purpose, the dynamic adsorption of the pure CO and CO_2 were performed at different temperatures in the range of 20-100 °C. After studying the temperature effect on the pure gases, the adsorption experiments were repeated at 100 °C for three selected binary CO/CO_2 mixtures, and the results were compared to the tests at 20 °C.

4.4 Results and discussions

4.4.1 Molecular modeling

Due to biochar molecule complexity, calculating the binding energies for CO and CO_2 on biochar was not feasible (requiring extreme computational time and memory). Therefore, the binding energies of adsorption of CO and CO_2 on seven different and common functional groups of biochar [34] were calculated. Figure 4.1 is a visual of the CO molecule and the seven functional groups after the optimization.

The calculated binding energies for CO and CO_2 on different functional groups on biochar surface are presented in Table 4.1. The negative numbers show that the energy is released as the result of adsorption, and a lower number (higher absolute value) can translate to higher affinity. The binding energy of CO and CO_2 on all functional groups were negative, showing that the biochar has affinities for both of the gases. Carboxyl had the lowest binding energy (highest released energy) among all the functional groups, which shows its stronger affinity to both of the gases, while methyl ether has the highest binding energy (lowest released energy) for both gases. For all of the functional groups, the released energy (binding energy) was higher for CO_2 compared to CO, meaning that biochar would most likely show a higher affinity for CO_2 compared to CO when both components are present. The higher affinity of carbon-based adsorbents toward CO_2 compared to CO has been reported by both simulation and experimental methods in other research works [8, 9].

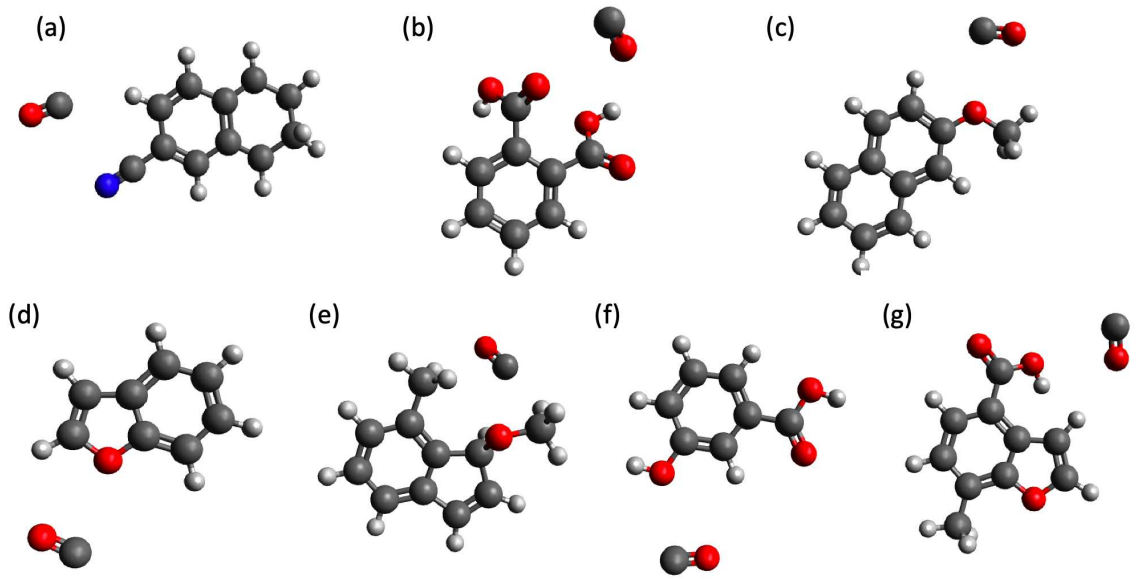

Figure 4.1: Seven functional groups put close to CO as a part of binding energy calculations: (a) nitrile (b) carboxyl (c) ether (d) furan (e) methyl ether (f) carboxyl hydroxyl (g) carboxyl furan. Nitrogen atoms are colored blue, oxygen atoms are colored red, carbon atoms are colored dark gray, and hydrogen atoms are colored light gray

Table 4.1: Calculated binding energy for seven different functional groups with CO and CO_2

Functional group	CO binding energy (kJ/mol)	CO_2 binding energy (kJ/mol)
Nitril	-6.743	-9.128
Carboxyl	-9.509	-17.557
Ether	-6.520	-12.409
Furan	-4.648	-11.232
Methyl ether	-3.064	-4.408
Carboxyl hydroxyl	-4.893	-11.482
Carboxyl furan	-6.294	-10.671

4.4.2 Adsorption isotherm

Different pure gas isotherms were studied for the CO and CO_2 adsorption equilibrium data and results are summarized in Table 4.2. The R^2 value of the isotherms suggests that the Dual-site Langmuir isotherm is the best representative for gases (Figure 4.2). This reflects the heterogeneity of the biochar surface.

The resulting IAST model of CO/CO_2 mixture at 100 kPa is presented in Figure 4.3. This figure shows the capacity for each of the gas components on biochar according to ideal adsorption solution theory at different levels of CO_2 based on the data from CO and CO_2 pure gas adsorption isotherms.

4.4.3 Pure gas dynamic adsorption experiments

Dynamic adsorption experiments for pure CO and pure CO_2 were performed using the ABR device, and breakthrough curves were collected. The breakthrough curves for pure CO and CO_2 are included in Figure 4.4 (Figure 4.4:(a) and Figure 4.4:(g)).

As noted in the plots, the CO and CO_2, the C/C_0 increased until a value of one is reached, where the adsorbent was saturated with the adsorbates, and no further adsorption occurs. Comparing the breakthrough curves of pure CO and CO_2 indicates that CO breaks through the adsorption bed faster than CO_2 (CO breakthrough time was 0.860 min and CO_2 breakthrough time was 4.568 min). The higher breakthrough time of an adsorbate translates to a higher affinity of the adsorbate and higher capacity (due to a longer time for the adsorbent to be saturated with the adsorbate)

Table 4.2: Fitted pure gas isotherm parameters for CO_2 and CO

Isotherm	Parameters	Adsorbate	
		CO_2	CO
Langmuir	q_m (mmol/g)	1.276	0.652
	K_L (1/kPa)	0.030	0.002
	R^2	0.998921	0.999984
Freundlich	K_F (mmol/(g $kPa^{1/n}$))	0.099	0.002
	n	1.979	1.131
	R^2	0.998909	0.999891
Langmuir-Freundlich	q_m (mmol/g)	1.897	0.815
	K_{LF} (1/kPa)	0.011	0.002
	n	0.754	0.973
	R^2	0.99999	0.999997
Dual-site Langmuir	q_{m1} (mmol/g)	0.281	0.078
	q_{m2} (mmol/g)	1.369	1.452
	K_{L1} (1/kPa)	0.151	0.008
	K_{L2} (1/kPa)	0.011	0.0007
	R^2	0.999995	0.999998

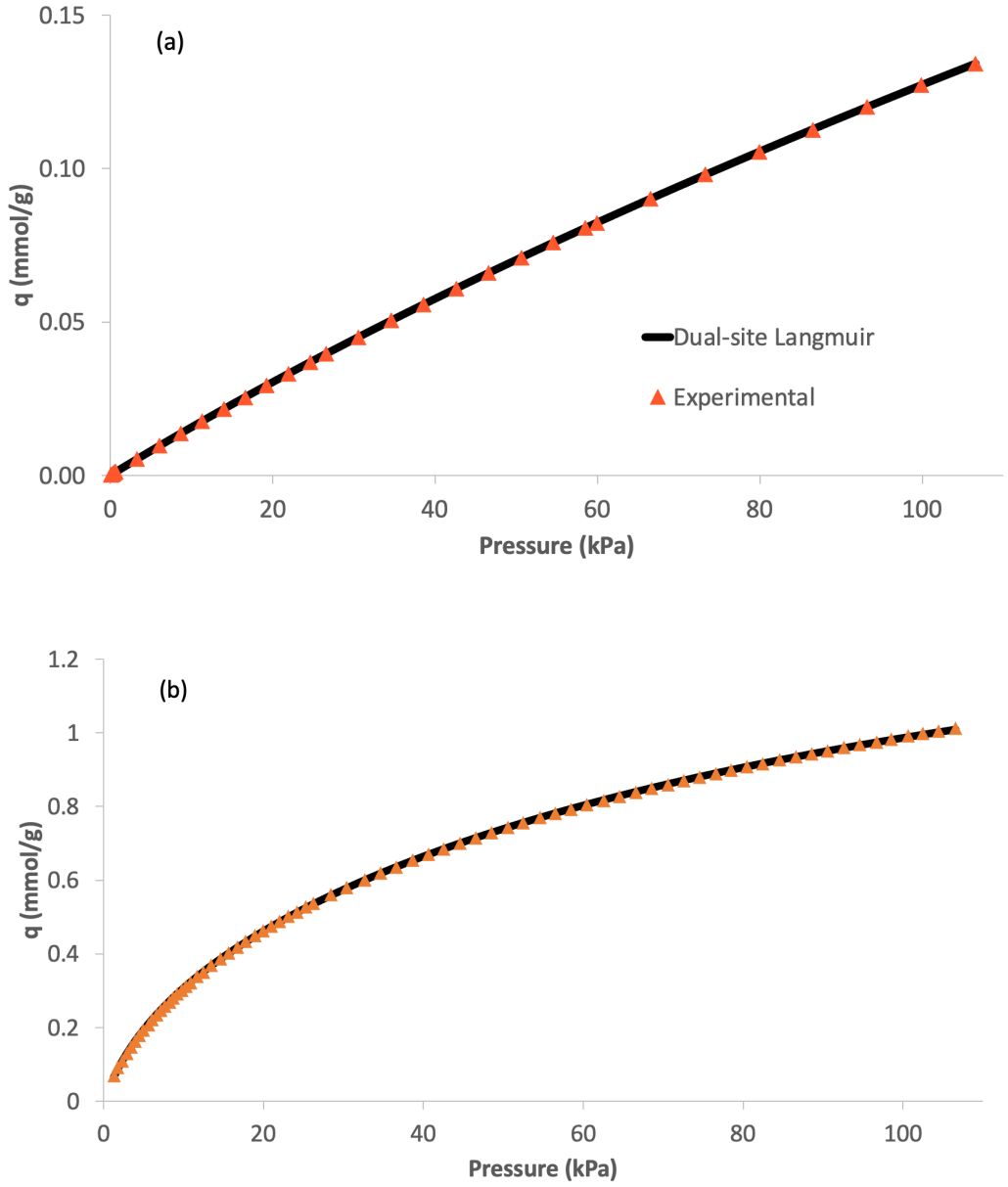

Figure 4.2: (a) CO and (b) CO_2 isotherms along with the fitted Dual-site Langmuir model

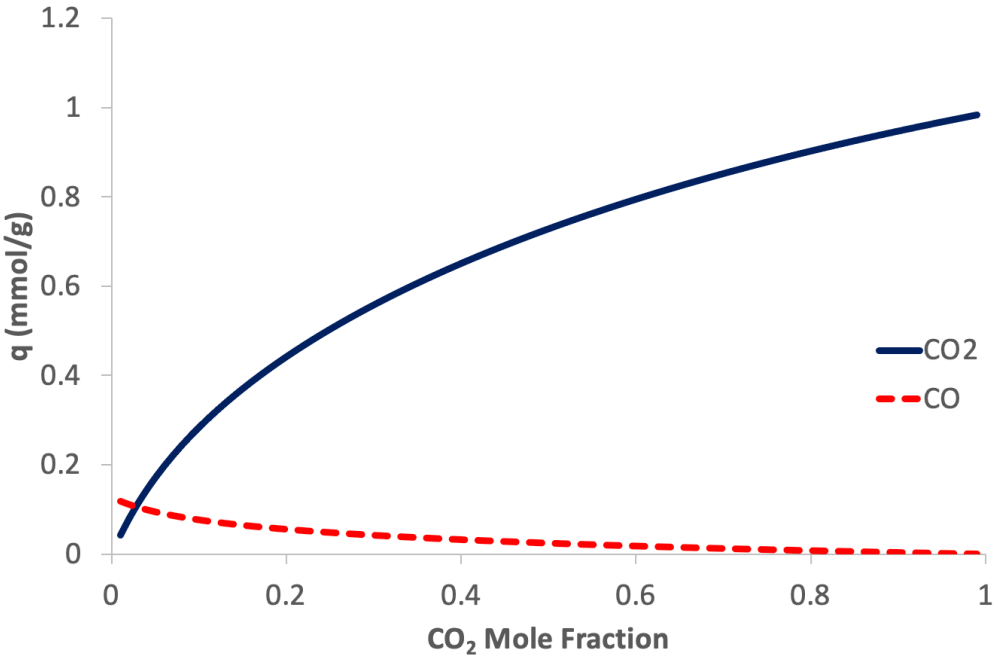

Figure 4.3: CO and CO_2 binary mixture adsorption isotherms derived from IAST

[35]. These results mirror the molecular modeling.

The capacities calculated using the breakthrough curves are presented in Table 4.4. The biochar adsorbs CO_2 and CO. However, the pure adsorption capacity of CO_2 (2.325 mmol/g) is much higher than CO (0.700 mmol/g). From our observations of the literature, there have not been any articles experimentally examining woody biochar pure CO adsorption, and as for CO_2, woody biochars produced in the range of 300-600 °C showed CO_2 adsorption capacities in the range of 0.379-2.4 mmol/g [3, 4, 11, 35]. This shows that the biochar in this work is on the high-end of adsorption of pure CO_2.

As mentioned in the materials and method section, the isotherms were derived from equilibrium adsorption data collected from the static experiments, while the dynamic adsorption experiments were performed in a continuous flow. Comparing the pure gas adsorption capacities from the static and dynamic adsorption experiments shows that the adsorbents showed higher capacities in the dynamic adsorption experiments. The biochar capacity for pure CO was 0.700 mmol/g at 20 °C in dynamic experiments, and in static experiments at the same temperature, the capacity was lower at 0.134 mmol/g. Likewise, the biochar CO_2 capacity was 2.325 mmol/g in the dynamic adsorption tests and 1.01308 mmol/g at the same temperature in the static experiments. The higher adsorption capacities in the dynamic adsorption experiments may be partially due to the higher pressure of the dynamic experiments (120 kPa) compared to the static experiments (max $\sim$ 100 kPa). However, calculated

capacities at 120 kPa using the fitted Dual-site Langmuir model (based on the static adsorption tests) still show lower biochar adsorption capacities for both of the gases at 120 kPa compared to that of the dynamic experiment (1.045 and 0.151 mmol/g for CO_2 and CO, respectively). The comparison of dynamic and static experiments in other research shows the same result with respect to higher adsorption under dynamic conditions [36, 37]. The reason is attributed to the difference in the static vs. dynamic nature of the experiments. In batch tests, a fixed volume of gas is introduced to the adsorbent, while in dynamic adsorption, the fresh feed is fed to the adsorbent constantly, resulting in a continuous driving force between the fresh feed and the adsorbed phase. This results in higher adsorption and a higher capacity [36, 38].

4.4.4 Adsorption kinetic

The dynamic adsorption experiment capacities, along with the fitted adsorption rate models for pure CO and CO_2 adsorption, are presented in Table 4.3. Comparing the R^2 values for both CO and CO_2 adsorption shows that the Avrami model represents the adsorption rate behaviors of both gases the best. This result indicates both physical and chemical forces were involved in CO and CO_2 adsorption. The Avrami exponent was higher than 1 for both of the components, which indicates adsorption on the surface of the biochar varies, reflecting the heterogeneity of the biochar surface.

Table 4.3: Fitted parameters of pseudo-first-order, pseudo-second-order, and Avrami kinetic models for the pure CO_2 and CO adsorption on biochar

Component	q_{exp}	Pseudo-first-order			Pseudo-second-order			Avrami			
	(mmol/g)	q_e	k_1	R^2	q_e	k_2	R^2	q_e	k_A	n	R^2
	±0.4 %	(mmol/g)	(min^{-1})		(mmol/g)	(g/mmol min)		(mmol/g)	(min^{-1})		
CO	0.70	0.67	1.127	0.964	0.73	2.684	0.856	0.68	1.061	1.457	0.988
CO_2	2.33	2.41	0.332	0.946	2.98	0.114	0.906	2.31	0.334	1.721	0.990

4.4.5 Binary CO/CO_2 dynamic adsorption experiments

The competitive adsorption of CO and CO_2 on biochar surface was studied by the dynamic adsorption experiments using the ABR device. The breakthrough curves of binary mixtures of CO and CO_2, along with their pure gas, are shown in Figure 4.4. Breakthrough curves of the gas mixtures are more complex than pure gases as they commonly contain a roll-up when the weaker adsorbed component is replaced by the stronger adsorbed component. This results in the outlet to inlet concentration (C/C_0) of the weaker adsorbed component to temporarily exceed one before decreasing back to one [39].

In the breakthrough curves for the binary CO/CO_2 mixtures, a roll-up can be noted for CO (component weaker adsorption). Initially, C/C_0 for both CO and CO_2 increased. The C/C_0 value for CO at some point temporarily exceeded one, indicating more CO in the gas outlet than in the inlet or some of the initially adsorbed CO was

being removed by the CO_2.

The capacities as a function of initial CO/CO_2 are provided in Table 4.4. Overall, it is evident that the biochar was more selective toward CO_2 compared to CO. For the tests with 10, 30, and 50 vol.% CO, the final capacity for CO was 0 mmol/g. The breakthrough curves show that in all of the tests, there was some CO loading on biochar initially; hence, it can be concluded that in the tests with up to 50 vol.% of CO, all of the initially adsorbed CO was later removed by the CO_2 molecules. In the tests with 70 and 90% CO, some of the CO was retained on the biochar. It is clear that CO_2 could replace CO more effectively at higher CO_2 partial pressures as a result of higher driving force and the resultant mass transfer. Even in the test with 90% CO, some CO molecules were removed by CO_2 (judging from the >1 C/C_0 values for CO in the breakthrough curve); however, the roll-up in the plot is not that visible as a result of lower CO_2 partial pressure and lower removal of CO compared to the other tests.

4.4.6 Impact of temperature

4.4.6.1 Pure CO and CO_2

The impact of temperature on CO and CO_2 adsorption was studied between 20-100 °C in the dynamic gas adsorption system. The breakthrough curves for pure CO and CO_2 at different temperatures are presented in Figure 4.5. As the temperature increased, the breakthrough and saturation time for CO_2 decreased, while for CO

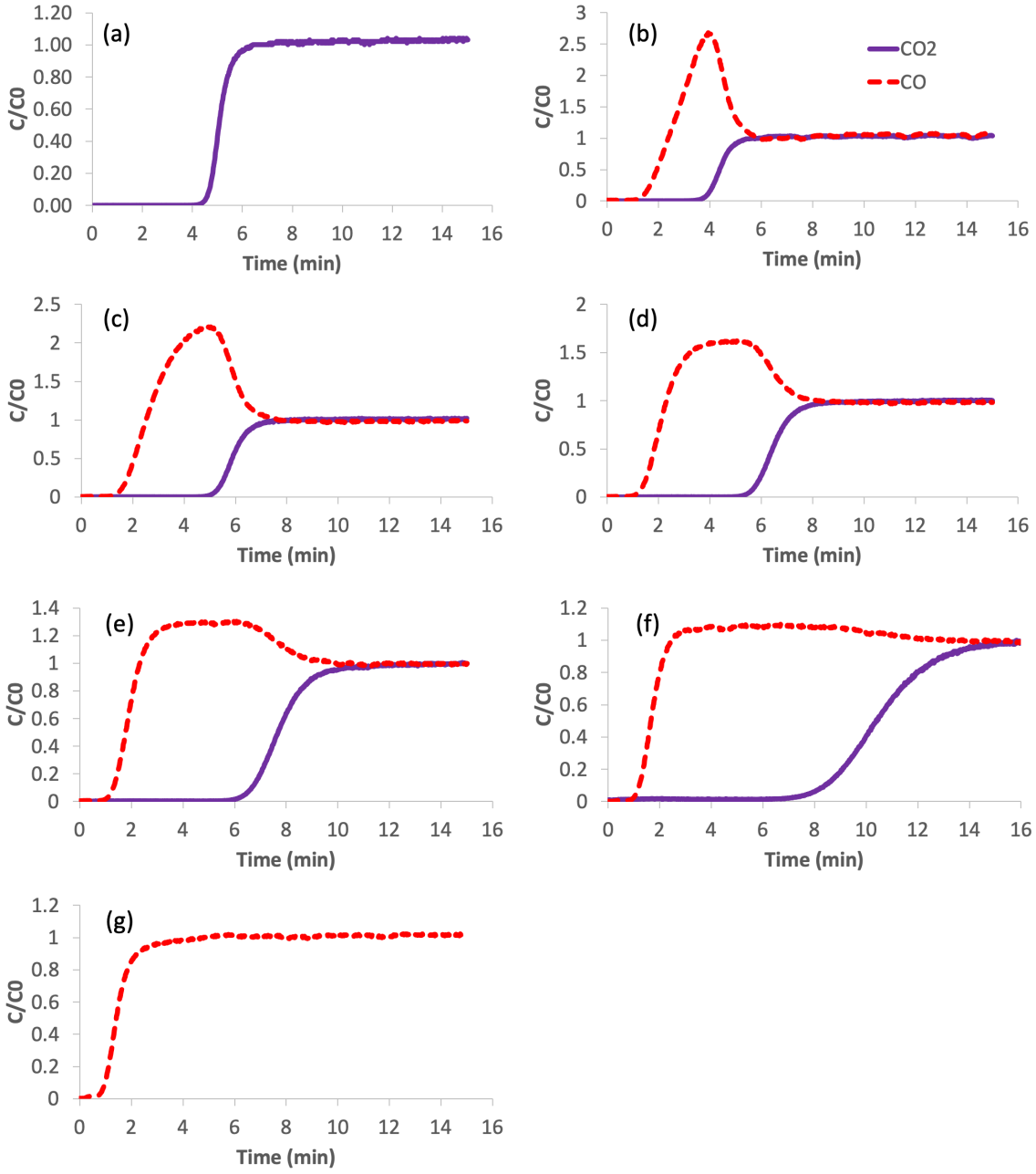

Figure 4.4: Breakthrough curves of dynamic adsorption experiments with various concentrations (vol.%) of CO and CO_2: (a) 100% CO_2, (b) 90%/10% CO_2/CO, (c) 70%/30% CO_2/CO, (d) 50%/50% CO_2/CO, (e) 30%/70% CO_2/CO, (f) 10%/90% CO_2/CO, (g) 100% CO

Table 4.4: Adsorption capacities of pure and binary CO/CO_2 from dynamic experiments

CO_2 (vol.%)	CO (vol.%)	Adsorption capacity (mmol/g) ±0.4 %	
		CO_2	CO
100	0	2.325	0
90	10	1.804	0
70	30	1.880	0
50	50	1.482	0
30	70	1.064	0.084
10	90	0.477	0.423
0	100	0	0.700

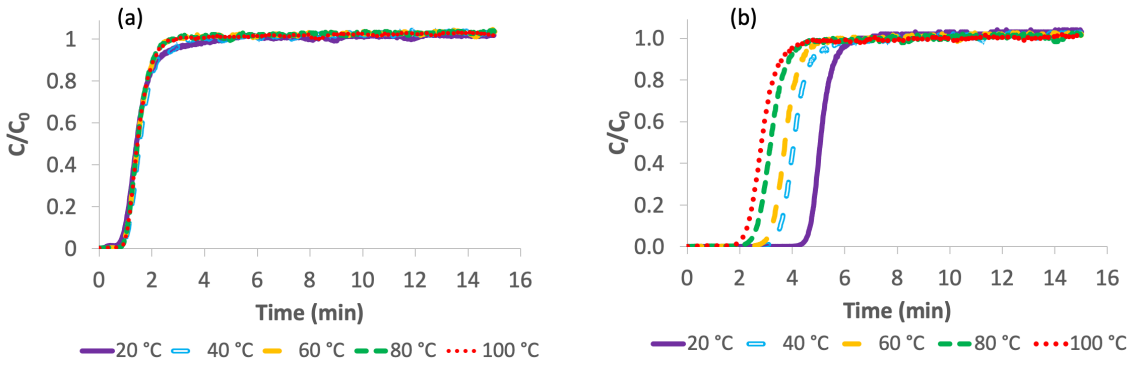

Figure 4.5: Breakthrough curves of adsorption of (a) pure CO and (b) pure CO_2 on biochar at different temperatures

there were no discernible changes with temperature.

The capacities calculated using the area above the breakthrough curves are reported in Table 4.5. The biochar CO_2 adsorption capacity decreased by 43.48% as the adsorption temperature increased from 20 to 100 °C (2.325 mmol/g at 20 °C and 1.314 mmol/g at 100 °C). This is a typical behavior of an exothermic process, where the process would shift to the direction of releasing less heat in response to the temperature increase.

The CO adsorption capacity did not show a notable change as the capacity fluctuated at approximately 0.700 mmol/g. The molecular modeling indicated that CO adsorption was also exothermic. However, the degree of exothermicity may be too low to show any impact at these conditions.

Table 4.5: Adsorption capacities of pure CO and CO_2 at different temperatures

Component	Temperature (°C)	Adsorption capacity (mmol/g) ±0.4 %
CO	20	0.700
	40	0.737
	60	0.684
	80	0.682
	100	0.686
CO_2	20	2.325
	40	1.877
	60	1.712
	80	1.468
	100	1.314

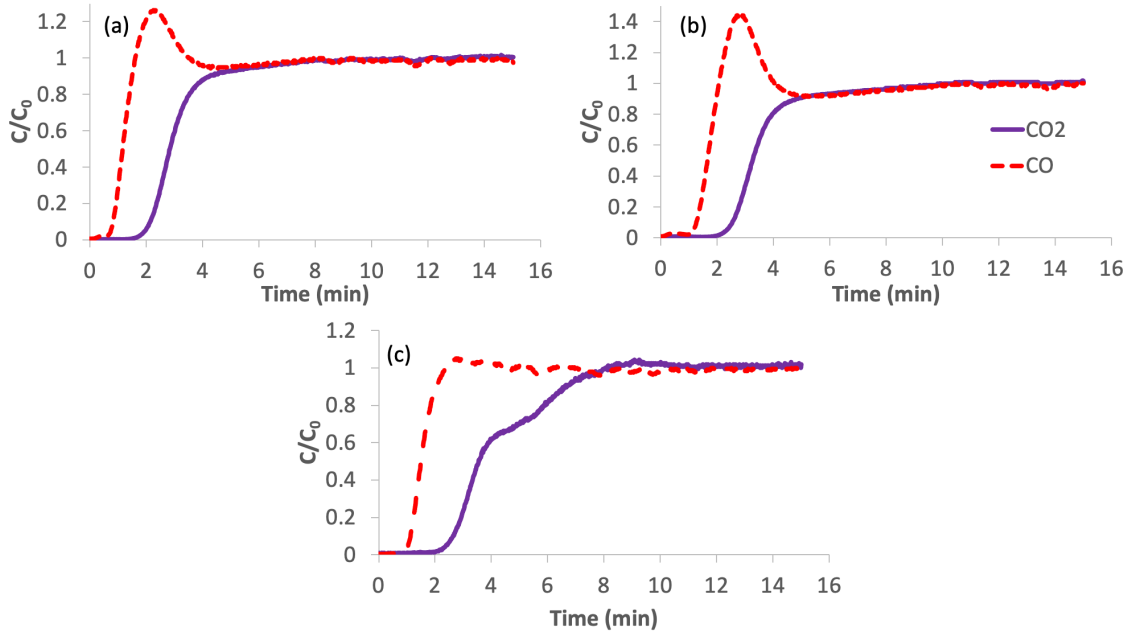

Figure 4.6: Breakthrough curves of dynamic adsorption experiments at 100 °C with (a) 50%50% CO_2/CO, (b) 30%/70% CO_2/CO, (c) 10%/90% CO_2/CO (vol.%)

4.4.6.2 Binary CO/CO_2 mixtures

In order to examine the adsorption of the binary mixture of CO and CO_2 at higher temperatures, three of the binary mixtures of CO/CO_2 were selected (CO/CO_2: 50%/50%, 70%/30%, and 90%/10%). These ratios were selected based on the results at 20 °C, which indicated CO adsorption. The breakthrough curves of these binary mixtures at 100 °C are presented in Figure 4.6. Similar to the binary gas adsorption experiments at 20 °C, a roll-up can be seen for CO, meaning that some of the initially adsorbed CO were later removed by CO_2, which had a stronger adsorption on the biochar surface.

Table 4.6: Adsorption capacities of selected binary CO/CO_2 mixtures at 20 and 100 °C

CO_2 (vol.%)	CO (vol.%)	Temperature	Adsorption capacity (mmol/g) ±0.4 %	
		(°C)	CO_2	CO
50	50	20	1.482	0
50	50	100	0.714	0.238
30	70	20	1.064	0.084
30	70	100	0.491	0.459
10	90	20	0.477	0.423
10	90	100	0.190	0.605

The capacities of CO and CO_2 for the experiments at 100 °C, along with the experiments with the same concentrations at 20 °C, are reported in Table 4.6. It can be noted that the CO adsorption capacity was higher in the experiments at 100 °C compared to the experiments at 20 °C. This is a result of the higher exothermicity of CO_2 adsorption, which resulted in less CO molecules removal by CO_2 molecules.

4.5 Conclusions

In this work, the co-adsorption of CO and CO_2 on wood biochar was studied. CO is always co-released with CO_2, and it was unclear if CO would also adsorb on

biochar and if there was going to be any competition between the two gases over the adsorption sites. The binding energies of different functional groups of biochar with CO and CO_2 were calculated separately to have an estimation of biochar affinity toward the gases before the adsorption tests. The results suggested that all of the functional groups on the biochar had a higher affinity toward CO_2 compared to CO. The isotherms of the two gases were derived from their batch equilibrium adsorption experiments. Fitting the adsorption experiments showed that the Dual-site Langmuir isotherm was best fitted to both of the gases equilibrium adsorption data, which showed that the biochar surface was not a homogeneous one. The pure dynamic adsorption tests also pointed to the same results as the molecular modeling (higher affinity of biochar for CO_2 compared to CO). The breakthrough time for pure CO_2 (4.568 min) was so much higher than that of pure CO (0.860 min), and the calculated capacity was also higher. The adsorption capacity for pure CO_2 (2.325 mmol/g) was more than 3 times greater than that of pure CO (0.700 mmol/g). The Avrami kinetic model fitted the pure dynamic adsorption experiments of CO and CO_2 on biochar the best, which showed that both chemical and physical forces were involved in the adsorption processes.

Based on molecular modeling and pure gas adsorption experiments, it was predicted that in the case of the competition between CO_2 and CO over biochar adsorption sites, CO_2 would be favored; however, dynamic co-adsorption experiments of CO and CO_2 were required to have a credible conclusion. Breakthrough curves of

biochar adsorption of binary CO/CO_2 (different concentrations in the range of 10-90 vol.%) indicated that both CO and CO_2 initially adsorbed on biochar; however, some CO were later removed by the more strongly adsorbed CO_2. The CO adsorption on biochar was not notable (0 mmol/g) in the binary adsorption tests for up to 50 vol% CO, as the result of CO and CO_2 competition over adsorption sites and CO_2 removing all of the initially adsorbed CO. However, at lower partial pressures of CO_2 (30 and 10 vol.%), CO_2 could not remove all of the initially adsorbed CO. The biochar CO capacity at 70 and 90 vol.% CO (30 and 10 vol% CO_2) was 0.084 and 0.423 mmol/g, respectively. This result suggested that for the gas streams at the ambient temperature if the CO_2 concentration is beyond 50 vol.%, biochar cannot adsorb a notable amount of CO.

It is clear that flue gas from power plants or syngas from gasification is released at higher temperatures than 20 °C. Therefore, biochar CO and CO_2 adsorption study at higher temperatures is required for examining the biochar adsorption performance at more practical operation conditions. In order to examine the impact of temperature on CO and CO_2 adsorption on biochar, pure CO and CO_2 adsorption tests were conducted at different temperatures in the range of 20-100 °C. The results of these adsorption tests suggested that CO_2 adsorption capacity on biochar declined as the temperature increased, but CO adsorption was not impacted by temperature. The results from three selected CO/CO_2 binary mixture adsorption on biochar at 100 °C showed that biochar CO adsorption from the binary mixture increased at 100 °C

compared to the same adsorption experiment at 20 °C. On the other hand, CO_2 adsorption from the binary mixture was reduced at 100 °C compared to the same experiment at 20 °C. This result showed that lower biochar capacity for CO_2 at higher temperatures caused CO_2 to not be able to remove as many CO molecules as in the experiments at 20 °C, suggesting that at the higher temperatures, the biochar CO adsorption would be enhanced as a result of declined adsorption of CO_2 on biochar.

Emitted gases from power plants or gasification (syngas) contain other compounds in the mixture as well. The next proper stage in the research in this area would be studying impact of other gases (such as CH_4, which is present in gasification syngas) on CO_2 adsorption, as well as studying mixtures of CO_2 containing more than just two gases at temperatures close to that of the power plant flue gas or gasification syngas.

4.6 Acknowledgements

This research was funded by the Natural Science and Engineering Research Council of Canada (NSERC) and Memorial University of Newfoundland. The authors would like to express their deepest gratitude to Dr. Peter Franshman from ABRI-Tech Inc., Dr. Oliver Stueker and Dr. Serguei Vassiliev from ACENET, and Etienne Guinand and Dr. Mason Lawrence for their valuable contributions to this research work.

Bibliography

[1] M. E. Boot-Handford, J. C. Abanades, E. J. Anthony, M. J. Blunt, S. Brandani, N. Mac Dowell, J. R. Fernández, M.-C. Ferrari, R. Gross, J. P. Hallett, *et al.*, "Carbon capture and storage update," *Energy & Environmental Science*, vol. 7, no. 1, pp. 130–189, 2014.

[2] J. C. Francis, A. Nighojkar, and B. Kandasubramanian, "Relevance of wood biochar on co2 adsorption: A review," *Hybrid Advances*, p. 100056, 2023.

[3] A. E. Creamer, B. Gao, and M. Zhang, "Carbon dioxide capture using biochar produced from sugarcane bagasse and hickory wood," *Chemical Engineering Journal*, vol. 249, pp. 174–179, 2014.

[4] L. Cao, X. Zhang, Y. Xu, W. Xiang, R. Wang, F. Ding, P. Hong, and B. Gao, "Straw and wood based biochar for co2 capture: Adsorption performance and governing mechanisms," *Separation and Purification Technology*, vol. 287, p. 120592, 2022.

[5] Z. G. Mamaghani, K. A. Hawboldt, and S. MacQuarrie, "Adsorption of co2 using biochar-review of the impact of gas mixtures and water on adsorption," *Journal of Environmental Chemical Engineering*, p. 109643, 2023.

[6] L. Huang, Z. Ning, Q. Wang, W. Zhang, Z. Cheng, X. Wu, and H. Qin, "Effect of organic type and moisture on co2/ch4 competitive adsorption in kerogen with

implications for co2 sequestration and enhanced ch4 recovery," *Applied Energy*, vol. 210, pp. 28–43, 2018.

[7] D. Nicks Jr, J. Holloway, T. Ryerson, R. Dissly, D. Parrish, G. Frost, M. Trainer, S. Donnelly, S. Schauffler, E. Atlas, *et al.*, "Fossil-fueled power plants as a source of atmospheric carbon monoxide," *Journal of environmental monitoring*, vol. 5, no. 1, pp. 35–39, 2003.

[8] S. M. Wilson, D. A. Kennedy, and F. H. Tezel, "Adsorbent screening for co2/co separation for applications in syngas production," *Separation and Purification Technology*, vol. 236, p. 116268, 2020.

[9] G. P. Lithoxoos, L. D. Peristeras, G. C. Boulougouris, and I. G. Economou, "Monte carlo simulation of carbon monoxide, carbon dioxide and methane adsorption on activated carbon," *Molecular Physics*, vol. 110, no. 11-12, pp. 1153–1160, 2012.

[10] Z. G. Mamaghani, K. A. Hawboldt, S. MacQuarrie, and M. Katz *Journal of random*, 3001in press.

[11] H. Bamdad, K. Hawboldt, S. MacQuarrie, and S. Papari, "Application of biochar for acid gas removal: experimental and statistical analysis using co 2," *Environmental Science and Pollution Research*, vol. 26, no. 11, pp. 10902–10915, 2019.

[12] M. J. Frisch, G. W. Trucks, H. B. Schlegel, G. E. Scuseria, M. A. Robb, J. R. Cheeseman, G. Scalmani, V. Barone, B. Mennucci, G. A. Petersson, H. Nakatsuji, M. Caricato, X. Li, H. P. Hratchian, A. F. Izmaylov, J. Bloino, G. Zheng, J. L. Sonnenberg, M. Hada, M. Ehara, K. Toyota, R. Fukuda, J. Hasegawa, M. Ishida, T. Nakajima, Y. Honda, O. Kitao, H. Nakai, T. Vreven, J. A. Montgomery, Jr., J. E. Peralta, F. Ogliaro, M. Bearpark, J. J. Heyd, E. Brothers, K. N. Kudin, V. N. Staroverov, R. Kobayashi, J. Normand, K. Raghavachari, A. Rendell, J. C. Burant, S. S. Iyengar, J. Tomasi, M. Cossi, N. Rega, J. M. Millam, M. Klene, J. E. Knox, J. B. Cross, V. Bakken, C. Adamo, J. Jaramillo, R. Gomperts, R. E. Stratmann, O. Yazyev, A. J. Austin, R. Cammi, C. Pomelli, J. W. Ochterski, R. L. Martin, K. Morokuma, V. G. Zakrzewski, G. A. Voth, P. Salvador, J. J. Dannenberg, S. Dapprich, A. D. Daniels, Farkas, J. B. Foresman, J. V. Ortiz, J. Cioslowski, and D. J. Fox, "Gaussian09 Revision E.01." Gaussian Inc. Wallingford CT 2009.

[13] M. D. Hanwell, D. E. Curtis, D. C. Lonie, T. Vandermeersch, E. Zurek, and G. R. Hutchison, "Avogadro: an advanced semantic chemical editor, visualization, and analysis platform," *Journal of cheminformatics*, vol. 4, no. 1, pp. 1–17, 2012.

[14] C. Chen, K. Xu, X. Ji, L. Miao, and J. Jiang, "Enhanced adsorption of acidic gases (co 2, no 2 and so 2) on light metal decorated graphene oxide," *Physical Chemistry Chemical Physics*, vol. 16, no. 22, pp. 11031–11036, 2014.

[15] M. A. Al-Ghouti and D. A. Da'ana, "Guidelines for the use and interpretation of adsorption isotherm models: A review," *Journal of hazardous materials*, vol. 393, p. 122383, 2020.

[16] C. Chilev, M. Dicko, P. Langlois, and F. Lamari, "Modelling of single-gas adsorption isotherms," *Metals*, vol. 12, no. 10, p. 1698, 2022.

[17] Q. Wu, L. Zhou, J. Wu, and Y. Zhou, "Adsorption equilibrium of the mixture ch4+ n2+ h2 on activated carbon," *Journal of Chemical & Engineering Data*, vol. 50, no. 2, pp. 635–642, 2005.

[18] I. Langmuir, "The constitution and fundamental properties of solids and liquids. part i. solids.," *Journal of the American chemical society*, vol. 38, no. 11, pp. 2221–2295, 1916.

[19] S. Alafnan, A. Awotunde, G. Glatz, S. Adjei, I. Alrumaih, and A. Gowida, "Langmuir adsorption isotherm in unconventional resources: Applicability and limitations," *Journal of Petroleum Science and Engineering*, vol. 207, p. 109172, 2021.

[20] S. Kalam, S. A. Abu-Khamsin, M. S. Kamal, and S. Patil, "Surfactant adsorption isotherms: A review," *ACS omega*, vol. 6, no. 48, pp. 32342–32348, 2021.

[21] R. Sips, "Combined form of langmuir and freundlich equations," *J. Chem. Phys*, vol. 16, no. 429, pp. 490–495, 1948.

[22] G. P. Jeppu and T. P. Clement, "A modified langmuir-freundlich isotherm model for simulating ph-dependent adsorption effects," *Journal of contaminant hydrology*, vol. 129, pp. 46–53, 2012.

[23] A. L. Myers and J. M. Prausnitz, "Thermodynamics of mixed-gas adsorption," *AIChE journal*, vol. 11, no. 1, pp. 121–127, 1965.

[24] K. S. Sing, F. Rouquerol, and J. Rouquerol, "Classical interpretation of physisorption isotherms at the gas-solid interface," *Adsorption by Powders and Porous Solids: Principles, Methodology and Applications*, vol. 2, pp. 159–189, 2013.

[25] S. Lee, J. H. Lee, and J. Kim, "User-friendly graphical user interface software for ideal adsorbed solution theory calculations," *Korean Journal of Chemical Engineering*, vol. 35, pp. 214–221, 2018.

[26] K. O. Yoro, M. Singo, J. L. Mulopo, and M. O. Daramola, "Modelling and experimental study of the co2 adsorption behaviour of polyaspartamide as an adsorbent during post-combustion co2 capture," *Energy Procedia*, vol. 114, pp. 1643–1664, 2017.

[27] M. S. Shafeeyan, W. M. A. W. Daud, A. Shamiri, and N. Aghamohammadi, "Modeling of carbon dioxide adsorption onto ammonia-modified activated carbon: kinetic analysis and breakthrough behavior," *Energy & Fuels*, vol. 29, no. 10, pp. 6565–6577, 2015.

[28] S. K. Lagergren, "About the theory of so-called adsorption of soluble substances," *Sven. Vetenskapsakad. Handingarl*, vol. 24, pp. 1–39, 1898.

[29] M. Avrami, "Kinetics of phase change. i general theory," *The Journal of chemical physics*, vol. 7, no. 12, pp. 1103–1112, 1939.

[30] F. Raganati, M. Alfe, V. Gargiulo, R. Chirone, and P. Ammendola, "Kinetic study and breakthrough analysis of the hybrid physical/chemical co2 adsorption/desorption behavior of a magnetite-based sorbent," *Chemical Engineering Journal*, vol. 372, pp. 526–535, 2019.

[31] C. Wang, B. He, S. Sun, Y. Wu, N. Yan, L. Yan, and X. Pei, "Application of a low pressure economizer for waste heat recovery from the exhaust flue gas in a 600 mw power plant," *Energy*, vol. 48, no. 1, pp. 196–202, 2012.

[32] Y.-C. Chiang, P.-C. Chiang, and C.-P. Huang, "Effects of pore structure and temperature on voc adsorption on activated carbon," *Carbon*, vol. 39, no. 4, pp. 523–534, 2001.

[33] N. Le-Minh, E. C. Sivret, A. Shammay, and R. M. Stuetz, "Factors affecting the adsorption of gaseous environmental odors by activated carbon: A critical review," *Critical Reviews in Environmental Science and Technology*, vol. 48, no. 4, pp. 341–375, 2018.

[34] H. Bamdad, S. Papari, S. MacQuarrie, and K. Hawboldt, "Study of surface

heterogeneity and nitrogen functionalizing of biochars: Molecular modeling approach," *Carbon*, vol. 171, pp. 161–170, 2021.

[35] S. Sethupathi, M. Zhang, A. U. Rajapaksha, S. R. Lee, N. Mohamad Nor, A. R. Mohamed, M. Al-Wabel, S. S. Lee, and Y. S. Ok, "Biochars as potential adsorbers of ch4, co2 and h2s," *Sustainability*, vol. 9, no. 1, p. 121, 2017.

[36] M. S. Mohd Musa, P. Y. Gopalan, N. Yekeen, and A. Al-Yaseri, "Influence of henna extracts on static and dynamic adsorption of sodium dodecyl sulfate and residual oil recovery from quartz sand," *ACS omega*, vol. 8, no. 14, pp. 13118–13130, 2023.

[37] P. B. Ramos, M. F. Ponce, F. Jerez, G. P. Barreto, and M. A. Bavio, "Assessment of industrial waste for adsorption and capture of co2: Dynamic and static capture system," *Journal of Environmental Chemical Engineering*, vol. 10, no. 3, p. 107521, 2022.

[38] J. Rouquerol, F. Rouquerol, P. Llewellyn, G. Maurin, and K. Sing, *Adsorption by powders and porous solids: principles, methodology and applications*. Academic press, 2013.

[39] R. Valenciano, E. Aylón, and M. T. Izquierdo, "A critical short review of equilibrium and kinetic adsorption models for vocs breakthrough curves modelling," *Adsorption Science & Technology*, vol. 33, no. 10, pp. 851–869, 2015.

Chapter 5

Conclusions and Recommendations for Future work

5.1 Summary and conclusions

Biochar is a green CO_2 adsorbent produced from the thermochemical conversion of biomass. The use of biochar for CO_2 adsorption offers sustainable waste management (by biochar production from waste materials) in addition to mitigating the CO_2 atmospheric emissions. In this thesis, after a thorough review of the previous research work in the literature (Chapter 2), we pinpointed the areas where further investigation is required to facilitate the industrial-scale application of biochar. It is evident that flue gas/ syngas from gasification is never pure CO_2 but rather a mixture of different gases. Since each of these impurities can potentially influence the adsorption of CO_2 on biochar by competing over adsorption sites, it is crucial to assess the effects of these impurities on biochar CO_2 adsorption. Such investigations are notably absent in the literature. In addition, the emitted gases are never dry and carry a significant moisture content. Examining the influence of water vapor on the adsorption of CO_2 by biochar is necessary before industrial-scale applications, as it can determine whether pre-treatment steps for removing water are necessary. Our observations indicate that not many research works have studied biochar CO_2 adsorption under humid conditions, and it is clear that more study is required in this area.

In this work, two of the important challenges in the industrial-scale application of biochar were tackled: the impact of water vapor on CO_2 adsorption (Chapter 3) and the impact of CO on CO_2 adsorption in co-adsorption of CO/CO_2 on biochar

(Chapter 4). In this thesis, we have shown fast pyrolysis wood-based biochar can capture CO_2 from CO_2/N_2 binary mixture, and the adsorption efficiency is not impacted by the presence of humidity. The study of co-adsorption of binary CO/CO_2 on biochar revealed that biochar favored CO_2 over CO when both gases were present in the gas mixture, and biochar adsorb CO_2 without any issues in the presence of CO. The summary and conclusions of each chapter are followed.

5.1.1 Literature review

In this chapter, two of the main production technologies (pyrolysis and gasification) and their biochar yields were discussed. The impact of biochar feedstock and its production conditions on its properties was analyzed, followed by a study of the impact of the biochar physical and chemical properties on its CO_2 adsorption capacity. The review of biochar-related literature suggested that for the same feedstock, the higher production temperature generally results in a higher surface area (it should be noted that for each feedstock, there is a max temperature before the surface area starts to decrease due to the pore destruction at high temperatures). A higher surface area usually results in a higher adsorption capacity. Aside from surface area, surface functionality also plays a role in the biochar CO_2 adsorption capacity and, in some cases, can even compensate for the lower surface area. For instance, basic functional groups have an enhancing impact on CO_2 adsorption on biochar, which is attributed to CO_2 slightly acidic nature.

In this chapter, the research gaps in biochar CO_2 adsorption study were identified. This chapter clearly showed a lack of research in biochar CO_2 adsorption from gas mixtures. Some research works suggested that acidic gases such as H_2S and SO_2 compete with CO_2 and decrease the adsorption capacity, while the other gases do not reduce the adsorption capacity to that extent. Nonetheless, there is not sufficient research in this area to validate this claim. This chapter also points out the research gap in biochar CO_2 adsorption in the presence of water vapor. A limited number of research works have been conducted in the area of carbon-based adsorbent CO_2 adsorption under humid conditions. Some of these research works suggested that carbon-based adsorbents would have a steady performance under humid conditions due to their hydrophobic surfaces, but due to the lack of research in the carbon-based adsorbents, especially biochar, CO_2 adsorption under humid conditions, more investigation in this area is necessary.

This chapter also presents a potential application of biochar in purifying components, such as H_2. Gasification syngas contains a notable amount of H_2, and if the biochar produced during gasification can be used for H_2 purification by adsorbing other syngas components and letting H_2 pass, it would be a cost-effective and sustainable way of purifying H_2. However, the review of the literature in this chapter showed that there are not many research works focused on carbon-based adsorbents, especially biochar, H_2 purification. Therefore, more research is required to assess the feasibility of this process, including an assessment of the capacity of biochar

to adsorb all other syngas components, an evaluation of potential additional steps requirements like the water-gas shift reaction (to convert syngas CO to CO_2), and a comparison of the attained level of purified H_2 with the required threshold for industrial H_2 utilization.

5.1.2 Impact of water vapor on biochar CO_2 adsorption

The impact of water on CO_2 adsorption on woody biochar was studied through computational and experimental methods. The binding energies of different functional groups of biochar and CO_2 were calculated under two conditions: dry and in the presence of water vapor as a solvent. Comparing the results suggested that all the functional groups of biochar had higher affinities for CO_2 (higher released energy and stronger adsorption) when water was present, which may be in part due to carbonate formation as a result of CO_2 solution/reaction with water. In order to check the affinity of the biochar for the formed carbonate (HCO_3^-), binding energies of biochar functional groups and HCO_3^- were also calculated. The results confirmed that all the studied functional groups of biochar had a much stronger affinity to HCO_3^- compared to CO_2.

The results from dynamic binary CO_2/N_2 adsorption tests under dry and humid conditions (where N_2 was saturated with water before being mixed with CO_2) at 20 °C and 1.2 bar showed that under both dry and humid conditions, biochar CO_2 adsorption capacity increased with CO_2 concentration in the feed gas. Comparing

the dry and humid adsorption tests indicated that biochar CO_2 adsorption capacity was not impacted by the presence of water for CO_2 levels of 20-60 vol.%; however, at 80 vol.% CO_2 the biochar CO_2 capacity increased by 38% under humid conditions compared to dry, which was attributed to the formation of carbonates. These findings confirmed that at the ambient conditions and 20-80% of humidity, the woody biochar CO_2 adsorption capacity was not negatively impacted by the water presence, and at higher CO_2 partial pressures ($>$ 80 vol.%), the capacity was even improved. Comparing the adsorption rates of biochar CO_2 adsorption under dry and wet conditions revealed that for all the adsorption tests (20-80 vol.% CO_2), the presence of water did not have a notable impact on the adsorption rate. It should be noted that water levels at this temperature (20 °C) are low (less than 2 vol.%).

5.1.3 Impact of CO on biochar CO_2 adsorption

The biochar CO/CO_2 co-adsorption was studied using computational (molecular modeling) and experimental methods. The binding energies of CO and CO_2 with different biochar functional groups showed that all the studied functional groups had a higher affinity for CO_2 compared to CO; therefore, it was predicted that biochar would favor CO_2 over CO if both gases were present in the feed stream. The results from pure CO and CO_2 adsorption tests on biochar at 20 °C and 1.2 bar supported the outcome from binding energies calculations (higher affinity of biochar for CO_2 compared to CO) as the adsorption capacity for pure CO_2 (2.325 mmol/g) was so

much higher than pure CO (0.700 mmol/g).

Although the results from molecular modeling and pure gas adsorption suggested the favored adsorption of CO_2 in co-adsorption of CO/CO_2 on biochar, binary co-adsorption experiments were required to have a reliable conclusion. The binary CO/CO_2 co-adsorption tests on biochar were conducted at 20 °C and 1.2 bar with 10-90 vol.% CO_2 balanced with CO. A roll-up was notable in all the CO breakthrough curves from CO/CO_2 binary adsorption tests on biochar, meaning that although there was some CO adsorption on biochar initially, some/all CO molecules were later removed by more strongly adsorbed CO_2 molecules, which resulted in the outlet to inlet ratio of CO concentration to be temporarily higher than 1. The calculation of CO and CO_2 adsorption capacities from the co-adsorption experiments showed that for up to 50 vol% CO, all of the initially adsorbed CO molecules were removed by CO_2, resulting in 0 mmol/g biochar CO adsorption capacity. However, for the tests with 70 and 90 vol.% of CO, not all of the initially adsorbed CO were removed by CO_2 due to CO_2 lower partial pressures in these tests, and that resulted in biochar CO adsorption capacity of 0.084 and 0.423 mmol/g, respectively.

As the CO_2 containing emitted gases (whether they are flue gas or syngas from gasification) are generally at higher temperatures than ambient, the study of temperature impact on CO and CO_2 biochar adsorption was necessary. The pure CO and CO_2 adsorption tests at temperatures in the range of 20-100 °C showed that although CO_2 adsorption decreased as the temperature increased, CO adsorption on

biochar was not impacted by the temperature as much. Results from the adsorption of selected binary CO/CO_2 mixtures on biochar at 100 °C indicated that CO_2 adsorption from the binary mixture decreased at 100 °C compared to 20 °C. The decrease of CO_2 adsorption at 100 °C resulted in lower removal of adsorbed CO and a higher final biochar CO adsorption capacity at 100 °C compared to 20 °C.

5.2 Recommendation for future work

- As mentioned in Chapter 2, there is a potential application of biochar in the purification of certain components, such as H_2. This potential application of biochar should be first examined at the laboratory scale with feed gas containing CO_2 and H_2. Subsequently, this study can be extended to biochar adsorption experiments in which the feed gas composition and temperature resemble those of gasification syngas.

- The CO_2 adsorption under dry and humid conditions were performed at 20 °C. The results from this research work created the baseline data on the impact of water vapor on biochar CO_2 adsorption. However, flue gas/gasification syngas is emitted at higher temperatures (stack gases are typically released at temperatures between 150-300 °C [1]), and gases can contain higher amounts of water at higher temperatures. Therefore, the experiments should be performed at different temperature levels to analyze the water vapor impact on biochar CO_2

adsorption at more realistic conditions.

- Adsorption experiments under humid conditions can be repeated using an alternative approach. Instead of introducing the water vapor by mixing it with the gas mixture, biochar can be wetted beforehand. Analyzing the outcomes of these sets of experiments could enhance the understanding of the process. In addition, examining the hydrophobicity of the biochar may provide additional insights into the results.

- A more detailed study of the change in the biochar surface before and after adsorption and after repeated adsorption cycles is required. This would inform the longevity of the biochar, mechanism of adsorption, changes in surface properties, etc., all of which are required for modeling transport phenomena at a larger scale.

- Other than CO and water vapor, there are other gases that are often co-released with CO_2, such as CH_4 and other hydrocarbons, SOx, NOx, H_2S, etc. [2]. It is important to study the co-adsorption of each of these components with CO_2 as a binary mixture to understand the impact of these components on CO_2 adsorption.

- After thoroughly understanding the impact of each flue gas component on biochar CO_2 adsorption, it is necessary to conduct adsorption experiments with gas mixtures containing more than two components with compositions

resembling powerplant flue gases or gasification syngas at temperatures close to real-life emissions.

Bibliography

[1] C. Song, W. Pan, S. T. Srimat, J. Zheng, Y. Li, Y.-H. Wang, B.-Q. Xu, and Q.-M. Zhu, "Tri-reforming of methane over ni catalysts for co2 conversion to syngas with desired h2/co ratios using flue gas of power plants without co2 separation," *Stud. Surf. Sci. Catal*, vol. 153, pp. 315–322, 2004.

[2] K. Kumar, D. Banerjee, and D. Das, "Carbon dioxide sequestration from industrial flue gas by chlorella sorokiniana," *Bioresource technology*, vol. 152, pp. 225–233, 2014.

Appendix A

A.1 Adsorption rate plots

The adsorption rate plots for pure CO and CO_2 at temperature range of 20-100 °C is followed:

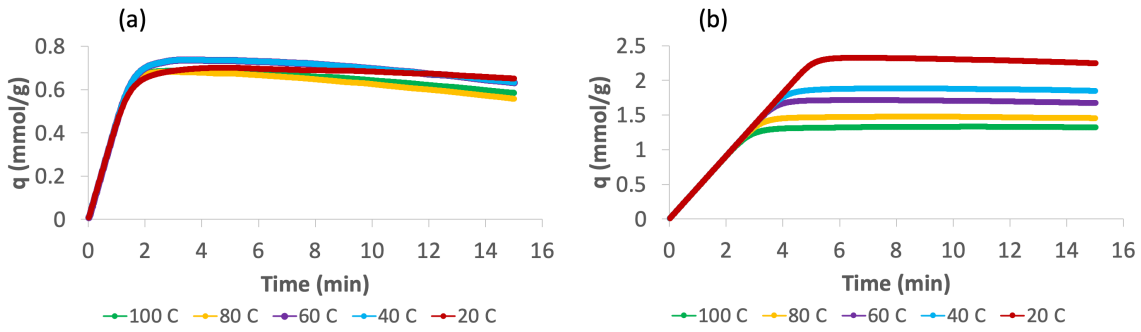

Figure A.1: Adsorption rate plots for (a) pure CO and (b) pure CO_2 at different temperatures

A.2 More detailed steps of molecular modeling

First, the biochar (functional groups) and the adsorbate (e.g. CO_2) should be drawn separately in the Avogadro software. The molecules then undergo an initial optimization step using the optimization tool in the Avogadro. Although molecules are optimized using the Avogadro built-in optimization tool, an additional more precise optimization stage is required. Therefore, the initial Gaussian calculation is optimization. The Gaussian input file is generated in the Avogadro (the type of cal-

culation is set as geometry optimization and the theory and basis set are chosen based on the type of molecules). The input files should be then uploaded to the ACEnet supercomputers (the ACEnet supercomputers were used in this work) and using the shell scripting tool the tasks should be requested, which will be then scheduled in the system. After the results are in, the next step would be creating the Gaussian input file for the frequency calculation using the optimized structures (from the Gaussian optimization calculation results). Figure A.2 shows how the Frequency calculation was requested in one of our calculations.

After the Gaussian frequency calculation is completed, the different molecular vibrations of the structure can be seen in the Avogadro. The energy of the structure can be read from the output text file in the A.U. unit. This energy would be used for the later calculations. The same procedure should be repeated when the adsorbates are put close to biochar functional groups (the initial distance of the adsorbent and adsorbate for these calculations were explained in the chapters of the thesis). The calculated energies of the adsorbent, adsorbate, and their combined structure would be used for binding energy calculation as discussed.

In order to repeat the calculations for adsorption under humid conditions, the SCRF keyword was used in Gaussian calculation input files (Figure A.3). Adding this keyword would result in the Gaussian calculations to be performed with the presence of the water as a solvent.

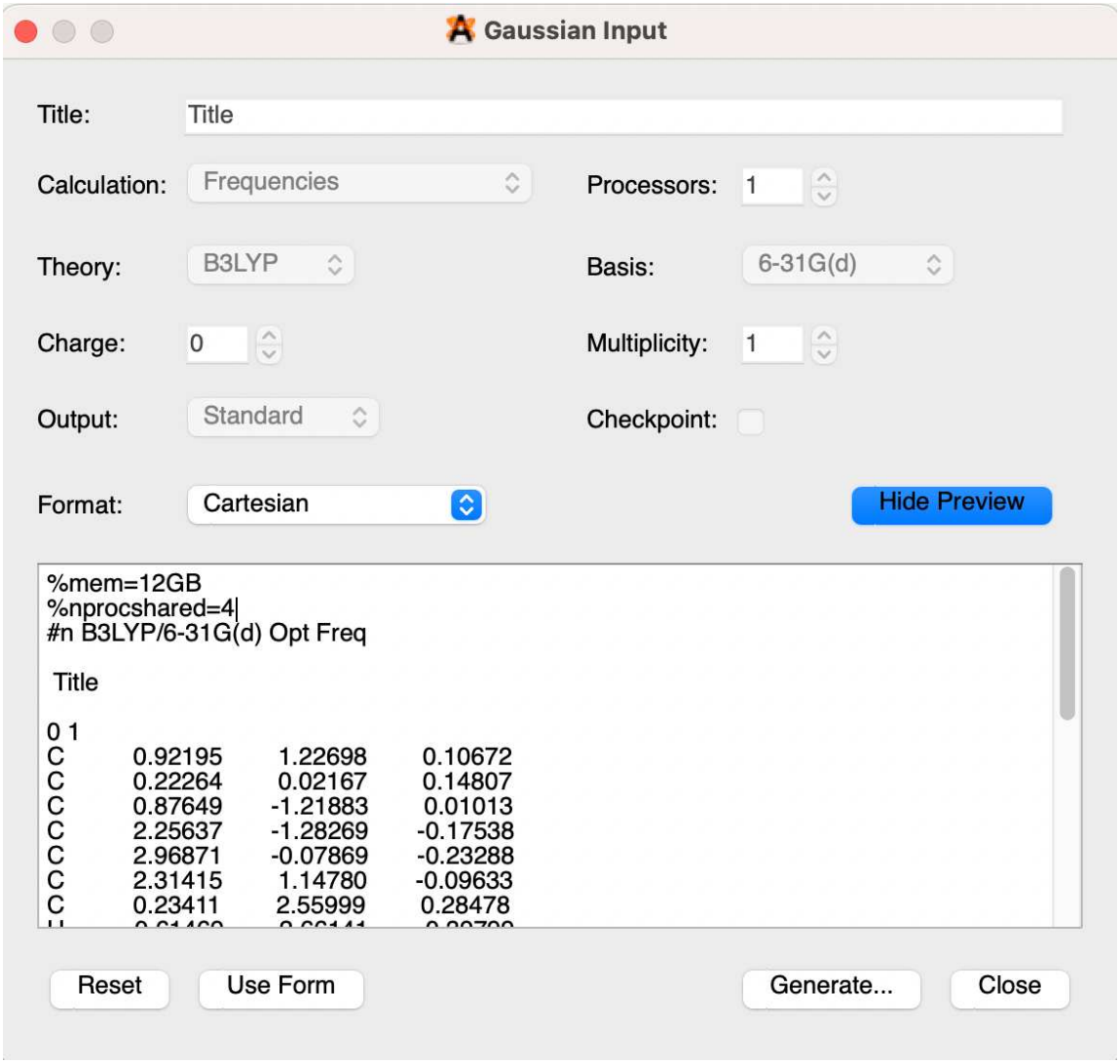

Figure A.2: Creating input file for frequency calculation in Gaussian (opt+freq keywords)

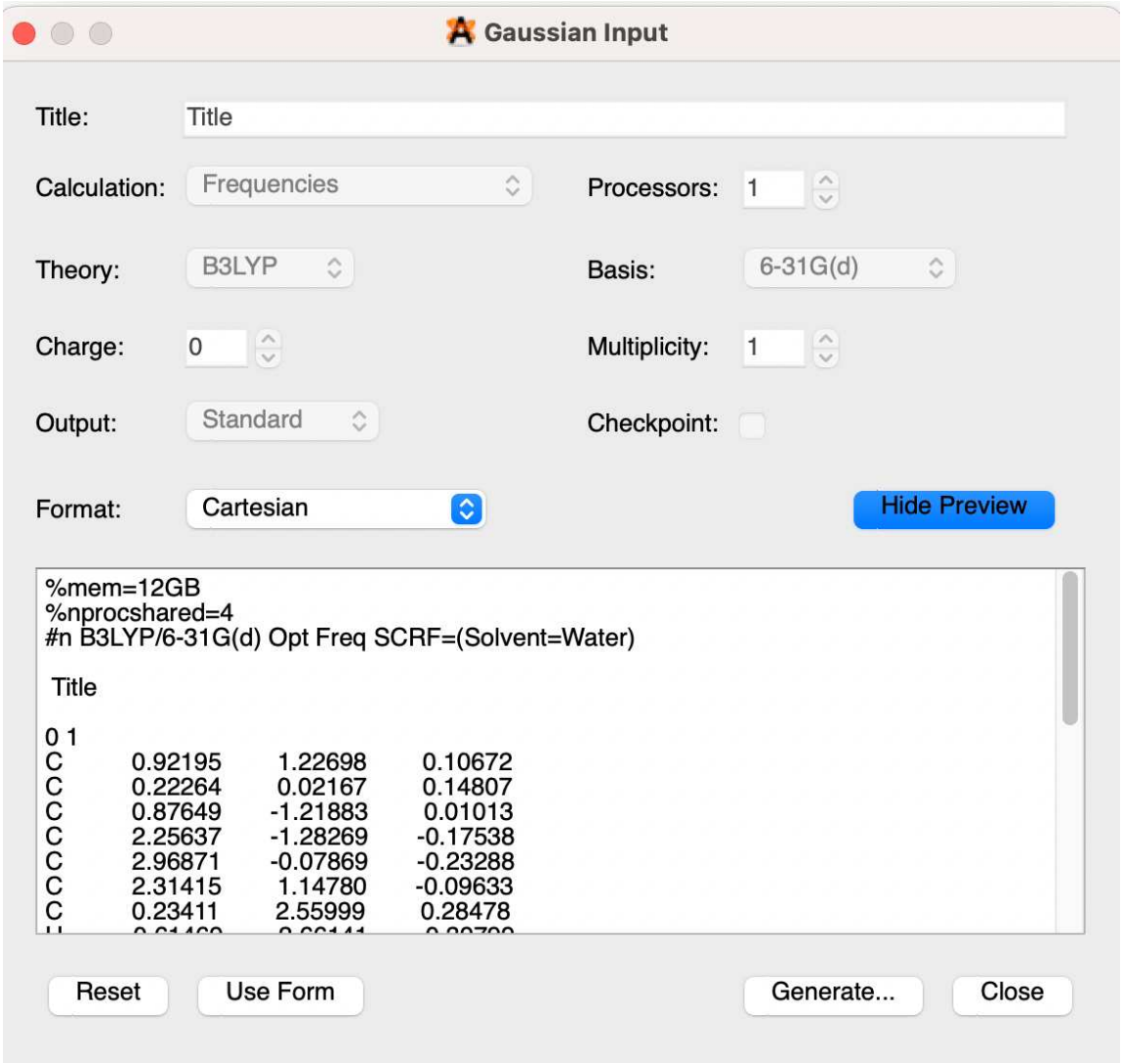

Figure A.3: Creating input file for frequency calculation in Gaussian in the presence of water as a solvent (SCRF keyword)